MultiBody Dynamic Analysis of a 3D Synchronizer Model

ScuDo
Scuola di Dottorato ~ Doctoral School
WHAT YOU ARE, TAKES YOU FAR

Doctoral Dissertation
Doctoral Program in Mechanical Engineering (31^{st} cycle)

Multi Body Dynamic Analysis of a 3D Synchronizer Model

By

Ali Farokhi Nejad

******

Supervisor(s):
Prof. Giorgio Chiandussi, Supervisor
Eng.Andrea Serra, Industrial tutor
Eng.Vincenzo Solimine, Industrial tutor

Doctoral Examination Committee:
Prof.Ian R.MCANDREW,Capitol Technology University
Prof.Katarina MONKOVA,Technical University of Kosice

Politecnico di Torino
2019

Declaration

I hereby declare that, the contents and organization of this dissertation constitute my own original work and does not compromise in any way the rights of third parties, including those relating to the security of personal data.

Ali Farokhi Nejad
2019

* This dissertation is presented in partial fulfillment of the requirements for **Ph.D. degree** in the Graduate School of Politecnico di Torino (ScuDo).

The world of knowledge is fast developing day to day, and only persons can be efficient who are dominant on today's knowledge. This thesis is dedicated to all people who endeavor to develop knowledge, and to my beloved and kind parents an my sisters who always supported me and filled my heart with nothing but their love.

Acknowledgements

I would like to express my deepest gratitude to Professor Giorgio Chiandussi, who always advised me with his perfect knowledge throughout the project. His constant support and invaluable suggestions made this work successful.
Many thanks to Oerlikon Graziano for supporting this project during my PhD program.

This research project would not have been possible without the help of many people especially Vincenzo Solimine and Andrea Serra.

Abstract

The synchronizer mechanism represents the essential component in manual, automatic manual and dual clutch transmissions. In order to carry out the experimental tests, three different synchronizers (single cone, double cone, and triple cone synchronizers) were used on the test rig machine. For the purpose of synchronizing time estimation, an analytical formulation is proposed. This model consider applied force as function of time. The time dependency of this method can be considered as the novelty of this method. The calculated error of this method in worse case was less than 11% in compare with experimental results. Another mathematical model for every phase of synchronization was stablished and the results of this model were compared with experimental data. There is a good agreement between extracted results. This model gives a rough estimation about dynamic behavior of synchronizer regarding fast calculation time. Because of rigid body assumption the reliability of this model in different loading conditions and changing the geometrical dimensions can be reduced. A FE model was generated to evaluate the natural frequency and modal dynamic behavior of the system. The modal responses of different synchronizers under various loading and boundary conditions were examined. The results highlighted the resonance frequency for each synchronizer based on transient modal dynamic. The developed FE model was modified in order to multi body dynamic analysis of three synchronizers. Two different MBD methods (rigid and flexible) were created and the results of those method were compare with experimental data. These three dimensional multi body dynamic models are developed to predict dynamic response of synchronizer especially for calculation of synchronization time. There is a good agreement between both model and experimental results. However the accuracy of flexible model is much closer to the real test condition. A sensitivity analysis was performed on the rigid MBD model and effect of changing the angle of friction cones was investigated. A new expression as a force ratio error was proposed as the outcome of this study. The flexible MBD model was simplified to a sub-model in order

to use for DOE optimization method. Furthermore the results of this validated model were used for DOE- RSM method in order to obtain the best operational condition for each kind of synchronizers. After performing different statistical verification tests some empirical model with more than 96% accuracy were proposed in order to predict the synchronization time, maximum contact pressure, and friction dissipated energy. The calculated synchronization time from DOE method was compared with experimental data and show less than 2% error for different synchronizer mechanism. Based on DOE method a sensitivity analysis was performed to study the effect of different factors when the friction cones have different tolerance dimensions. After applying verification test on the statistical models the final empirical models for each condition were presented. In general, different models which expressed in this thesis can be applicable for different applications. The proposed methodology provides dynamic behavior of synchronizers regarding computational cost and detail information of synchronization during shifting process.

Contents

List of Figures **xi**

List of Tables **xvii**

Nomenclature **xix**

1 Introduction **2**

1.1 Background of Research 2

1.2 Problem Statement 3

1.3 Objectives of Research 5

1.4 Significance of Research 5

1.5 Organization of Thesis 6

2 Literature Review and Theories **8**

2.1 Introduction 8

2.2 Different shifting Mechanisms 11

2.2.1 Diversity of design elements 11

2.3 Power break in the shifting process 13

2.3.1 Shifting with power interruption 13

2.3.2 Shifting without power interruption 15

2.4 Synchronizer mechanism 16

2.5 Shifting process phases 20
2.6 Different models for synchronization simulation 22
2.7 Qualitative factors 24
2.7.1 Shifting Comfort 24
2.8 Important parameters through synchronization 26
2.9 Theories on the current study 30
2.9.1 Fundamental of multibody dynamic 30
2.9.2 Frequency Analysis 33
2.9.3 Design of Experiment method 36
2.10 Summary of this chapter 40

3 Research Methodology 42

3.1 Introduction 42
3.2 Setup of experiments 45
3.2.1 Preparation of the test setup 45
3.2.2 Experimental procedure 49
3.3 Analytical approach 51
3.3.1 Time estimation analysis 51
3.3.2 Multibody dynamic formulation for different phases of synchronization 55
3.4 Numerical approach 64
3.4.1 Geometry preparation and CAD model 64
3.4.2 Physical condition and applied loading and boundary condition 66
3.4.3 Connector element implementation 66
3.4.4 Dynamic Friction Coefficient 67
3.4.5 Contact modeling 68
3.4.6 Material properties 69

3.4.7 Modal dynamic analysis 69
3.4.8 Rigid MBD model 75
3.4.9 Flexible MBD model 79
3.5 DOE technique 81
3.5.1 Sensitivity analysis through DOE method 82
3.6 Summary of this chapter 84

4 Results and Discussion 85
4.1 Introduction 85
4.2 Numerical approach 86
4.2.1 Natural frequency of synchronizer mechanism 86
4.2.2 Transient modal dynamic analysis of synchronizer mechanism 92
4.2.3 Rigid MBD model 98
4.2.4 Sensitivity analysis through rigid MBD 106
4.2.5 Flexible MBD model 108
4.3 Results of analytical model 114
4.3.1 Dynamic behavior of analytical model 114
4.3.2 Comparison between Analytical and Numerical approaches 116
4.4 DOE analysis 118
4.4.1 Results of DOE method for SC-74 118
4.4.2 ANOVA analysis of second response; Contact Pressure . . . 123
4.4.3 ANOVA analysis of third response; friction dissipated energy 126
4.4.4 Results of DOE method for DC-170 129
4.4.5 Results of DOE method for TC-100 132
4.5 Sensitivity analysis through DOE technique 135
4.6 Summary of this chapter 144

5 Conclusion **145**

5.1 Introduction 145

5.2 Conclusion 145

5.3 Recommendations and future works 147

References **148**

Appendix A Appendix1 **155**

List of Figures

2.1 A section view of an MT gearbox for a passenger car [1]. 9

2.2 A section view of a CVT design in a hybrid gearbox [2]. 9

2.3 A section view of a DCT system for passenger cars [3]. 10

2.4 An AMT gearbox view for passenger cars [4]. 10

2.5 Two different shifting mechanisms with (a) frictional cone and (b) fork mechanism for constant meshing [5, 6]. 12

2.6 Two engagement mechanism with (a) dog clutch and (b) Sliding gear mechanism [6, 7]. 13

2.7 The schematic sample of the direct synchromesh shifting mechanism [8]. 14

2.8 The schematic of external features for a gear shifting mechanism in a passenger car [8]. 15

2.9 (a) A free-wheel mechanism and (b) the multi-plate clutch [9, 10]. . 16

2.10 The schematic view of the Baulk-ring synchronizer. 17

2.11 The different parts of (a) single cone (b) double cone and (c) triple cone synchronizers in the exploded view. 19

2.12 (a) to (h) eight different phases of synchronization. 21

2.13 Five different phases of synchronization [8]. 22

2.14 An example of scraping on the gear teeth. 25

2.15 An example of fracture area on the synchronizer ring teeth. 26

2.16 The free body diagram related to the breakthrough on the sleeve and strut detents. 27
2.17 The schematic view of the applied axial loading of synchronization. 28
2.18 The reaction forces from fork motions and indexing torque. 29
2.19 A spatial four-bar linkage with two spherical joints and two revolute joints. 31
2.20 The different kind of kinematic joint that are implemented in ABAQUS [11]. 32
2.21 The design configurations for CCC, CCF, and CCI methods. 39

3.1 The flowchart of the research methodology of this thesis. 43
3.2 (a) A 74 mm single cone synchronizer (SC-74), (b) a 170 mm double cone synchronizer (DC-170) and (c) a 100 mm triple cone synchronizer (TC-100). 44
3.3 The location of the inertia weight (left) and the sensor position (right). 45
3.4 (a) Lubrication system, (b) the fork mechanism, (c) the actuator and (d) The position of load cell. 46
3.5 The applied inertia (left) and the torque convertor stage (right). . . . 47
3.6 Measuring the gap between synchro ring and clutch cone the synchro by feeler gauge. 48
3.7 The PLC interface and the ready to start test rig machine. 49
3.8 The schematic of the synchronizer test rig machine. 50
3.9 The first phase of the synchronization process (Free flying). 56
3.10 The second phase of the synchronization process.The axial moving of the sliding sleeve to the synchronizer ring. 58
3.11 the third phase of synchronization process (first indexing). 60
3.12 The fourth synchronization phase (synchronization phase). 62
3.13 The fifth phase of synchronization second indexing and final engagement. 63

3.14 An imported geometry (a) with error surface and (b) after improvement. 65

3.15 The final assemblies of (a) SC-74, (b) DC-170 and (c) TC-100 were used for FE modeling. 65

3.16 The applied connector to the strut detent mechanism regarding coordinate system. 67

3.17 The procedure of contact modeling in ABAQUS. 69

3.18 The schematic of connecting shafts to the synchronizer. 71

3.19 The applied boundary conditions to the FE model (modal dynamic) of SC-74. 72

3.20 The applied boundary conditions to the FE model (modal dynamic) of DC-170. 72

3.21 The applied boundary conditions to the FE model (modal dynamic) of TC-100. 73

3.22 The applied load as the excitation force in a short period of time. . . 74

3.23 The different steps for setting up the modal dynamic solver in ABAQUS. 75

3.24 The converted solid geometry of synchronizer hub to the rigid shell body. 76

3.25 The applied boundary conditions for rigid MBD analysis of (a) SC-74, (b) DC-170 and (c) TC-100 synchronizer models. 77

3.26 The three friction cones configurations for sensitivity model. 78

3.27 Comparison between the full and sub model for flexible MBD analysis. 80

4.1 The natural frequency of separate parts of SC-74 after mesh convergence study. 87

4.2 The natural frequency of separate parts of DC-170 after mesh convergence study. 88

4.3 The natural frequency of separate parts of TC-100 after mesh convergence study. 89

4.4 The first ten mode shapes of frequency with free-free condition for SC-74. 90

4.5 The effect of sleeve position on the natural frequency of the system for (a) SC-74, (b) DC-170 and (c) TC-100. 91

4.6 The modal responses of SC-74 with different shaft size configuration. 92

4.7 The modal responses of DC-170 with different shaft configurations. 93

4.8 The modal responses of DC-170 with different shaft configurations. 94

4.9 The maximum modal responses of different synchronizers (SC-74, DC-170 and TC-100). 94

4.10 Different sleeve positions in different shaft configurations for SC-74. 95

4.11 Different sleeve positions in different shaft configurations for DC-170. 96

4.12 Different sleeve positions in different shaft configurations for TC-100. 97

4.13 The modal responses of different synchronizers regarding nominal and minimum backlash. 98

4.14 The difference between angular velocities of input and output shafts for SC-74. 99

4.15 Comparison the results of experimental and rigid MBD model for sleeve motion of SC-74. 100

4.16 The difference between angular velocities of input and output shafts for DC-170. 101

4.17 Comparison the results of experimental and rigid MBD model for sleeve motion of DC-170. 102

4.18 The difference between angular velocities of input and output shafts for TC-100. 103

4.19 Comparison the results of experimental and rigid MBD model for sleeve motion of TC-100. 104

4.20 Energy balance through simulation for (a) SC-74, (b)DC-170 and (c) TC-100 synchronizers. 105

4.21 Effect of tolerance dimension on the performance of the SC-74 during synchronization process. 106

4.22 The maximum contact pressure for SC-74 with different tolerance dimension. 107

4.23 Effect of tolerance dimension on the force ratio error. 108

4.24 (a) The difference between angular velocities of input and output shafts and (b) representation of sleeve motion for SC-74. 110

4.25 (a) The difference between angular velocities of input and output shafts and (b) representation of sleeve motion for DC-170. 111

4.26 (a) The difference between angular velocities of input and output shafts and (b) representation of sleeve motion for TC-100. 113

4.27 The difference between angular velocities of input and output shafts from analytical solution and experimental test for (a) SC-74, (b) DC-170 and (c) TC-100. 115

4.28 Comparison between different models for synchronization time estimation of (a) SC-74, (b) DC-170 and (c) TC-100. 117

4.29 Post ANOVA verification tools for prediction of synchronization time of SC-74. 122

4.30 Effect of changing main control factors on the response of the synchronization time for SC-74. 123

4.31 Post ANOVA verification tools for prediction of contact pressure of SC-74. 125

4.32 Effect of changing main control factors on the response of the contact pressure for SC-74. 126

4.33 Post ANOVA verification tools to predict the fiction dissipated energy of SC-74. 128

4.34 Effect of changing main control factors on the response of the friction dissipated energy for SC-74. 129

4.35 Effect of changing main control factors on the response of the synchronization time for DC-170. 130

4.36 Effect of changing main control factors on the response of contact pressure for DC-170. 131

4.37 Effect of changing main control factors on the response of friction dissipated energy for DC-170. 132

4.38 Effect of changing main control factors on the response of the synchronization time for TC-100. 133

4.39 Effect of changing main control factors on the response of contact pressure for TC-100. 134

4.40 Effect of changing main control factors on the response of friction dissipated energy for TC-100. 135

4.41 Post ANOVA verification tools for prediction of synchronization time of SC-74 with varies cone angle. 137

4.42 Effect of changing main control factors on the response of synchronization time for SC-74 with varies cone angle. 138

4.43 Post ANOVA verification tools for prediction of contact pressure for SC-74 with varies cone angle. 140

4.44 Effect of changing main control factors on the response of contact pressure for SC-74 with varies cone angle. 141

4.45 Post ANOVA verification tools for prediction of friction dissipated energy for SC-74 with varies cone angle. 143

4.46 Effect of changing main control factors on the response of friction dissipated energy for SC-74 with varies cone angle. 143

List of Tables

2.1 Different methods of DOE technique based on the number of runs and outcomes. 40

3.1 The dynamic specifications of the SC- 74, the DC-170 and the TC-100 synchronizers. 51

3.2 The components terminology and their dependent parameters. . . . 55

3.3 The inertial and mass properties of SC-74, DC-170 and TC-100. . . 66

3.4 The applied joints between different parts and their bodies' coordinates. 66

3.5 The material properties of different materials were used for different models. 69

3.6 The dimension of connecting shafts of synchronizer mechanism. . . 71

3.7 The main factors for SC-74 synchronizers were used for DOE analysis. 82

3.8 The main factors for DC-170 synchronizers were used for DOE analysis. 82

3.9 The main factors for TC-100 synchronizers were used for DOE analysis. 83

3.10 The main factors for SC-74 with different geometries were used for DOE analysis. 83

4.1 The modal dynamic characteristics of SC-74, DC-170 and TC 100 under different operational conditions. 98

4.2 Design of Experiment's table for SC-74 119

4.3 ANOVA analysis for synchronization time as the first response of DOE method for SC-74. 120

4.4 ANOVA analysis for contact pressure as the second response of DOE method for SC-74. 124

4.5 ANOVA analysis for friction dissipated energy as the third response of DOE method for SC-74. 127

4.6 ANOVA analysis for synchronization time as the first response of DOE method for SC-74 with varies cone angle. 136

4.7 ANOVA analysis for contact pressure as the second response of DOE method for SC-74 with varies cone angle. 139

4.8 ANOVA analysis for friction dissipated energy as the third response of DOE method for SC-74 with varies cone angle. 142

A.1 Design of Experiment's table for DC-170 156

A.2 Design of Experiment's table for TC-100 157

A.3 Design of Experiment's table for SC-74- sensitivity analysis 159

A.4 ANOVA analysis for synchronization time as the first response of DOE method for DC-170. 161

A.5 ANOVA analysis for contact pressure as the second response of DOE method for DC-170. 161

A.6 ANOVA analysis for friction dissipated energy as the third response of DOE method for DC-170. 161

A.7 ANOVA analysis for synchronization time as the first response of DOE method for TC-100. 162

A.8 ANOVA analysis for contact pressure as the second response of DOE method for TC-100. 162

A.9 ANOVA analysis for friction dissipated energy as the third response of DOE method for TC-100. 162

Nomenclature

Greek Symbols

α	Cone angle
$\Delta\omega$	Difference of angular velocity between gearbox shafts
Ω	Angular velocity

Subscripts

1	subscript index of Gear clutch body
2	subscript index of sliding sleeve
3	subscript index of synchronizer ring
4	subscript index of strut detents
5	subscript index of hub
6	subscript index of fork
i	subscript index
j	subscript index

Acronyms / Abbreviations

M_0	Initial torque
a	Constant in the parabolic equation
b	Constant in the parabolic equation

F_{app} Applied load

ALL_{CCDW} Contact discontinuity work

ALL_{CCE} Contact elastic energy

ALL_{FD} Friction dissipation energy

ALL_{IE} Kinetic energy

ALL_{JD} Heat dissipation energy

ALL_{SD} Static dissipation

ALL_{VD} Viscous dissipation

ALL_{WK} External work

CBR_{max} Maximum tolerance dimension of clutch body ring

CBR_{min} Minimum tolerance dimension of clutch body ring

E_{TOT} Total energy

F_{err} Force ratio error

F_{max} Maximum applied load

F_{RA} Reaction force

I_R Applied Inertia

$Ring_{max}$ Maximum tolerance dimension of synchro ring

$Ring_{min}$ Minimum tolerance dimension of synchro ring

T_s Synchronization time

t_{lim} Limited time

U_x Axial displacement along X axis

UR_x Internal energy

UR_x Rotational displacement along X axis

****

Chapter 1

Introduction

1.1 Background of Research

Fuel consumption and ecological issues lead car manufacturers to develop more efficient vehicles. Generally, the transmission systems are 94-96% efficient. However, reportedly, up to 15% of energy loss arises from the transmission system based on driving conditions such as different gear ratios and applied torque [12, 13].The synchronizer mechanism plays a crucial role in Manual Transmissions (MTs), Automatic Manual Transmissions (AMTs) and Dual Clutch Transmissions (DCTs). Synchronizers are tasked to synchronize the different rotational speed of engine and gearbox output shafts. Synchronizer mechanisms are widely used in passenger cars and commercial vehicles, e.g. trucks [14–16]. The effect of the friction coefficient, the thermal condition, the lubrication flow, and other physical properties during the shifting process in manual transmission systems have been evaluated in many studies [17–19].Noise and vibration analysis in DCTs have also been studied according to several research [20]. Spreckels and Wanli et al. [21, 22] have utilized test rigs equipped with instruments to calculate different rotational velocities, reaction forces, applied inertia, and friction coefficients to realize the overall behavior of a synchronizer. However, these kinds of test rigs could not analyze the shifting process. Therefore, mathematical and empirical models have been proposed to simulate the synchronizers dynamic behavior [23, 24]. The effect of applied forces, drag torques and dynamic friction coefficients have been analytically evaluated by those models. Lovas et al.[25] have defined eight different phases for one cycle shifting and have

derived the dynamic governing equation for each phase. Razaki [26] has proposed a different definition of shifting process with five different steps and has identified the analytical formulation for the dynamic behavior of every synchronization step. Pastor et al.[27] have developed a model based on the existing model [25] regarding separated governing equations for each part of synchronizer at different phases of the process. To assess the dynamic response of many systems in automotive industries, Multi-Body Dynamic (MBD) analysis is carried out [28]. Compared with empirical models, implementation of MBD models of the transmission system is not straightforward. Nevertheless, MBD models provide more detailed and accurate outcomes in terms of shifting process description. Hoshino [29] has developed an MBD model to simulate the synchronization of a heavy-duty vehicle under different shifting conditions, and has evaluated the effect of reaction forces and abnormal shifting during the synchronization process under different operational conditions. When a large shift effort is required at the shift lever by downshifting into lower gear, two methods have been proposed to tackle this problem. One method is to increase the gear shift ratio: however, unpleasant vibration and noise can occur during the shifting process. The other method is to apply a multi-cone synchronizer to reduce both the shifting effort and shifting time. Although using multi-cone synchronizers increases the transmission system capacity, geometrical constraints and production costs do not allow the manufacturers to use more than three cones in the synchronizer mechanism [30].Despite of a great deal of research conducted on single-cone synchronizers, the study of multiple cone synchronizer mechanisms has been neglected. Moreover, during the manufacturing process of synchronizer components, the geometrical tolerance is applied to the synchronizer assembly. The synchronization performance may also be influenced by changing the geometrical dimension, which has yet to be taken into consideration.

1.2 Problem Statement

The synchronizing time is one of the significant factors that can influence the transmission system efficiency. Reducing the shifting time minimizes the energy loss during the shifting procedure. To reduce emissions and optimize fuel consumption, some research has been carried out based on real test conditions such as the New European Driving Cycle (NEDC). The results show that optimizing the shifting

procedure will significantly influence both fuel consumption and emission reduction. Their findings suggest the importance of accurate estimation of the shifting time in the transmission system [31, 32].MBD models can be used as a precise tool to estimate the synchronization time [33]. Although some analytical formulations were presented to calculate the shifting time, those models do not have enough accuracy to predict the correct shifting time. The main problem of the previous models is that the force applied by the shifting lever is time dependent, which has been neglected so far [34]. The role of dynamic analysis of rotational systems, like geared systems, in the reduction of noise and vibration should not be taken for granted. Some research has been conducted on natural frequencies and vibration modes of rotating machines such as automotive transmission systems, turbo engines, helicopter and etc.[35, 36]. Parker and his colleagues [37] have developed two different models to present some sources of nonlinearity in a planetary gear system. Walker et al. [38] have presented a lumped model to study on the response of DCT powertrain during the engagement process with and without engine harmonic induced vibration. Although the various components of the transmission system have been studied before [39, 40],less attention has been paid to the vibrational effects of the shifting mechanism. Since the synchronizer is involved transitionally in the dynamic behavior of the transmission system, a transient analysis is needed to investigate the dynamic responses of the shifting mechanism. The materials and software that are used in this study are as follow:

1. Three different types of synchronizers mechanism were used for MBD analysis i.e. single cone (ϕ74 mm), double cone (ϕ170 mm) and triple-cone (ϕ 100 mm) synchronizer.

2. ABAQUS software V6.14 was used to perform FE simulation of rigid and flexible multibody dynamics analysis.

3. A universal test rig machine was used to extract experimental data for the purpose of results validation.

4. Design Expert software was used in order to perform statistical analysis with the design of experiment (DOE) method.

5. Eulerian method for the conservation of angular momentum was considered to estimate synchronizer time as a function of applied loading.

1.3 Objectives of Research

The main objectives of this thesis can be introduced as follow:

1. To develop an integrated 3D finite element (FE) model to evaluate the dynamic behavior of a synchronizer mechanism for a transmission system.
2. Establish a set of equations to evaluate dynamic responses and shifting time estimation of a synchronizer mechanism.
3. To investigate the significant parameters during the synchronizing process.
4. To optimize the outcome responses as a function of the design parameter in order to achieve optimum synchronization performance.
5. To validate the analytical, numerical and FE results through a series of experiments

1.4 Significance of Research

The MDB analysis provides great advantages over existing analytical models from different aspects such as results accuracy and provision of detailed information. A three-dimensional MBD model to simulate the shifting process for three different types of synchronizers was presented. Moreover, two different MBD approaches, i.e. a rigid model and a flexible model, were developed to evaluate the overall and the detailed behavior of the system, respectively. The dynamic behavior of a synchronizer during the shifting process was validated with experimental data extracted from a test rig. Besides, the effect of geometrical tolerance for different types of synchronizers was investigated by considering shifting time and synchronizer performance. To investigate the significant parameters in the synchronization process, the DOE technique was used and after different statistical analyses, the best operational condition for each type of synchronizer was presented. In addition, the statistical-empirical models for multi-objective optimization with more than 96% accuracy were obtained. Since the synchronizer is involved transitionally in the dynamic behavior of the transmission system, a transient analysis is needed to investigate the dynamic responses of the shifting mechanism. In terms of modal dynamic

analysis, a FE model suitable for extracting the natural frequencies of a particular synchronizer and for the evaluation of the effects of different boundary conditions on the dynamic response of the synchronizer mechanism was developed. To estimate the synchronization time regarding time-dependent applied force, a new formulation is presented and compared with the outcome of MBD and the experimental results.

1.5 Organization of Thesis

This thesis includes five chapters. The first chapter is the introduction. It overviews the background of synchronization modeling and different approaches to investigate the shifting process. The rest of the report is arranged as follows. Chapter 2 is concentrated on the literature reviews. This chapter highlights the background knowledge on different transmission systems, different synchronizer mechanisms, identification of different steps in the shifting process, significant physical parameters during synchronization and different methods to model the shifting process. Chapter 3 presents the research methodology of this study that includes five main sections as follow:

- The detailed procedure to run experimental tests in order to carry out the model validation.
- Establishing the analytical equation to estimate synchronization time and driving the dynamic governing equations for different phases of synchronization.
- Generating an FE model to evaluate the natural frequency and modal dynamic behavior of the system.
- Development of the FE model for rigid and flexible MBD analysis for different types of synchronizer mechanism.
- Implementation of DOE techniques to investigate the significant parameters of the synchronization process.

Chapter 4 focuses on the numerical and analytical study and their validation by experiments. The chapter provides a comparison between rigid and flexible MBD models with experimental data. Furthermore, the results of these validated models

were used for the DOE method in order to obtain the best operational condition for each kind of synchronizer. Besides, the results of the FE model for modal analysis with different loading conditions were demonstrated in this chapter. Chapter 5 summarizes the conclusions, outlines the significant contributions from the findings and finally suggests recommendations for future works.

Chapter 2

Literature Review and Theories

2.1 Introduction

Transmission systems have three main categories that were mentioned in chapter 1. In this chapter, the brief history of different transmission systems will be presented. After introducing the transmission systems the different internal and external mechanism for gear shifting will be described. A detailed explanation about the transmission system with or without power interruption is discussed. Furthermore, the different synchronizer mechanism will be presented in this chapter. Moreover, the shifting process through synchronization with a different definition is addressed. The existing model to simulate the synchronization process will be mentioned in the following section and the significant parameters for the shifting process from the previous literature will be introduced. A manual transmission system (MT) includes synchronized manual transmission (SMT) and unsynchronized or constant mesh transmission (CMT).Figure 2.1 shows an MT gearbox for a passenger car.

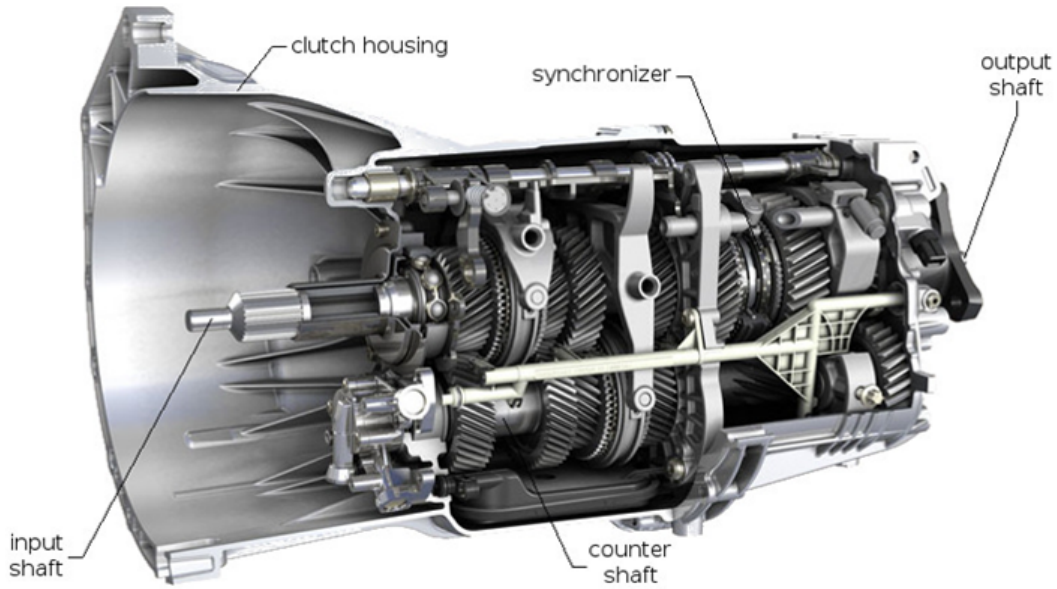

Fig. 2.1 A section view of an MT gearbox for a passenger car [1].

The second branch of the transmission system is continuously variable transmission (CVT) which mostly is used in electro-mechanical transmission (EMT) systems. Figure2.2 demonstrates a CVT design in a hybrid gearbox.

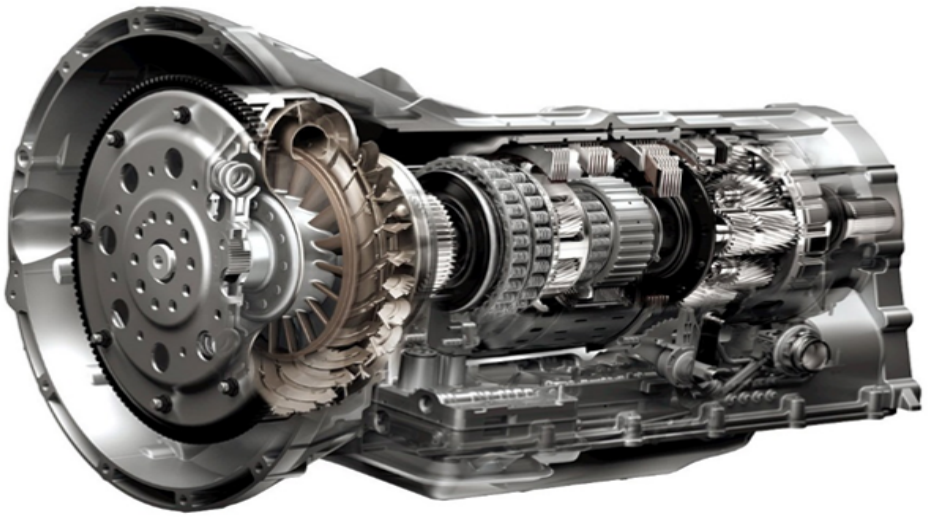

Fig. 2.2 A section view of a CVT design in a hybrid gearbox [2].

The third group consists of an automatic transmission (AT) which includes automatic planetary transmission (APT), dual clutch transmission (DCT) and automated manual transmission (AMT) [41]. Figure 2.3 and Figure2.4 show a DCT and an AMT system for passenger cars, respectively.

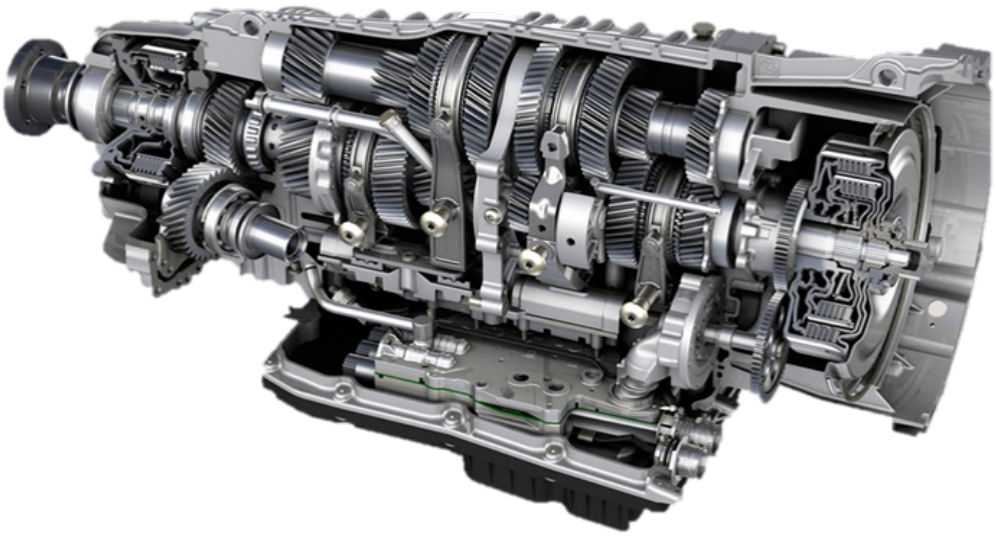

Fig. 2.3 A section view of a DCT system for passenger cars [3].

Fig. 2.4 An AMT gearbox view for passenger cars [4].

The synchronizer mechanism represents the essential component in MT, AMT and DCT systems. When a multi-speed MT is designed, the running gear train is engaged even if does not transfer the power [42]. However, if a specific angular velocity is needed, the main shaft will be connected to the free wheel and the corresponding torque can be transferred from power flow. At this stage, the necessity of using synchronizer can be realized [43].

2.2 Different shifting Mechanisms

2.2.1 Diversity of design elements

Various designs and implementation of different technologies, to use internal and external gear-shifting features, lead to several kinds of shifting mechanisms. The shifting features can be categorized in the following sections.

1. External shifting actuator: To activate the shifting mechanism, different transmission manufacturers used different systems such as linkage, multiple linkages, cable control and shift by wire [44].

2. The applied force generator: Manual mechanical, electro-mechanical, electro-hydraulic, electromagnetic, and electro-pneumatic systems were implemented in transmission systems to apply the force on the shifting mechanism [44].

3. Gear selection mechanism: to transfer the applied loading for changing the position of the gear selector bars, levers, ball joints, four bar linkage, selector shaft, and gear shifting drum were proposed by different designs [45].

4. Positioning components: to change the position of shifting gear, the different gearboxes were equipped with different actuation systems e.g. fork, swing fork, or actuated hydraulic piston. Generally, MT systems use the fork mechanism due to the lower cost in comparison with the other mechanism. However, using the fork mechanism needs more space to be installed [46].

5. Frictional connections: to make synchronization between rotating elements in transmission systems, the different frictional connections were employed. Some examples of them are single or multiple cones, spread ring, multiple

plates, belt, and spring freewheel [45]. Figure2.5 (a) and 2.5(b) shows two different shifting mechanisms that including (a) frictional cone and (b) fork mechanism for constant meshing.

6. 6- Engagement feature: dog clutch engagement, pin engagement, drew key and sliding gear engagement has been used in different kinds of the shifting mechanism [47]. Sliding gear normally is designed as the reverse gear in passenger and commercial vehicles. Figure 2.6 (a) and 2.6 (b) shows the dog clutch and sliding gear mechanism, respectively.

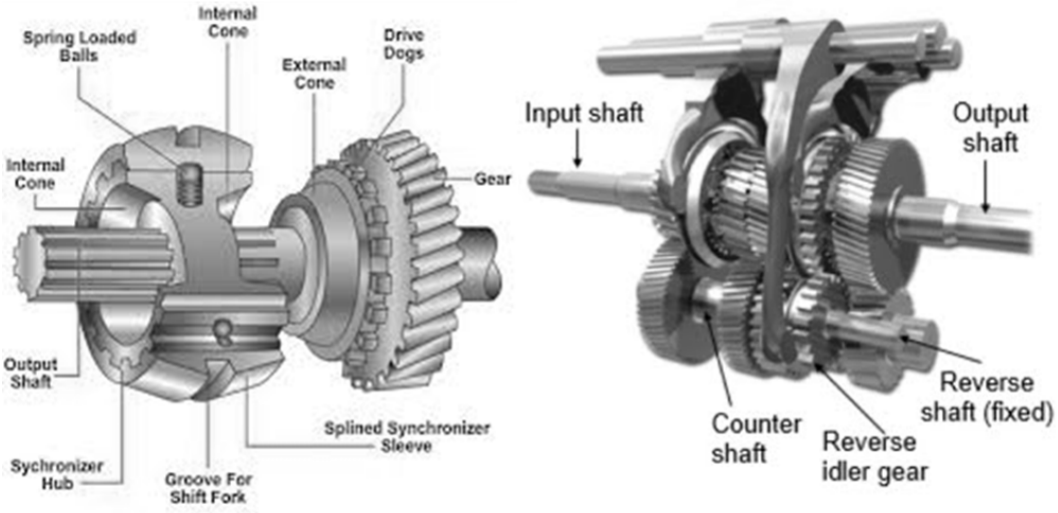

Fig. 2.5 Two different shifting mechanisms with (a) frictional cone and (b) fork mechanism for constant meshing [5, 6].

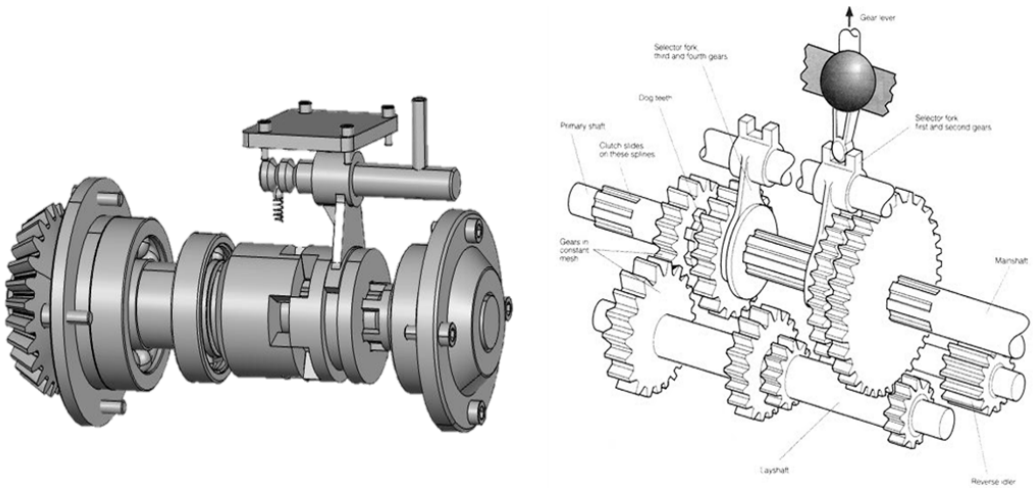

Fig. 2.6 Two engagement mechanism with (a) dog clutch and (b) Sliding gear mechanism [6, 7].

2.3 Power break in the shifting process

2.3.1 Shifting with power interruption

Shifting process can be performed with or without power interruption. Gear shifting can be accomplished without load, i.e., the power flow between the initial motion and the wheels is stopped in the shifting process. This breakage can be the reason for speed loss depending on the gear ratio or rolling resistance. Shortening the shifting time is an option to limit this speed and energy loss. Due to this phenomenon, the shifting process should be completed in less than one second. When the speed of the vehicle is not reduced significantly over shifting process, the transmission with power break can be applied. The power interruption can be implemented in MT and also it is applicable for AT while the master clutch is opened during the shifting process [48].Manual gear shifting requires a smoother running operation on the shifting actuator due to the necessity of bringing gear wheel to the power flow. In passenger cars, some characteristics such as short shifting strokes, smooth changing and low applied force should be taken into account. Therefore, the interaction between internal and external shifting components such as the lever, linkage bars, fork, and detents can be highlighted as a significant factor. Figure2.7 shows the schematic sample of the direct synchromesh shifting mechanism with three different selector

bars [8]. The lever 1 and the ball joint 2 are used as the pivot mechanism to reduce manual shifting effort.

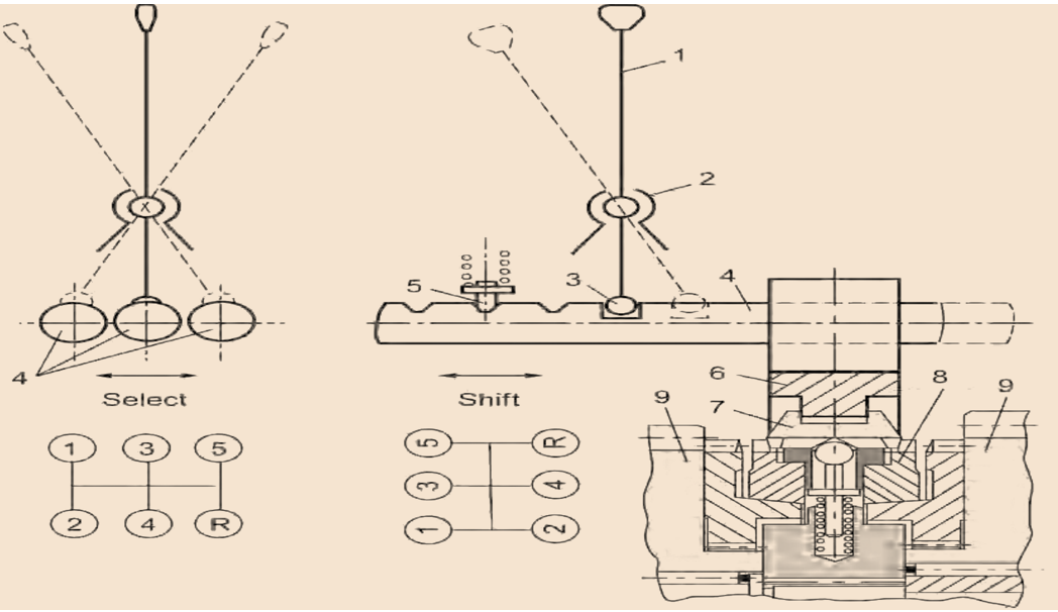

Fig. 2.7 The schematic sample of the direct synchromesh shifting mechanism [8].

External gear shifting mechanism is used to remove vibration and reaction of load changing from gearbox housing and gear shifting lever. Figure 2.8 shows the external and some internal features of a gear shifting mechanism for a passenger car [8].

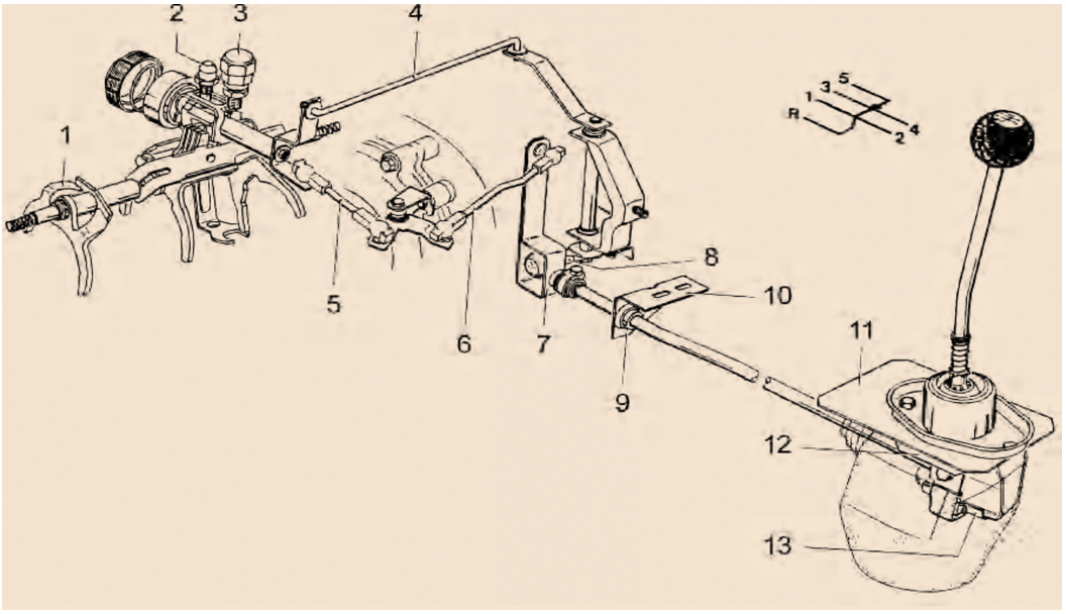

Fig. 2.8 The schematic of external features for a gear shifting mechanism in a passenger car [8].

2.3.2 Shifting without power interruption

In contrast with interrupted shifting conditions, the transmission systems with frictional elements do not have break or interruption over the shifting process. In this case, changing from different gear ratios can be carried out without power interruption and the engagement can be occurred under load by using the clutch mechanism. Therefore, the gear ratio can be changed from one set of gear to another, with no speed reduction of the vehicle [49]. AMT and DCT are examples of power shift transmission systems. The use of the friction elements helps to bring the shifted gear into the power flow without breakage on the power transmission process. Moreover, in a particular way, the gear shifting mechanism without power interruption can be installed on the CVT systems. The most important internal features for gear shifting in AT and AMT gearboxes are multiple-plate clutches and freewheels. Multi-plate clutches work in a pressurized oil housing and are activated from an external force. Freewheel clutches rotate in one direction and they will be locked in the reverse direction. Through freewheels, the connecting shafts are linked together. With higher relative rotational speed between connecting shafts, freewheel clutch will be released from locking conditions and it can rotate freely. At the same speed, freewheels

are linked and torque can be transferred. This gripping process can be taken into account as a step function with respect to the torque enhancement. Various kinds of freewheels have been proposed for different designs such as roller freewheel, ball freewheel, and spring free-wheel. In order to transfer torque in a short time (synchronous speed), freewheels are the best clutches. However, they are large and have problems with overloading. Therefore, the flanking solution should be considered when the transmission system is subject to high loading conditions. Figure2.9 (a) and (b) illustrates the samples of a free-wheel mechanism and the multi-plate clutch.

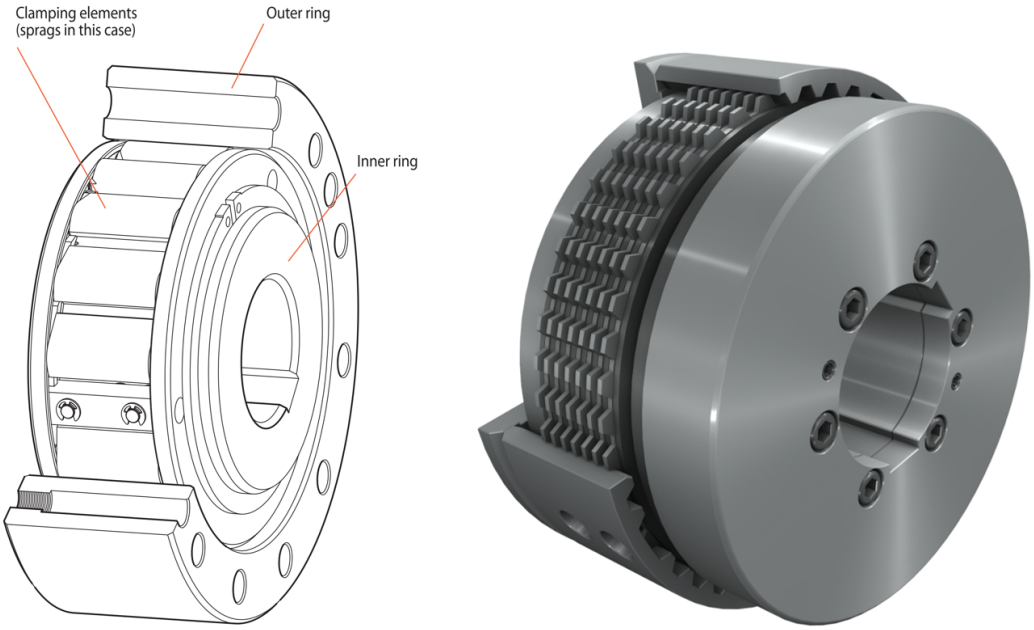

Fig. 2.9 (a) A free-wheel mechanism and (b) the multi-plate clutch [9, 10].

2.4 Synchronizer mechanism

Over the time the synchronizer mechanism has been developed. The most applicable synchronizers were Clark type or pin type synchronizer, planetary gears synchronizer, Lever-type synchronizer and Baulk-ring synchronizer [27, 8].The most common type of synchronizer for MT and DCT is Baulk-ring synchronizer. Figure2.10 shows the schematic view of the Baulk-ring synchronizer. In commercial vehicles and heavy-duty vehicles, increasing the shifting effort can be observed. To overcome this problem, the self-energizer synchronizer was suggested. Self-energizer synchronizers

utilize the boost surfaces and ramps to enhance the engagement force on the friction cones. Therefore, there is an additional axial force by the driver on the lever mechanism.

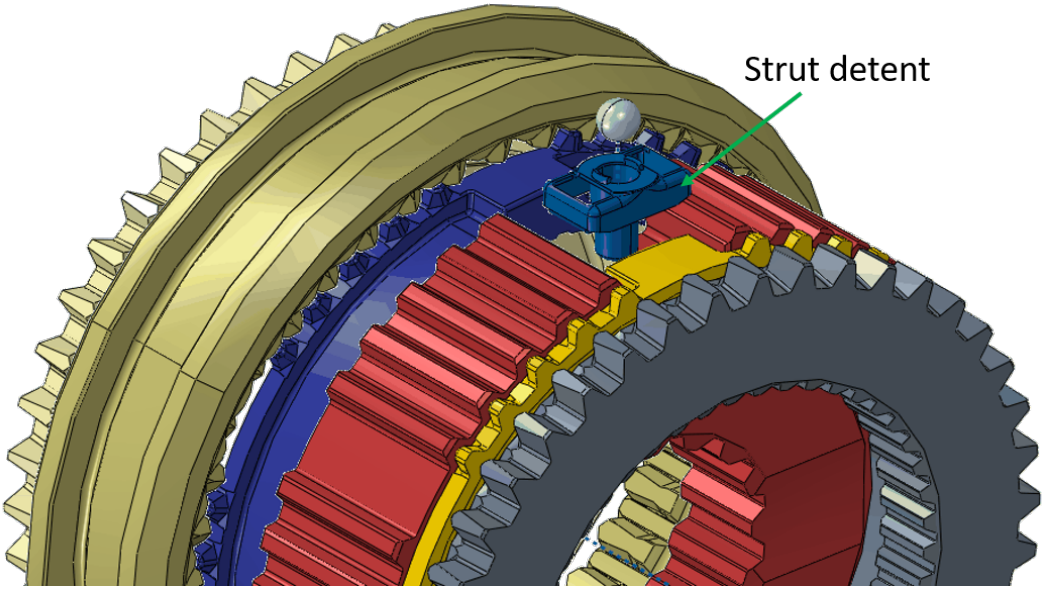

Fig. 2.10 The schematic view of the Baulk-ring synchronizer.

In the present study, the Baulk ring-type mechanism was considered as a reference synchronizer which consists on: synchronizer hub, sliding sleeve, synchronizer ring, friction cone(s), three sets of strut detents and clutch body ring. The synchronizers are generally installed alternatively on the input or on the output shaft of a generic transmission while they rotate with different rotational speeds. The synchronizer hub is connected to the input shaft and also it is in contact with the sliding sleeve at the neutral position. There are three strut detents in this kinds of synchronizers as shown in figure 2.10. They transfer the axial force from the sliding sleeve to the synchronizer ring over the synchronization process. The strut detents are placed in the hub grooves and they have two axial and vertical relative motions inside of the hub's grooves. In addition, the steel ball sets of the strut detents are in contact with the internal grooves of the sliding sleeve. When the shifting process begins, the sliding sleeve is in a neutral position and its axial motion can be started by means of a fork lever. Using multiple friction cones is an option to increase the output torque and design space that is taken into account by some manufacturers. However, the cost and the design complexity of multi cones synchronizers are a negative matter

for using them. The other method to increase the output torque is increasing the diameter of friction cones or using a longer lever arm in the actuator mechanism. It helps to apply much force on the friction cones. However, the size and weight constraints are the obstacles to implement this method. Synchronizers with two or three friction cones are well-known synchronizers for transmission system designers. The different parts of (a) single cone (b) double cone and (c) triple cone synchronizer are shown in figure 2.11 in the exploded view.

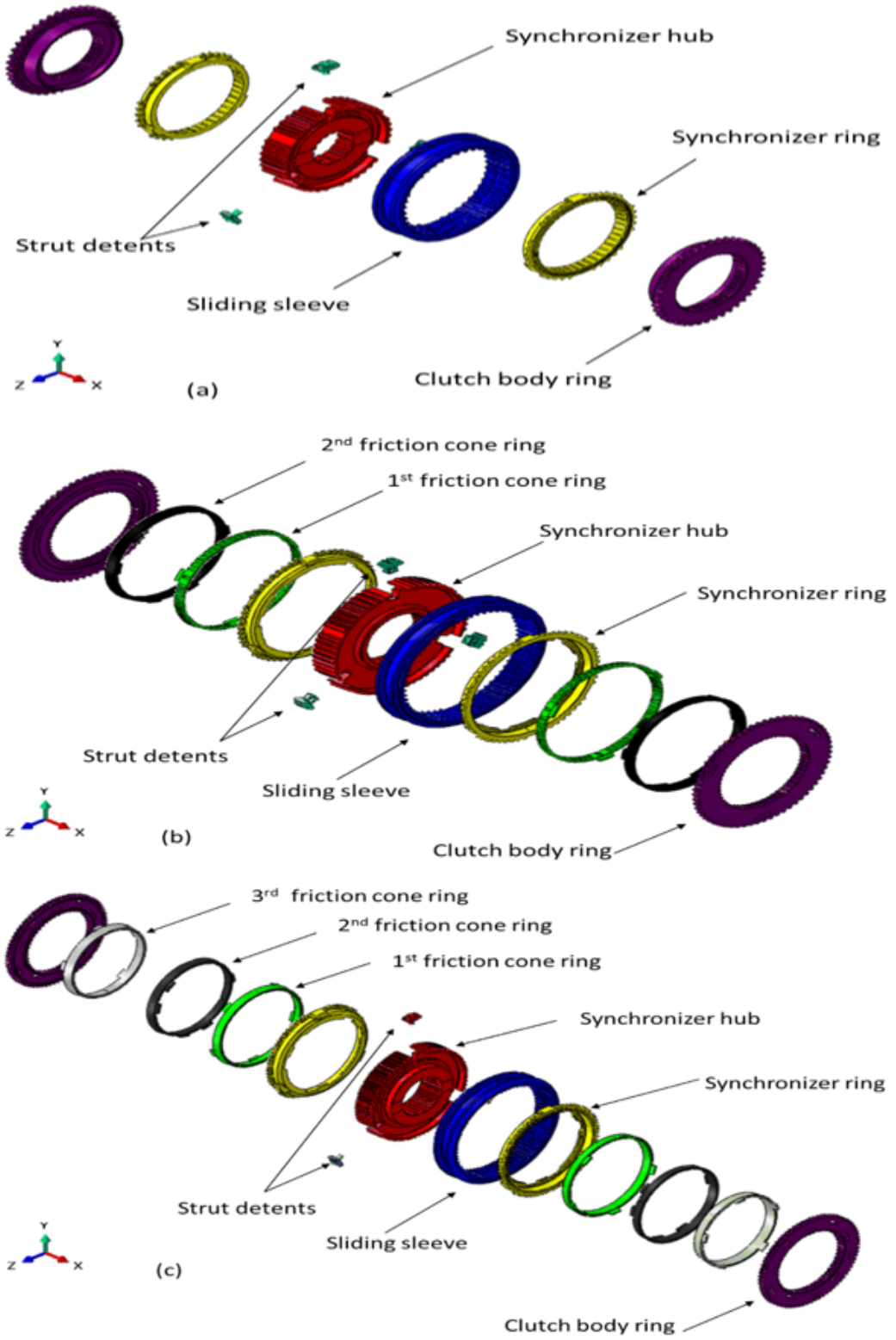

Fig. 2.11 The different parts of (a) single cone (b) double cone and (c) triple cone synchronizers in the exploded view.

2.5 Shifting process phases

In order to clarify the dynamic behavior of the synchronizer mechanism, it is better to separate each step of the shifting process. Many studies have been conducted to identify the synchronization stages. Lovas et al.[50] have defined eight different phases for one cycle shifting. Their first phase is free flying. It means that in this phase sliding sleeve and hub rotate with the same velocity and the clutch body ring has a different angular velocity. In this phase, there is no contact between the synchronizer ring and the clutch body ring. The second phase of synchronization is initial velocity for synchronization. In this step, the strut detents start moving axially and generate a frictional force on the synchronizer ring. The next phase is increasing the axial force: the sliding sleeve and the synchronizer ring have the same angular velocities. At the 4th step, the diameter of the synchronizer ring will be reduced and the contact between the synchronizer ring and clutch body ring will happen. In this phase, the first meshing between the synchronizer ring and the sleeve has been completed. The 5th step is free flying: all parts rotate together with the same velocity. During the 6th step, the sleeve moves axially and the first contact between sleeve teeth and clutch body teeth can be observed. In the 7th step, the sleeve moves to the final position and the engagement will be completed. The last phase of the shifting process will happen when all parts rotate as an integrated set with the same velocity. Figure 2.12 (a) to (h) illustrates the Lovas et al. synchronization phase identification.

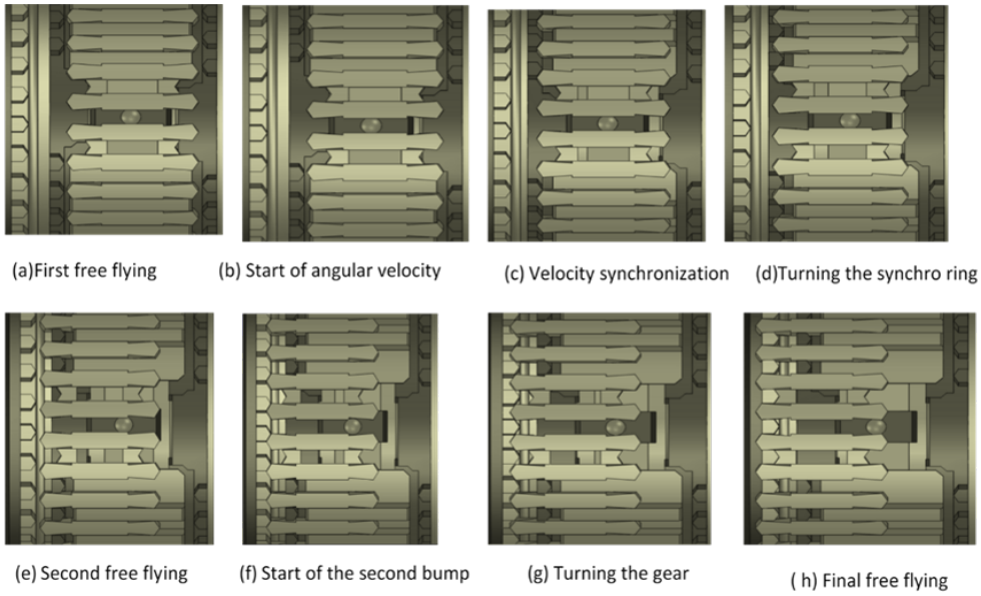

Fig. 2.12 (a) to (h) eight different phases of synchronization.

Another synchronization phase definition assumes five phases that are more realistic. In fact, some phases of the previous definition are infinitesimal and can be combined in a single phase. Hoshino has developed a model and considers five phases of synchronization as follow: 1- Free flying 2- sleeve starts moving 3- finishing first indexing 4- synchronization 5- final indexing and engagement [8]. Figure 2.13 shows the five phases definition for synchronization process.

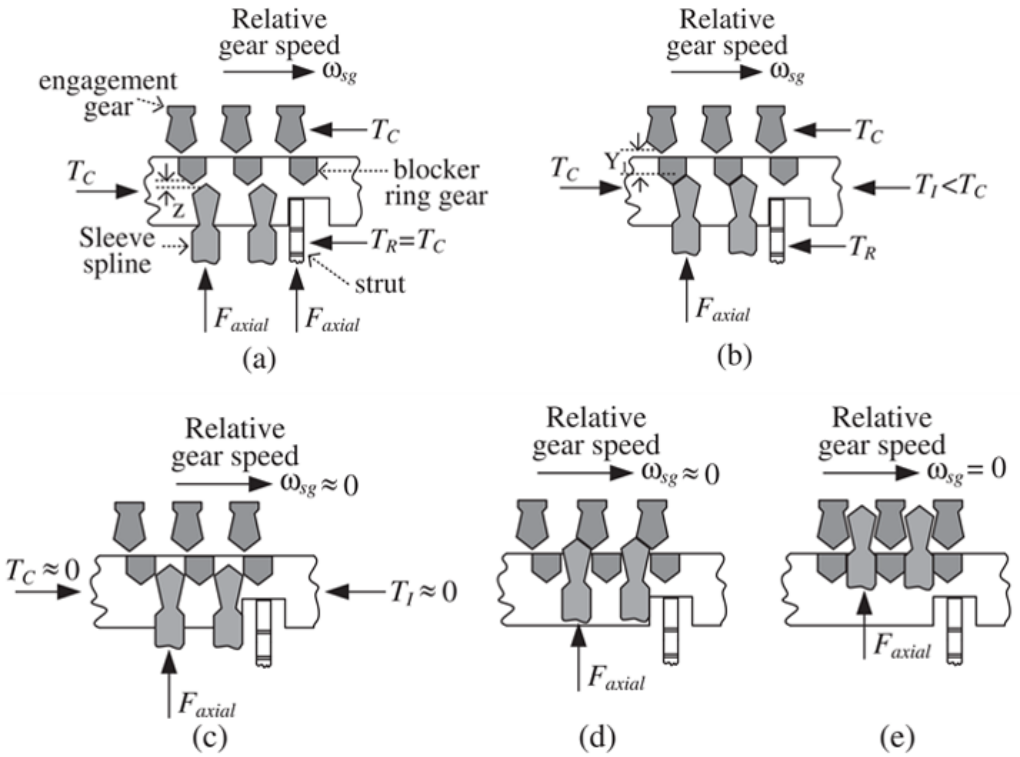

Fig. 2.13 Five different phases of synchronization [8].

2.6 Different models for synchronization simulation

Many mathematical and empirical models have been proposed to simulate the synchronizers dynamic behavior [23, 25, 50]. The effect of applied forces, drag torques and dynamic friction coefficients have been analytically evaluated by those models. Lovas et al. [25] have defined eight different phases for one cycle shifting and have derived the dynamic governing equation for each phase. Razaki [26] has proposed a different definition of shifting process with five different steps and has identified the analytical formulation for the dynamic behavior of every synchronization step. Pastor et al. [27] have developed a model based on the existing model [25] regarding separated governing equations for each part of synchronizer at different phases of the process. To assess the dynamic response of many systems in automotive industries, Multi-Body Dynamic (MBD) analysis is carried out [28]. Compared with empirical models, implementation of MBD in the transmission system is not straightforward. Nevertheless, MBD models provide more detailed and accurate outcomes in terms

of shifting process description. Hoshino [29] has developed an MBD model to simulate the synchronization of a heavy-duty vehicle under different shifting conditions, and to evaluate the effect of reaction forces and abnormal shifting during the synchronization process under different operational conditions. The problem with his model was that he used a rigid connector between components. Using this technique may increase the reaction force and unwanted bumping effect in the numerical model. Furthermore, the validity of this model was not evaluated. The estimated synchronizing time is one of the significant factors that can influence the transmission system efficiency. Reducing the shifting time minimizes the energy loss during the shifting procedure. To reduce the emission and optimize fuel consumption, research has been carried out based on real test conditions such as the New European Driving Cycle (NEDC). The results show that optimizing the shifting procedure will significantly influence both the fuel consumption and the emission reduction. Findings suggest the importance of accurate estimation of the shifting time in the transmission system [31].The MBD model can be used as a precise tool to estimate the synchronization time [32]. Although some analytical formulations were presented to calculate the shifting time, those models do not have enough accuracy to predict the correct shifting time. The main problem of the previous models is that the force applied by the shifting lever is time dependent which has been neglected so far [34]. The role of dynamic analysis of rotational systems such as geared systems in the reduction of noise and vibration should not be taken for granted. Research has been conducted on natural frequencies and vibration modes of rotating machines such as automotive transmission systems, turbo engines, helicopter, ... [35, 36]. Parker and his colleagues [37] have developed two different models to present some sources of nonlinearity in a planetary gear system. Walker et al. [38] have presented a lumped model to study the response of DCT powertrain during the engagement process with and without engine harmonic induced vibration. Although the various components of the transmission system have been studied before [39, 40],less attention has been paid to the vibrational effects of the shifting mechanism. Since the synchronizer is involved transitionally in the dynamic behavior of the transmission system, a transient analysis is needed to investigate the dynamic responses of the shifting mechanism.

2.7 Qualitative factors

2.7.1 Shifting Comfort

Smooth gear changing and comfortable shifting can be a result of a sequential and uniform synchronization process. In manual shifting gearbox, the applied force by the driver is transferred by the gearshift lever and transmission linkages to the gearshift fork and sleeve. In this case, the shifting comfort is much important for drivers. The efficiency of the shifting effort from the linkage mechanism with a variable transmission ratio (normally 7-12) [8] is reported less than 70 % [27]. In order to increase the shifting comfort, the precise design of the synchronizer component and identifying the appropriate clearances for the linking mechanism should be taken into account. The standard values for the passenger cars in terms of the maximum permissible slipping time was 0.15-0.25 s and the maximum permissible manual effort was 80-120 N [51].The cold temperature has significant effects on the slipping time and shifting comfort, however, after warming up the gearbox oil this phenomenon will disappear. Moreover, driving style and traffic conditions will influence the shifting effort. Sticking, upshifting grating and shifting noise are the major shifting comfort problems in the synchronization process [52].

Sticking and double bump effect

Before completing the engagement, when the synchronizer has been unlocked and the clutch body gear has been synchronized, the shifting effort should decrease noticeably for the driver. At this moment, the synchronizer ring should rotate with minimum effort and it should be easily pushed into the engaged position. However, the friction between strut detents and sleeve exists. If the fiction is high or the geometrical tolerance between these parts is not appropriate, a high shift effort is needed to turn synchronizer ring and also a large residual stress can be observed on the synchronizer ring. More axial force is required to release the gear shift mechanism and to turn the synchronizer ring from sticking conditions. This state has been named as the double bump effect [18].To overcome this problem, the inertia, elasticity, damping of synchronizer ring, and the link between the sliding sleeve and the fork can be modified. Some optimization methods were carried out to reduce the double bump effect [53].

Gear up Grating

Upshift grating or cold scraping will occur in very low ambient temperature. Generally, these conditions will happen between the first and the second gears and when the oil temperature is lower than 10 C. During the synchronization phase and engagement, the clutch body ring has some residual stress. At this time, the drag torque due to oil viscosity is high and it can be the cause of relative speed between sliding sleeve and clutch body gear. In the final indexing phase and engagement, the internal teeth of sleeve scraps the idler gear teeth. Figure 2.14 shows a sample of scraping on the gear teeth.

Fig. 2.14 An example of scraping on the gear teeth.

Engagement noise

The sliding sleeve can be engaged with the clutch body ring before they become synchronized. In this case, the noise and scraping can be expected. This kind of noises depend on the driver's action during gear shifting. If the changing process occurs rapidly, the grating can happen on the engaged gear. Due to rapid motion of sliding sleeve before completion of synchronization, the sleeve reaches the gear clutch and it may generate torsional vibration. This vibration will have an effect on the powertrain as a source of backlash. Moreover, this vibration can be considered

as the excitation force against friction coefficient. Mostly, this shaking problem can be observed on the sliding sleeve dog and synchronizer ring teeth. Figure 2.15 demonstrates a sample of fracture area due to torsional vibration on the synchronizer ring teeth.

Fig. 2.15 An example of fracture area on the synchronizer ring teeth.

2.8 Important parameters through synchronization

The axial distance from the pointing teeth between sliding sleeve and synchronizer ring can be called as proximity. To fill up the proximity gap between the sliding sleeve and the strut detents, a push through load is necessary. This load corresponds to the fork load [24]. Figure 2.16 shows the free body diagram related to the breakthrough load and corresponding force to the ball-spring mechanism.

$$F_{fork} = F_{sp}\frac{\mu\cos\varphi + \sin\varphi}{\cos\varphi - \mu\sin\varphi} = F_{sp}\frac{\mu + \tan\varphi}{1 - \mu\tan\varphi}$$

$$BTL = n_p.F_{fork}$$

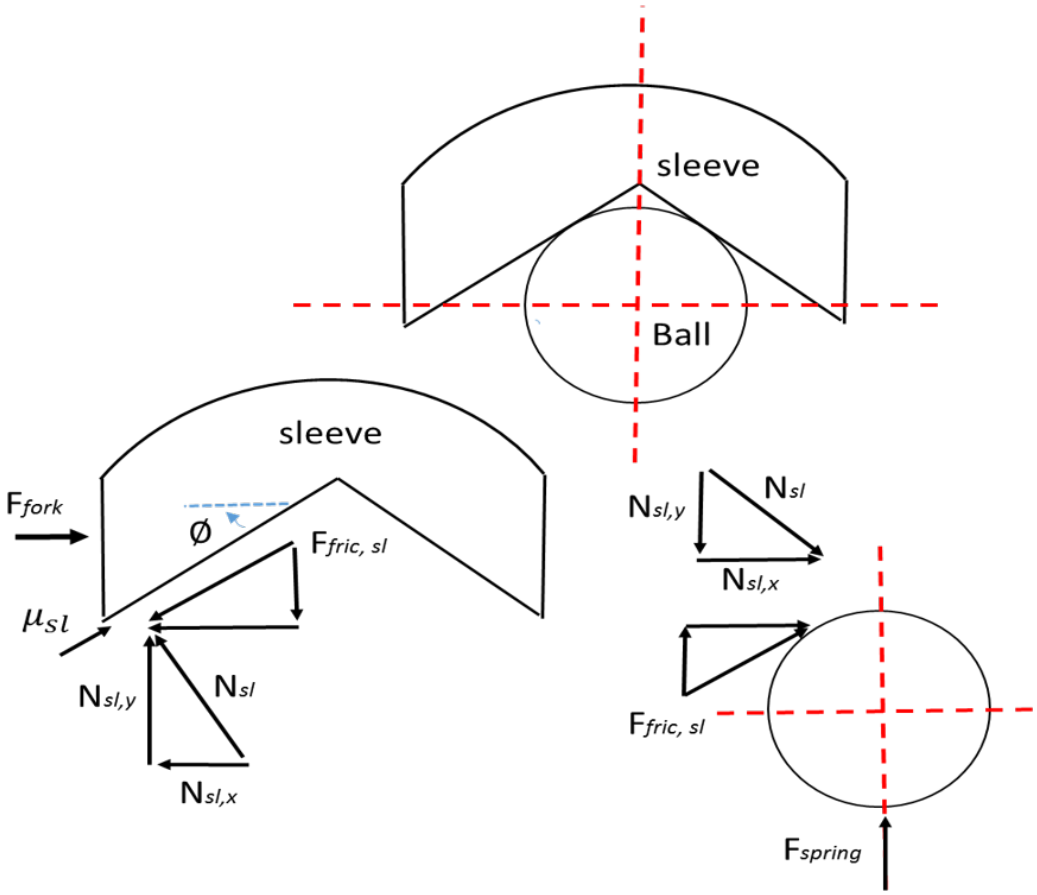

Fig. 2.16 The free body diagram related to the breakthrough on the sleeve and strut detents.

When the sliding sleeve starts moving, a friction force between the friction surface and cone angle is generated. This force will be converted to the synchronizer ring and it is known as the synchronization torque [24]. Figure 2.17 shows the schematic view of the applied axial loading and the outcome torque of synchronization.

$$T_s = T_c \pm T_D$$

$$T_C = \frac{\mu \; F_{fork} \; R_C}{\sin\alpha_c}$$

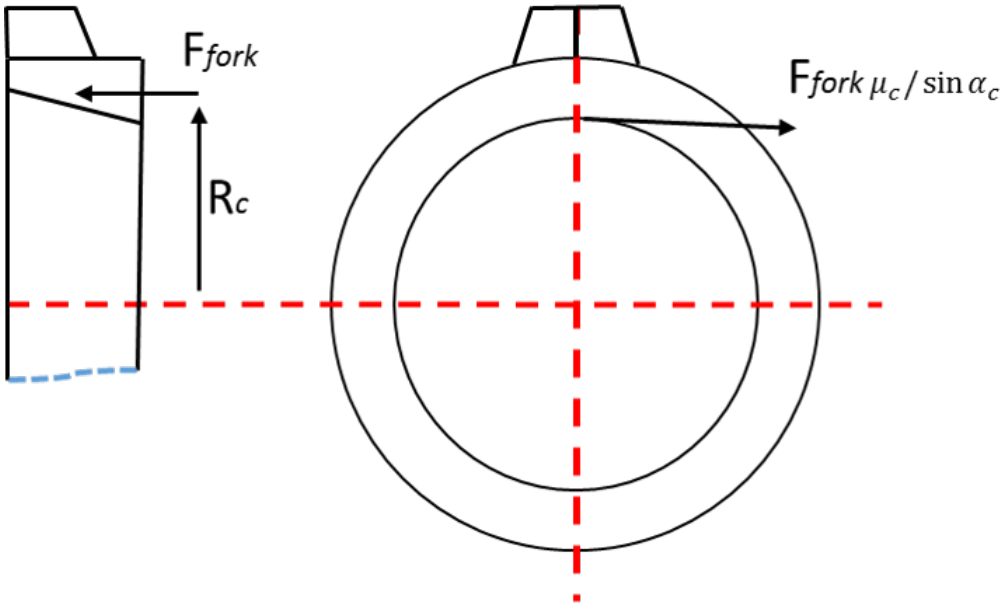

Fig. 2.17 The schematic view of the applied axial loading of synchronization.

At the pointing angle between the teeth from sleeve and synchronizer ring during first indexing process, the index torque due to the existing friction at this area will be generated. This torque can be assumed as a function of axial loading, teeth pointing angle, friction coefficient and pitch diameter of the blocking ring. Figure 2.18 depicts the reaction forces from fork motions and indexing torque [12].

$$T_I = F_{fork} R_{sl} \frac{\cos\beta + \mu \sin\beta}{\sin\beta - \mu\cos\beta} = F_{fork} R_{sl} \frac{1 - \mu\tan\beta}{\tan\beta + \mu}$$

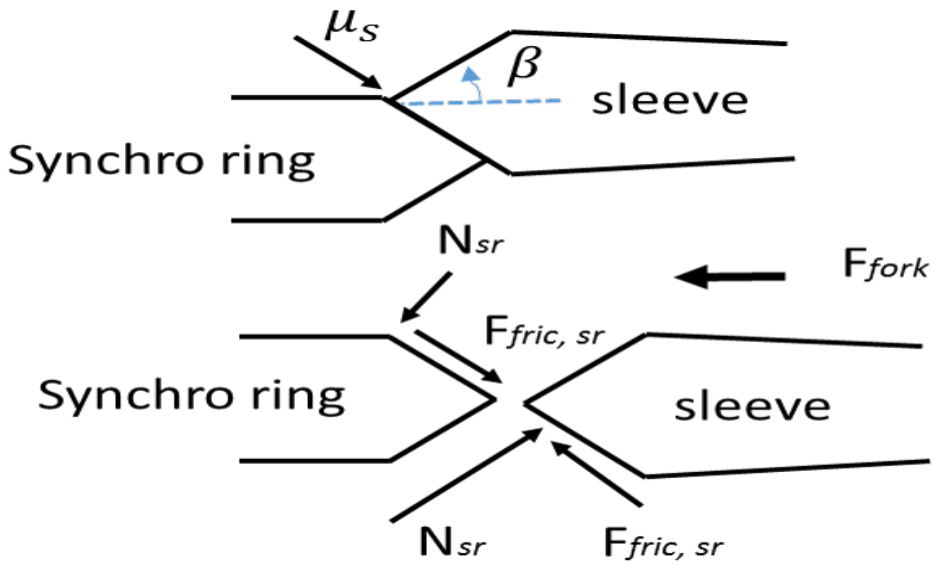

Fig. 2.18 The reaction forces from fork motions and indexing torque.

The power losses from oil churning, rotation of friction components and clutch drag will generate a negative effect on the shifting process that is called drag torque. In a normal situation, this number can exceed 10 N.m [18].

$$T_D = T_{CD} + T_{fc} + T_{fric}$$

By applying the pressure from the shift knob to the shifted gear, an impulse can be observed during the shifting which has some effects on the gear shift performance and shifting time. Moreover, an additional force will be generated due to the ramp surface of the hub circumference that it will increase the shifting force. This load can be defined as the boost force [8]. The coefficient of friction varies between different contact surfaces in the synchronizer mechanism. For instance, the friction coefficient between friction cones and the synchronizer ring, due to different lubricant film thickness, would vary in different operational and temperature conditions. By increasing the force from sliding sleeve, the axial load increases the friction coefficient between friction cones. After finishing the engagement the contact surfaces will be separated and the friction coefficient will decrease [54].Thus, the friction coefficient can be assumed as a function of the material properties, ambient temperature, and lubrication viscosity. Torque transferred by the synchronizer is highly dependent on the friction coefficient. In order to reduce the time of shifting, materials with high friction resistance such as brass, molybdenum or carbon

fiber were used for the cone surfaces of the synchronizers [8]. However, the high coefficient of friction reduces the durability of the synchronizer by creating higher adhesive wear. Moreover, the geometrical constraint should be applied to avoid self-locking phenomena. The following equation presents the condition for geometrical conditions for designing the angle of friction cone [23].

$$\mu_c \leq \tan \alpha_c$$

2.9 Theories on the current study

2.9.1 Fundamental of multibody dynamic

Before establishing the governing dynamic equations of a system, it is crucial to know how to describe the dynamic system. The system variables should be able to characterize the dynamic motion of all components over the time. In addition the coordinate system, material points and center of masses should be identified in a dynamic system. The generalized coordinate system should satisfy linear and radial coordinates [55].The minimum number of variables required to describe a dynamic system can be called as the system's degree of freedom (DOF) [56].For instance, when a multibody dynamic system is defined completely by the coordination of one of its bodies, the system can be called as one DOF problem. The number of independent orientations required to describe the system configuration is equal to the system's degree of freedom. The knowledge of the degree of freedom for a multibody system is the essential matter for system modeling. There are six DOF to be identified for a spatial dynamic system. However, using kinematic joints between bodies' constraints the number of system's DOF. It is obvious that the number of DOF depends on the constraints and the type of applied joints. By using GrüeblerKutzback criterion, the number of DOF for a multibody system can be evaluated [57].

number of DOF=$6n_b$-m

where nb is the number of bodies that create the multi-body system and m is the number of independent constraints. If the number from the above equation is negative, it means that the system is not solvable. The degree of freedom equals to zero shows that the system is static and positive number shows the degree of freedom

for a dynamic multibody mechanism. However, there are some exceptions to use this criterion. Figure 2.19 shows a spatial four-bar linkage with two spherical joints and two revolute joints. As a result, this system has six constraints from spherical joints and ten constraints from revolute joints. The system degree of freedom is equal to two.

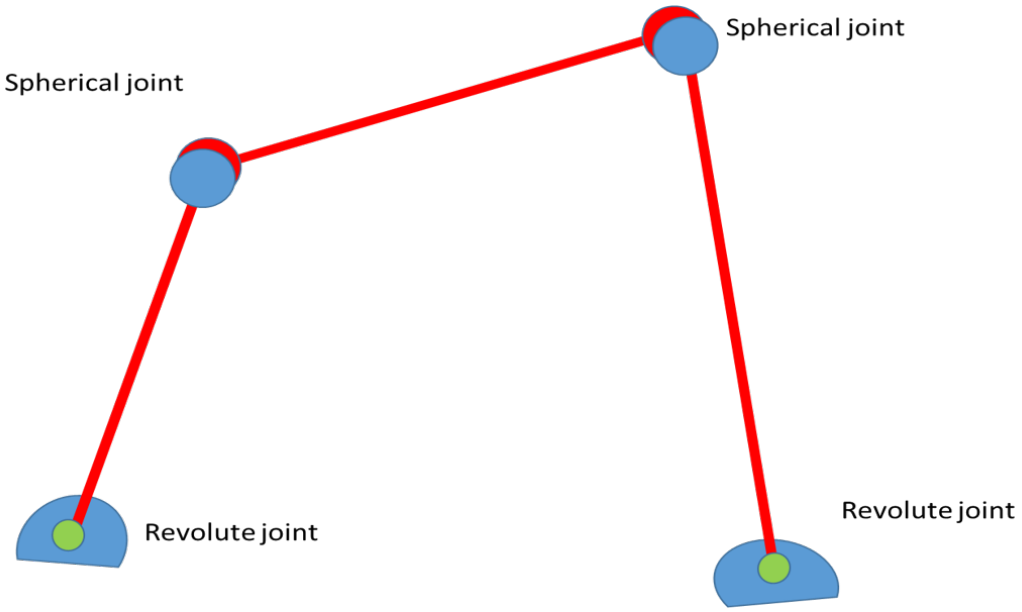

Fig. 2.19 A spatial four-bar linkage with two spherical joints and two revolute joints.

Defining the coordinate system for a specific dynamic mechanism doesn't follow a standard regulation. Frequently, dependent and independent coordinate systems are the two main groups to generalize a coordinate system for a multibody mechanism [58].]. The dependent coordinate systems are free to move arbitrary and the independent coordinate systems follow the applied constraint to satisfy the problem's governing equations. The dependent coordinate system is categorized with the absolute coordinate, relative coordinate, and natural coordinate systems [59–61]. In order to derive equations of motion for a multi-body system, different types of coordinate systems can be implemented. Different studies have been conducted by [62, 63]to compare the effects of using different coordinate systems in terms of complexity and calculation time of a dynamic problem. Choosing an appropriate coordinate system for a flexible multi-body system shows a significant effect on the system responses [64]. Applying kinematic joint, brings an appropriate degree of freedom to the multibody system. Every specific kinematic joint provides a relative motion

between two bodies and constrains them in the desired motion direction. Figure 2.20 shows different kind of kinematic joints that are implemented in the ABAQUS commercial finite element software for the multi-body dynamic analysis.

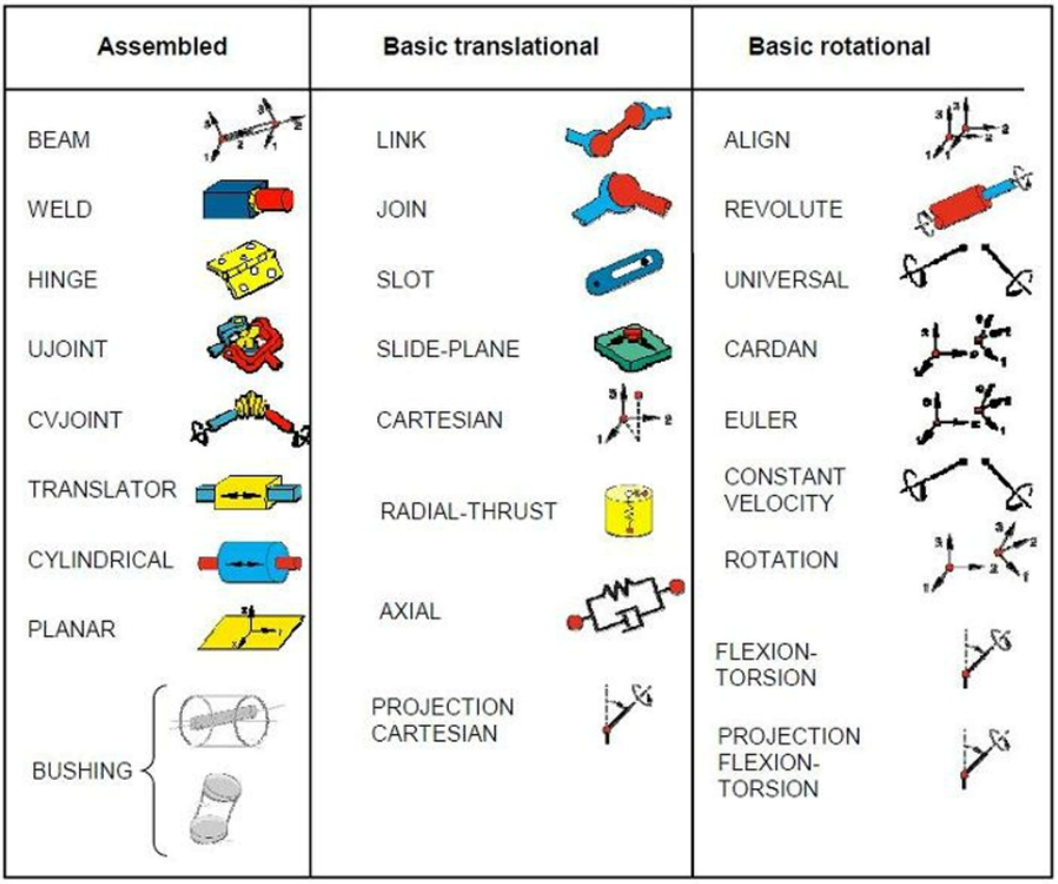

Fig. 2.20 The different kind of kinematic joint that are implemented in ABAQUS [11].

To develop a multi-body dynamic analysis, two main steps can be developed. These steps consist in the presentation of the mathematical formulation and the implementation of the numerical model. After developing the model, the numerical simulation can be performed and the dynamic behavior of the multibody system can be evaluated. Body coordinate and point coordinate formulation are the main approaches for presenting a multibody dynamic model. In body coordinate approach, the coordinates are considered as the bodies and constraints are the joints whereas, in the point approach it is vice versa [65]. Using point coordinate describes a multibody system as multi particles which are connected to each other by points. The intersection points are considered as the joints and every point with a set of

constraints provides the DOF for that components. Therefore, the number of degrees of freedom depends on the type of implemented joints and the applied constraints on the system components. When the governing equations are derived based on the bodies coordinates, the point approach is much convenient. To obtain the dynamic equations for a body coordinate system, the dynamic formulation can be derived based on Newton–Euler equations. This type of formulations expresses absolute coordinates and velocities of involved bodies that are involved in dynamic motion. Compared with other methods, the results of the number of equations are large and the computational calculation is recommended for solving the set of dynamic equations. In order to solve the kinematic formulation of a multi-body system, the second order differential equation was recommended [66, 67].

2.9.2 Frequency Analysis

Natural frequency extraction

There are many areas in mechanical engineering which are necessary to extract the eigenvalue and natural frequency of the mechanical system. Moreover, solving an eigenvalue problem can be associated with the bifurcation of kinematic instability and vibration of a mechanical system. The eigenvalue problem is one of the classical areas of research in mechanical engineering with a broad range of application in finite element analysis [68]. The calculated eigenvalue of a system will be used in the finite element code to obtain a participation factor, the generalized mass, and the related modal damping for every selected mode. The eigenvalue problem for a finite element model can be calculated as:

$$(-\omega M^{MN}+K^{MN})\varphi^{N}=0, \tag{2.1}$$

where M^{MN} is the mass matrix, K^{MN} is the stiffness matrix regarding the initial stiffness effects, φ^{N} is the eigenvector (the mode of vibration), and M and N are the component's degrees of freedom.

To extract the natural frequency, the Automatic Multi-level Sub-structuring (AMS) Eigen solver was used. The AMS method consists of three steps. The first step consists of a reduction process. In this step, a full system is reduced with a very efficient eigensolution method. This method combines sparse factorization

based on the multilayer super node elimination tree and a local eigensolution at each super node. Starting from the lowest level super nodes, a Craig-Bampton substructure reduction technique is used to successively reduce the size of the system [69].The second step consists of the reduced eigenproblem solution. In this phase, the eigensolution of the reduced system that comes from the previous phase is calculated. Although the reduced system typically is two orders of magnitude smaller in size than the original system, generally it still is too large to be solved directly. Thus, the system is further reduced mainly by truncating the retained eigenmodes and then solved using a single subspace iteration step. The last step is recovery. In this phase, the eigenvectors of the original system are recovered using eigenvectors of the reduced problem and local substructure modes [70].

There are some different ways to introduce the system damping for a linear dynamic analysis. Some of the most important damping categories can be listed as follow:

Critical damping factors

For every natural frequency, the eigenmode can be assumed as a fraction of critical damping. Therefore, if the system is damped critically, after fluctuation and system disturbance, the system becomes stable statically. Generally, less than 10% of critical damping is allocated to damping of each mode. However, this assumption is not precise in nonlinear systems due to changing the equation of motion over the calculation time [71].

Rayleigh damping

A linear combination of mass and stiffness matrices leads to mixed damping matrices that is introduced as the Rayleigh damping. In this damping matrix, the eigenvectors of damped and undamped systems are equal. Therefore, it can be considered as a fraction of the critical damping for each mode of frequency. For nonlinear problems, the Rayleigh damping can be used in a different way. In this case, the mass damping factors will be used as the independent variables although the stiffness damping factors are assumed as the viscoelastic behavior that is equivalent

to the proportional elastic damping in the linear problem [72].

Composite modal damping

When different materials are used in the simulation, a damping value for each material is allocated as the fraction of critical damping of those materials. The damping value will be converted as the weight average of each mode of frequency [65].

Structural damping

The structural damping is commonly used for solid materials in low frequencies where the damping forces and the damping factors are proportional to frequency. This type of damping can be implemented when the velocity or displacement is 90° out of phase or the system's excitation is sinusoidal. This damping formulation can be called structural damping which is used in steady state or random response problems. Any combination between mass and stiffness damping factors can be added to the structural damping. Usually, structural damping is used for damping modeling of a system with complex stiffness. Furthermore, the application of structural damping for frequency domain analysis has less difficulty in comparison with time domain analysis. For time domain analysis, the structural damping will be converted to the equivalent viscous damping in order to reduce the degree of system's complexity [73].

Modal Dynamic analysis

As mentioned in the previous section, given the transient behavior of the synchronizer, it is necessary to perform the modal transient analysis to examine the dynamic response of the system. In order to analyze a linear system, the dynamic equation for a time response problem can be written as [74]:

$$[M]_\beta[\ddot{u}]_\beta + [C]_{\beta\alpha}[\dot{u}]_\alpha + [K]_\beta[u]_\beta = (f_t)_\beta \tag{2.2}$$

where M is the mass matrix, C is the viscous damping matrix, K is the stiffness matrix, α and β indices span the eigen space and U is the generalized displacement of the mode β. The substitution of $\omega = \sqrt{}$ (K / M) in 2.2 yields:

$$[\ddot{u}]_\beta + [C]_{\beta\alpha}[\dot{u}]_\alpha + \omega^2[u]_\beta = (f_t)_\beta \tag{2.3}$$

Moreover, to simplify the 2.3 the ζ_β (damping ratio) can be calculated as:

$$2\zeta_\beta \omega_\beta = \frac{C_\beta}{M_\beta} \tag{2.4}$$

And the full system dynamic equation with diagonal damping matrix can be written as:

$$[\ddot{u}]_\beta + 2\zeta_\beta \omega_\beta [\dot{u}]_\alpha + \omega^2[u]_\beta = (f_t)_\beta \tag{2.5}$$

However, for a coupled system, the viscous damping matrix should be split into the diagonal and off-diagonal matrix as follow:

$$C = C_{diag} + C_{off} \tag{2.6}$$

The solution to the coupled equations is obtained readily as a particular integral for the loading and a solution to the homogeneous equation. These solutions can be combined and written in the general form:

$$\begin{aligned} \begin{Bmatrix} u_t + \Delta t \\ \dot{C} + \Delta t \end{Bmatrix} &= \begin{bmatrix} a_{11} & a_{12} - b_{11}C_{off} \\ a_{21} & a_{22} - b_{21}C_{off} \end{bmatrix} \begin{Bmatrix} u_t \\ \dot{u}_t \end{Bmatrix} \\ + \begin{bmatrix} b_{11} & b_{12} \\ b_{21} & b_{22} \end{bmatrix} \begin{Bmatrix} u_t \\ \dot{u}_t \end{Bmatrix} &+ \begin{bmatrix} 0 & -b_{11}C_{off} \\ 0 & 0 \end{bmatrix} \begin{Bmatrix} u_t + \Delta t \\ \dot{u}_t + \Delta t \end{Bmatrix} \end{aligned} \tag{2.7}$$

Since the loading only varies linearly over the time increment (Δf/Δt), The a_{ij} and b_{ij}, are constants and i,j=1,2. To calculate a and b constants in more detail see[65].

2.9.3 Design of Experiment method

According to the theory of optimization, when the design variables with respect to the specific rule change and the responses of the tests can be measured, therefore,

this procedure can be called as the experiment. Based on Montgomery [75, 76]], experiments can be implemented in any field such as machines combination, techniques and other sources of transferred inputs and outputs. During the experiment, some variables are controllable and others not. The experiment objectives are to identify the most significant variables on the experiment responses, and setting the significant controllable parameters to obtain the response near to the optimum value. Design of Experiments (DOE) is one of the techniques which guide the operator to perform the experiments in an optimal way. The experimental error can be called as the analysis noise. This kind of noise will have an effect on the final results. Therefore, an appropriate statistical method can discriminate the experiment noise. Generally, replication, random test, and test blocking are the basic principles of a statistical method. In order to obtain accurate results, replication or test repeating should be performed. By applying standard deviation and considering the mean values, the experimental error can be calculated. To eliminate the effect of sequential runs on each other, it is necessary to perform the experiments in a random order. In other word, the model prediction will be unbiased. The other tool to generate unbiased system is to implement the blocking method. In addition, blocking helps to clarify the main effects over statistical analysis. DOE technique exploits all these characteristics to evaluate the result of a set of experiments statistically. Box and Wilson [77] developed the response surface method (RSM) as the statistical tool for industrial experiment evaluation. Taguchi [78]] has extended the DOE method in order to improve the quality. Moreover, many methods with the basis of DOE were introduced for a particular purpose in different industries [79]. Before starting the DOE analysis, some prerequisite actions should be considered. The design factors, design space or area of interest, the upper and lower bound of each parameter are the factors that should be identified by the user. In addition, the level of a different factor has to be defined before DOE analysis. In the other word, the level means that the different values of factors that user allows to discretize the values of different variables. The objective of the experiment in DOE can be called as system response. In a DOE analysis, the number of responses can be varied from the single response or multi-objective DOE analysis. Based on the mentioned characters of DOE approach different methods for different applications have been developed. The following section introduces some of the most important DOE techniques.

Randomized Complete Block Design

During the experimental tests, some factors are uncontrollable. Therefore, to observe the effects of this kind of factors, the randomization can be helpful. Considering the average value of random factors can eliminate the effect of uncontrollable factors. For the purpose of randomization, Randomized Complete Block Design (RCBD) regarding DOE methodology has been proposed. Moreover, when the effect of particular factors on a specific response is interesting, the RCBD method is recommended [80].

Latin Square

when a randomized method is used, the number of factors will increase rapidly. To reduce the number, experiments without neglecting the effect of important variables the Latin Square (LS) method based on the RCBD method has been presented. The difference between the LS method and RCBD is that in LS method every single experiment is performed in a specific block [81].

Full Factorial

One of the most common DOE techniques is the full factorial design. In the simple form, there are a number of controllable factors s and two levels for each factor. Therefore every combination can be considered in the experiment design. In this method, the high level and a low level is assumed from +1 to -1. This definition helps to keep the factors in the sample space while the factors change over time. Moreover, this way allows observing the effect of each variable on the response independently. The central point between higher and lower level was used to make the experimental test as the orthogonal design. If we have three factors and two levels, the design combination can be placed on the corners of a cube. Therefore, using a central point at the center of cube creates an orthogonal combination for this set of experiments. The orthogonal terminology came from the scalar product of two orthogonal vectors (factors column) that it becomes zero. The difference between RCBD and full factorial method is that the full factorial design considers the effect of all factors on the response; however, the RCBD only focuses on the primary variable.

By using RCBD, the design space and the order of performing the experiment can be neglected. In addition, implementation of the adjustable full factorial method will evaluate the main effect and their interaction effects. Avoiding confounding the effect of different factors on each other is the main advantage of the full factorial design. On the other hand, the number of experiments increases exponentially with the number of levels and the number of variables [82].

Central Composite

The central composite design is a modified method of the full factorial design. In this method, the central point and star points are added to the 2k full factorial, where k is the control factor. The star points or axial points are the points with a mean value which are remaining value in terms of distance with the center point. If the distance from design points and the center point is normalized to one, the axial points can be defined in different ways. By changing the distance from the central point to the axial point, different configurations of central composite design can be achieved. Central composite circumscribed (CCC), central composite faced (CCF) and central composite inscribed (CCI) are some examples of central composite design methods with different levels to perform experiments [76]. Figure 2.21 shows the design configurations for CCC, CCF, and CCI.

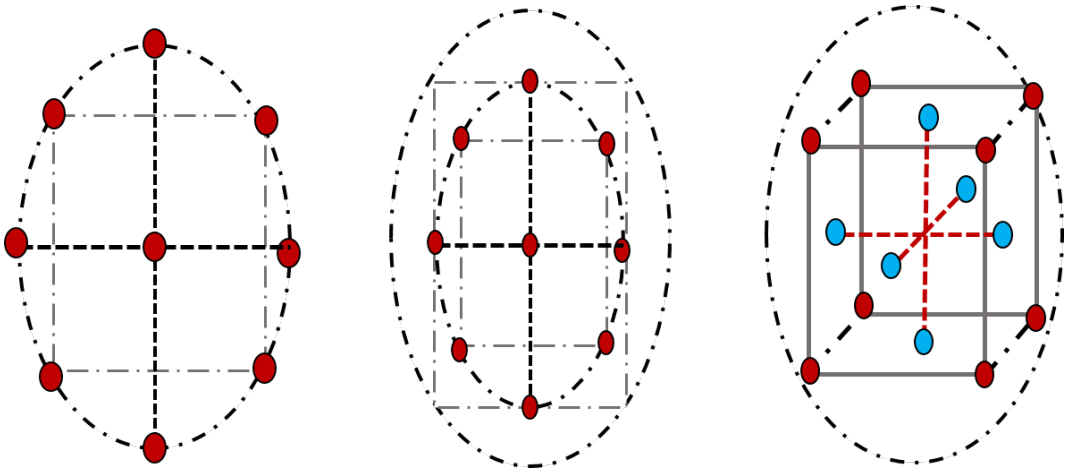

Fig. 2.21 The design configurations for CCC, CCF, and CCI methods.

Many DOE methods exist to design of experiment. However, for the optimization process, choosing the best method is not the main problem. The most important

issue on choosing the DOE methods depends on the objective of the problem to be investigated. Moreover, the time of each experiment is important to select the DOE methods. For instance, there is a big difference to choose a DOE technique for a simple simulation and a very complex laboratory test. The number of variables also exponentially grows up the time of the experiment that should be selected wisely. Based on the aim of experiment, the type of DOE technique can be selected. For instance, to obtain a precise analysis of a set of experiments and investigating the main and interactions effect, the full factorial design can be implemented. On the other hand, the Plackett-Burman method can be used to give a rough estimation of the effects of an experiment's factors. To evaluate the effect of a primary factor in an experiment the LS or RCBD are suggested. The Box-Behnken, factorial design and central composite design are the methods to perform response surface method (RSM). The advantage of RSM is a good compatibility with DOE technique which can influence the quality of results significantly. Table 2.1summarizes the different DOE methods with respect to the number of runs and their outcomes [82].

Table 2.1 Different methods of DOE technique based on the number of runs and outcomes.

DOE method	Number of run	Application
RCDB	N(L_i)	Finding the primary factor
Latin square	N(L)=L^2	Finding the primary factor rapidly
Full factorial design	N(L,k)=L^k	Evaluating the main factors and their interaction and plotting the response surfaces
Fractional factorial	N(L,k,p)=L^(k-p)	estimating the main factors and their interaction
Central composition	N(k)=2^k+2k+1	plotting the response surfaces
Box-Behnken	N(k) from table	plotting the quadratic response surfaces

2.10 Summary of this chapter

Over the time different mechanisms have been developed to transfer the power from engine to the wheels of vehicles. This chapter illustrates a critical review on the literature of different transmission systems. The shifting mechanism through the transmission system is the crucial component in power transmission sector. The shifting mechanism was divided into two main categories namely, external and internal shifting mechanism. The external mechanisms include the different linkage system to change the position of driving gears from outside of gearbox. The internal mechanism are placed inside of gearbox and they are linked to the external shifting mechanism. Many design have been implemented in different transmission system

over previous decades. One of the most common and efficient shifting mechanism is synchronizer. Moreover, the detail of shifting phases with synchronizer mechanism is explained in this chapter and important parameters from different literatures were addressed. The qualitative and quantitative factors during synchronization process were listed. In addition some possible damage phenomena due the inappropriate operational condition were presented. Some analytical and numerical models that were used to simulate the dynamic behavior of synchronizers were mentioned and their research outcomes were listed as influential parameters of synchronization. The last part of this chapter is a summary about the fundamental theories that were used in this thesis. The fundamental of multibody dynamics and different method to identify a multibody system is the first theory that is explained in this chapter. The second theory is a short background about the modal analysis and the Automatic Multi-level Sub-structuring method for calculation of a system natural frequencies. The third theory is related to the design of experiment method and different statistical models based on DOE technique. According to previous studies, it can be said that using multibody dynamic based on FE method is the new approach to study the dynamic behavior of synchronizer mechanism. Moreover, utilizing DOE technique to find significant variables of synchronization process through numerical simulation can be the other method that is not reported so far.

Chapter 3

Research Methodology

3.1 Introduction

In this chapter a methodology to study the dynamic behavior of different synchronizer mechanisms is explained in detailed. Three main approaches are used to study the dynamic behavior of a synchronizer model. The first is the experimental approach. The purpose of the experimental approach is to create a baseline for validation and verification of mathematical based data. The second is the analytical approach. Two analytical models are presented in this thesis. The first model was created to calculate the synchronization time and the second model to solve the governing dynamic equations for each phase of synchronization based on multibody method. The third approach of this study is based on the implementation of a numerical model based on the MBD method. This multibody model simulates the dynamic behavior of the synchronizer with different methods such as rigid model, full flexible model, sub flexible model, modal dynamic model. The natural frequencies of the system were extracted and the effect of different boundary conditions on the modal behavior of the system was evaluated. Moreover the effect of linear backlash was investigated and the worst case condition of transient modal response of the system is listed. Moreover, the results of rigid and flexible models are compared with experimental data and after validation the verified data can be used for DOE optimization technique. In order to save computational time, the results of flexible sub model was considered for DOE analysis. Statistical DOE analysis for different synchronizer model were performed and the significant parameters over synchronization were addressed.

Also a sensitivity analysis was performed to study the effect of cone angle on the performance of single cone synchronizer model. Figure 3.1 shows the flowchart of the research methodology of this thesis.

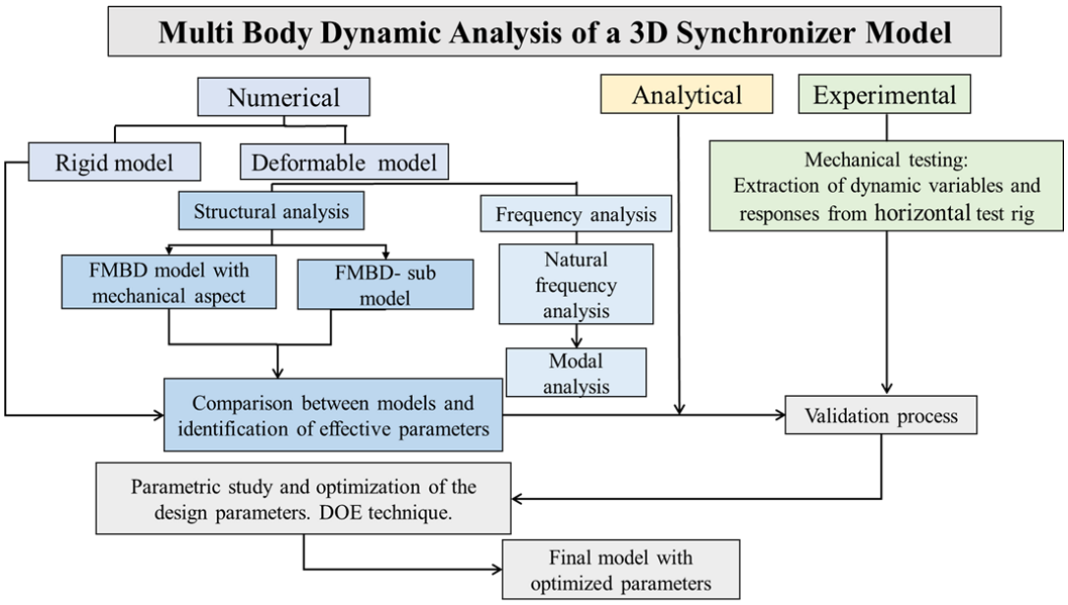

Fig. 3.1 The flowchart of the research methodology of this thesis.

The synchronizer hub is connected to the input shaft and also it is engaged with the sliding sleeve at the neutral state. In the current study the synchronizers with three strut detents were used. They are tasked to transfer the axial force from the sliding sleeve to the synchronizer ring. The strut detents are placed in the hub grooves and are free to move axially. In addition, the steel ball sets of the strut detents are in contact with the internal grooves of the sliding sleeve. In this study, three synchronizers, i.e. a 74 mm single cone synchronizer (SC-74), a 170 mm double cone synchronizer (DC-170) and a 100 mm triple cone synchronizer (TC-100) were linked to the testing machine. Figure 3.2, a, b and c represents the SC-74, Dc170 and TC-100 synchronizers, respectively.

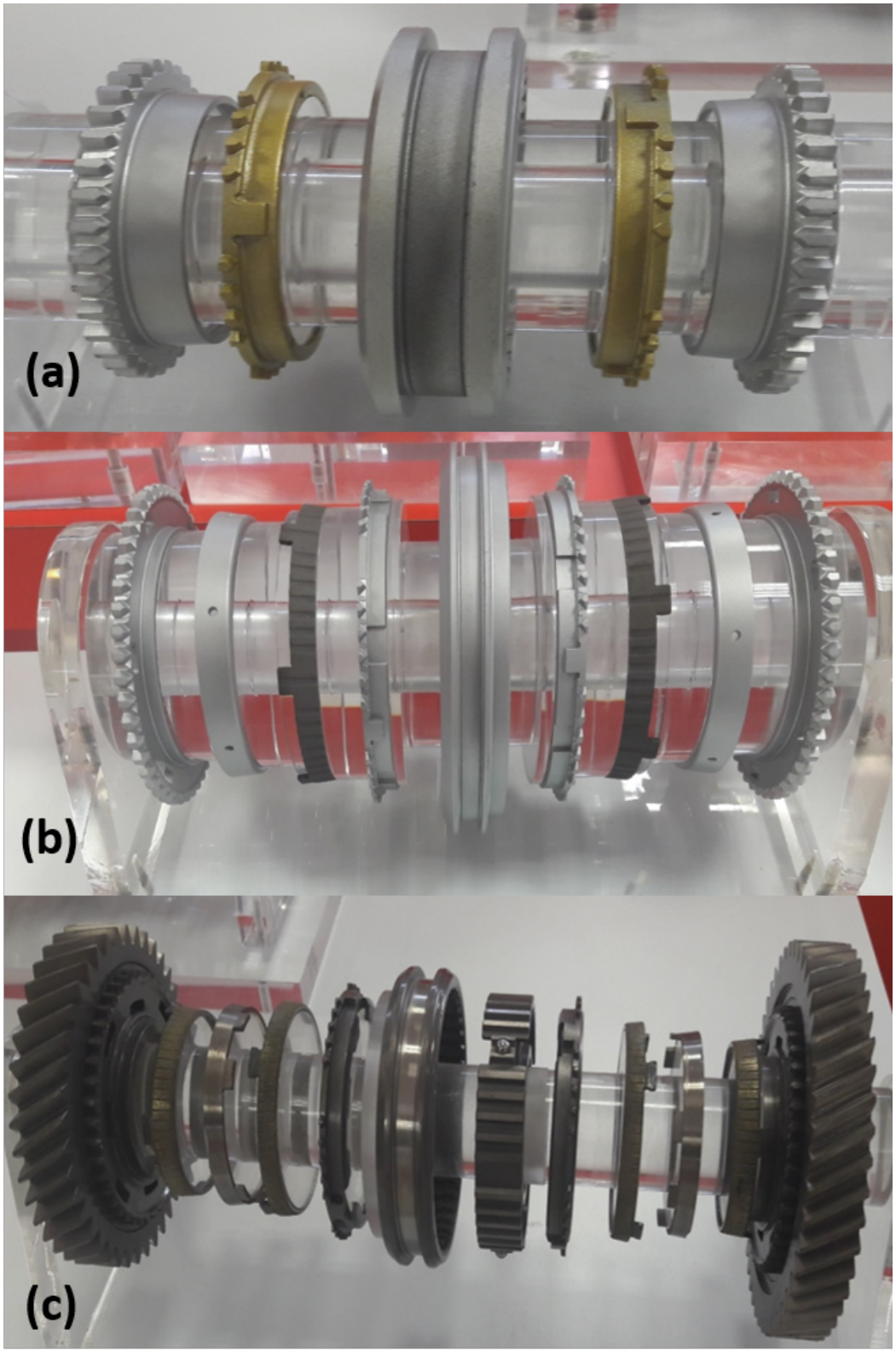

Fig. 3.2 (a) A 74 mm single cone synchronizer (SC-74), (b) a 170 mm double cone synchronizer (DC-170) and (c) a 100 mm triple cone synchronizer (TC-100).

3.2 Setup of experiments

3.2.1 Preparation of the test setup

Before performing the experimental tests, some preliminary actions should be considered. The following steps explain how a test should be prepared before starting the test: 1- Controlling the Machine: in this step the operational condition of machine such as the location of the sensors and the position of applied inertia should be checked. Figure 3.3 shows the location of the inertia weight (left) and the sensor position (right).

Fig. 3.3 The location of the inertia weight (left) and the sensor position (right).

2- Adjusting the actuator stroke and load cell: to control the actuator stroke and attached load cell to the fork mechanism, the suitable distance can be reached by adjusting the stopper pin that is connected to the cylinder head. After reaching the stroke distance, the synchronizer set is assembled and installed between input and output shafts. Then the backlash distance between fork and sliding sleeve also can be adjusted. At the end of this step the lubrication system can be checked. Figure 3.4 shows the position of the load cell, lubrication system, actuator, and fork mechanism.

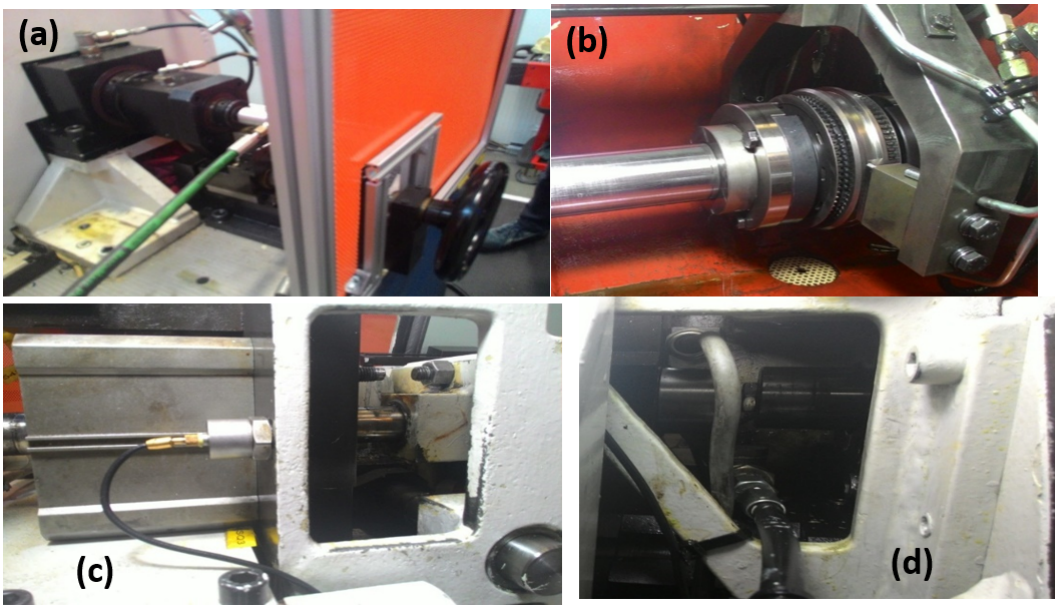

Fig. 3.4 (a) Lubrication system, (b) the fork mechanism, (c) the actuator and (d) The position of load cell.

3- Applying the Inertial Load: based on the test requirement the amount of the load that corresponds to the applied inertia will be applied to the machine. So the subsequent torque due to applying the load is measured by torque meter which is connected to the inertia shaft. Then it will be attached by universal joint to the synchro mechanism. Figure 3.5 shows the applied inertia (left) and the torque convertor stage (right).

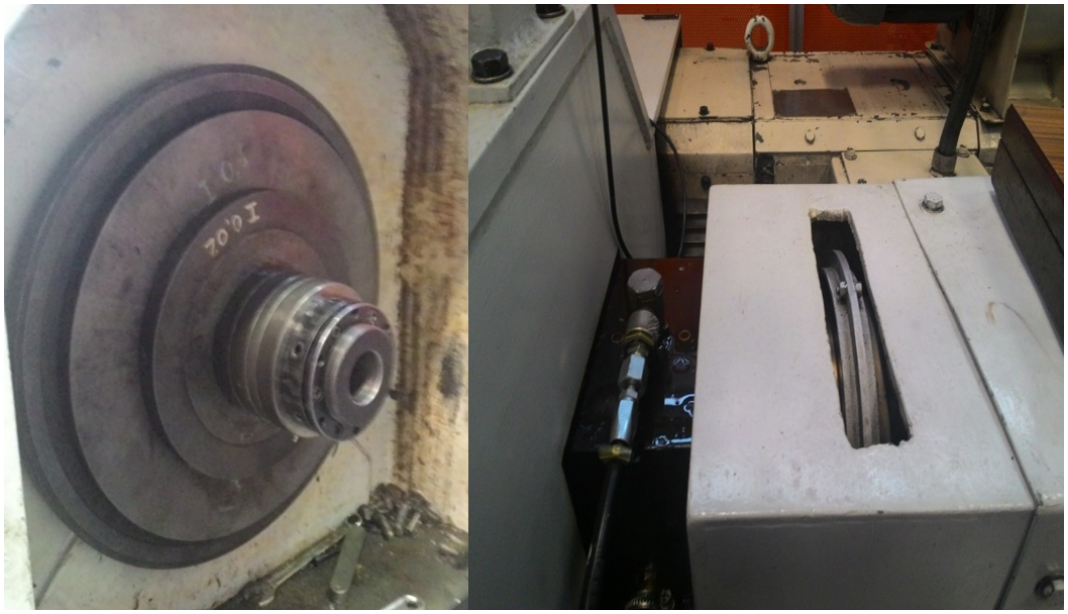

Fig. 3.5 The applied inertia (left) and the torque convertor stage (right).

4- Removing the Synchro Set: in order to measure the gap between the synchro ring and the clutch cone, the synchro set was removed and the distance was measured by feeler gauge as shown in Figure 3.6. After finishing the test this gap will be measured again to control the effect of axial loading and other parameters.

Fig. 3.6 Measuring the gap between synchro ring and clutch cone the synchro by feeler gauge.

5- Reassembling the Synchro and Setting the Test Requirements: after measuring the distance between the ring and the clutch cone, the synchro mechanism was reassembled and the hydraulic pressure was adjusted and all the pump and valves are checked then the safety doors were closed. The PLC interface was set based on test requirement e.g. rotational speed, time span of each stroke, number of cycle and etc. (see Figure 3.7).

Fig. 3.7 The PLC interface and the ready to start test rig machine.

3.2.2 Experimental procedure

In order to evaluate the dynamic parameters of the synchronizer, some experimental tests were carried out. Figure 3.8, shows the 2D schematic and a picture of the synchronizer test rig machine. For the purpose of the results repeatability for each product, ten tests were carried out. Two electric motors with different controllers were connected to the input and output shafts to obtain the specified angular velocities. To measure the absolute angular velocity, two different magnetic encoders with ± 0.1% error were attached to each rotating shaft. A hydraulic actuator was attached to the fork linkage mechanism. To measure the applied force a 5 kN load cell with ± 1N precision was utilized and the data was collected in every 0.01ms. To provide the allowable rotational inertia based on each testing condition, the inertia weights were mounted to the output shaft. This weight is equivalent to the inertia that is applied to the car wheels. The applied torque corresponding to the applied force and inertia was calculated by a 10 kN.m torsiometer with ± 0.1% error. A splash lubrication system through the input shaft was connected to the synchronizer. Before and after the test, the backlash was measured. To control the rate of wear production, the backlash should be in the allowable range that is considered in the design step.

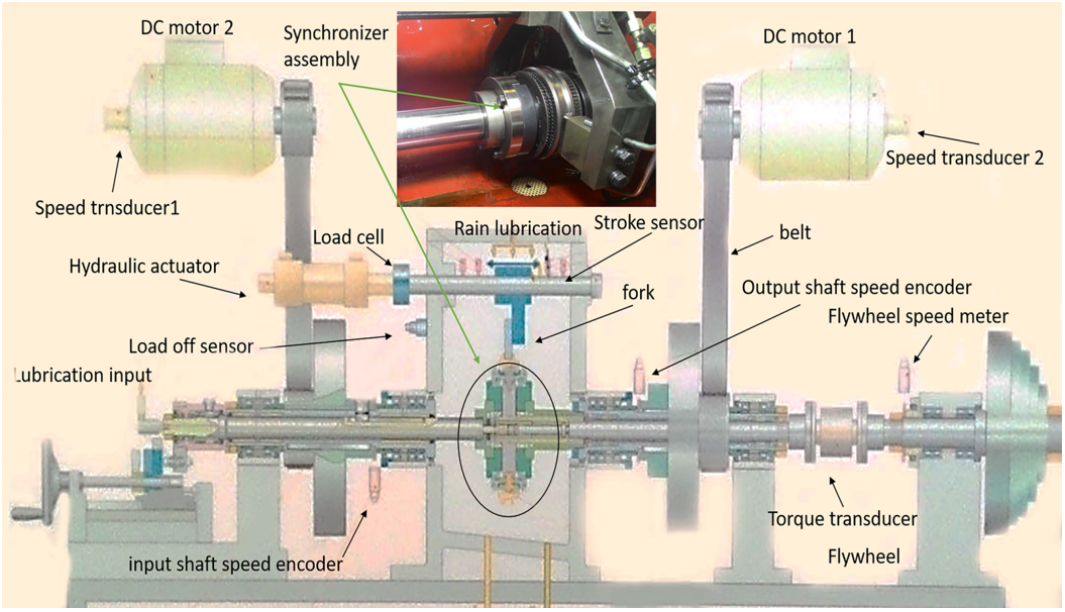

Fig. 3.8 The schematic of the synchronizer test rig machine.

For the purpose of validation, according to the real application, a single cone synchronizer with 74 mm diameter of the friction cone was used. The input rotational speed was set to 1000 rpm and the output shaft was adjusted with 2000 rpm. A ramp force within 200 ms was applied from a hydraulic actuator to the fork until the maximum load reached to 1400 N. In this test, the applied inertia was 0.169 kg.m2. Moreover, for the second test, a double cone synchronizer with 170 mm friction cone diameter was installed in the test rig. The input shaft rotational speed was 300 rpm while the output shaft angular velocity was set to 900 rpm. A 1500 N ramped force was applied to the actuator within 180 ms and the applied inertia was 0.895 kg.m2. The third test sample was 100 mm synchronizer with three different friction cones. The input shaft velocity was 1000 and the output shaft velocity was set to 2000 rpm. The applied inertia at the output shaft was 1.05 kg.m2. A ramp force with 1500 N was induced within 220 ms. The output data e.g. actuator axial motion, the time of synchronization, the friction coefficient and reaction force are extracted by the test rig data logger. Table 3.1 shows the dynamic specifications of the SC- 74, the DC-170 and the TC-100 synchronizers.

Table 3.1 The dynamic specifications of the SC- 74, the DC-170 and the TC-100 synchronizers.

characteristic	unit	Code		
		SC-74	DC-170	TC-100
Cone diameter	mm	74	165/170	90/95/100
Angular velocity	rpm	1000/2000	300/900	1000/2000
$\Delta\omega$	rpm	1000	600	1000
μ	–	0.06	0.1	0.09
Applied inertia	$kg.m^2$	0.17	0.9	1.05
Applied force	N	1400	1500	1500
t_{app}	s	0.2	0.18	0.22

3.3 Analytical approach

3.3.1 Time estimation analysis

The general form of dynamic equation to calculate the synchronization time regarding constant applied load is presented as follow [34]:

$$t_{synch} = \frac{I_R \Delta\omega \sin\alpha}{\mu c R_c F_{max}}, \tag{3.1}$$

where I_R is the equivalent applied inertial, $\Delta\omega$ is the difference of rotational speed between gearbox shafts, F_{max} is th emaximum axial load. Some parameters influence shifting time such as friction coefficient, the applied inertia, the difference velocity between the transmission system shafts and time of applied force from actuator. It can be expected that, when a time-dependent load is taken into account the synchronization time can be estimated more accurately. To derive the time dependency formulation of the applied force, the general form of torque calculation can be written based on the system equilibrium.

$$M_{max} = \frac{(\mu_c R_c F_{max})}{\sin\alpha} = \frac{I\Omega}{\Delta T}, \tag{3.2}$$

$$M_t = \begin{cases} \frac{M_0 + (M_{max} - M_0)}{T_t} & \nabla t < T \\ M_{max} & \nabla t \geq T \end{cases}, \tag{3.3}$$

where M_{max} is the maximum torque corresponding to the maximum applied force, M_0 is the initial torque, T is the duration of the applied ramp load and t is the processing time. Starting from the balance equation:

$$M_t = \frac{-Id\omega}{dt} = \frac{M_0 + (M_{max} - M_0)}{T}t, \tag{3.4}$$

It follows that $\omega(t)$ is a parabolic function:

$$\omega(t) = at^2 + bt + c, \tag{3.5}$$

$$\frac{d\omega}{dt} = 2at + b, \tag{3.6}$$

The substitution of the initial condition leads to:

$$\frac{-Id\omega}{dt}|_{t=0} = \begin{cases} M(0) = M_0; b = \frac{-M_0}{I} \\ b \end{cases}, \tag{3.7}$$

$$\Omega(0) = at^2 + bt + c; c = \Omega, \tag{3.8}$$

where Ω is the difference between the input and output shaft angular velocities. Therefore, the angular velocity and acceleration can be rewritten as:

$$\omega(t) = at^2 + \frac{-M_0}{I}t + \Omega, \tag{3.9}$$

$$\frac{d\omega}{dt} = 2at - \frac{M_0}{I}, \tag{3.10}$$

In case of $t_s < T$, the equilibrium at $\omega_{(ts)} = 0$ can be written as:

$${t_s}^2 + \frac{-M_0}{I}t_s + \Omega = 0, \tag{3.11}$$

$$\frac{d\omega}{dt}|_{ts} = 2at_s - \frac{M_0}{I}, \tag{3.12}$$

where t_s is the synchronization time

$$M(t_s) = M_0 + \frac{(M_{max} - M_0)}{T} t_s = \frac{-Id\omega}{dt}|_{t_s}, \tag{3.13}$$

$$a = \frac{-(M_{max} - M_0)}{2IT}, \tag{3.14}$$

If $M_0 = M_{max}$ then $a = 0$. Thefrore, the angular velocity equation can be written as:

$$\omega(t) = \frac{-(M_{max} - M_0)}{2IT} t^2 - \frac{M_0}{I} t + \Omega, \tag{3.15}$$

Simplifying the angular velocity equation at the synchronization time, yields:

$$(M_{max} - M_0) t_s^2 + 2M_0 T t_s - 2IT\Omega = 0, \tag{3.16}$$

and when $M_{max} = M_0$:

$$t_s = \Delta T = \frac{I\Omega}{M_{max}}, \tag{3.17}$$

However, when $M_{max} \neq M_0$ the synchronization time can be written as:

$$t_s = \frac{-M_0 T + \sqrt{M_0^2 T^2 + 2IT\Omega(M_{max} - M_0)}}{((M_{max} - M_0))}, \tag{3.18}$$

Moreover, if $M_0 = 0$ the synchronization time would be :

$$t_s = \sqrt{\frac{2IT\Omega}{M_{max}}} = \sqrt{2T\Delta T}, \tag{3.19}$$

When $t_s = T$, (the synchronization is completed at the end of the ramp), the 3.17 becomes:

$$t_{lim} = \frac{2I\Omega}{(M_{max} + M_0)}, \tag{3.20}$$

t_{lim} is the synchronization time for which the above condition is fulfilled.

When $M_0 = 0$, the limit time can be written as:

$$t_{lim} = \frac{2I\Omega}{M_{max}} = 2\Delta T, \tag{3.21}$$

$$\omega(t) = \frac{-\Omega}{2T\Delta T}t^2 + \Omega, \tag{3.22}$$

In case of $t_s \geq T$ the equilibrium at $\omega(T)$ as a parabolic curve and at the $\omega_{ts} = 0$ as a linear line can be written as:

$$\omega|_{t_s \geq T} \Rightarrow \begin{cases} \omega(T) = \frac{-(M_{max}-M_0)}{2IT}T^2 - \frac{M_0}{IT} = \frac{-\Omega T}{\Delta T} + b \\ \Omega - \frac{\Omega_{ts}}{\Delta T} + b = 0; b = \frac{\Omega_{ts}}{\Delta T} - \Omega \end{cases}, \tag{3.23}$$

Rewriting 3.23 leads to:

$$\frac{-(M_{max} - M_0)}{2I}T - \frac{M_0}{IT} = \frac{-\Omega T}{\Delta T} + \frac{\Omega_{ts}}{\Delta T} - \Omega, \tag{3.24}$$

Simplifying (3.24) express the synchronization time in the specified time domain as follow:

$$t_s = \frac{-(M_{max} + M_0)T\Delta T + 2I\Omega(T + \Delta T)}{2I\Omega}, \tag{3.25}$$

Regarding different testing conditions, the input data can be implemented in (3.17), (3.18), (3.19) or (3.25) .

Table 3.2 The components terminology and their dependent parameters.

Component code	description	Degree of freedom's (DOF)dependent parameters
C1	Gear clutch body (input shaft)	J_1, ω_1
C2	Sliding sleeve	$J_2, \omega_2 m_2, x_2, f_2$
C3	Synchro ring	J_3, ω_3, m_3, x_2
C4	Strut detent	$J_4, \omega_4 m_4, x_4, y_4, k_{sp}$
C5	Hub	J_1, ω_1
C6	Fork	f_6

3.3.2 Multibody dynamic formulation for different phases of synchronization

This section expresses a body coordinate multi body formulation for evaluating the different components during different synchronizer phases. Table 3.2 presents components terminology and their dependent parameters. These parameters and degree of freedom can be used to establish dynamic equations for each components over every single phase.

Phase 1-first free flying

When the shifting process begins, the sliding sleeve is in neutral position and its axial motion can be started by means of a fork lever. At the first phase of the synchronization process, the sliding sleeve, the synchronizer hub and the strut detents have the same angular velocity as the gearbox input shaft. Figure 3.9 shows the first phase of the synchronization process.

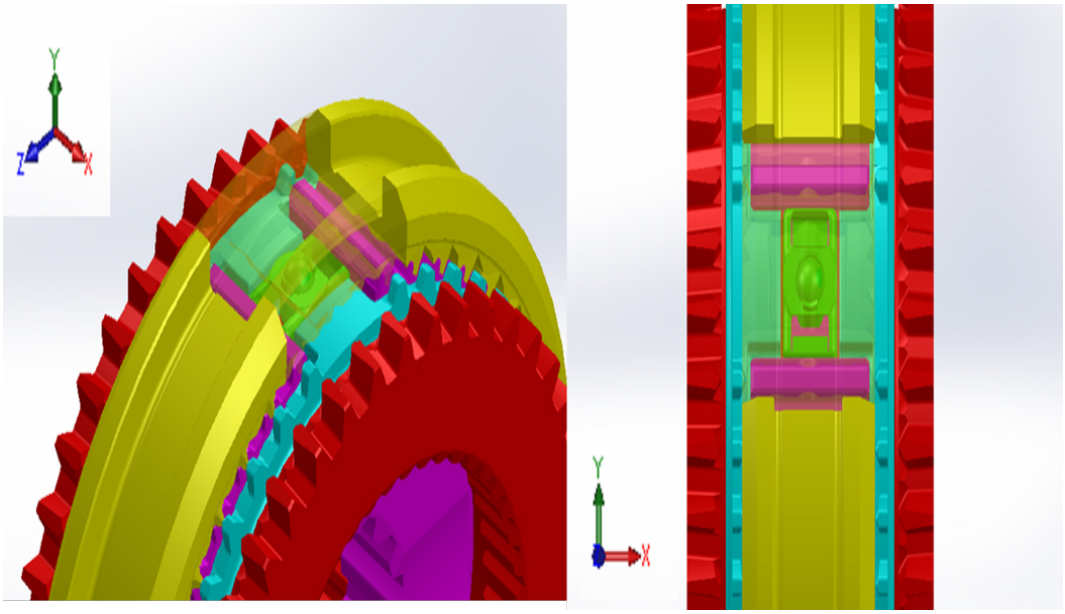

Fig. 3.9 The first phase of the synchronization process (Free flying).

The available degree of freedom for different component is as follow:

$\omega_1, \omega_2, \omega_3, \omega_4$, ω_5, x_2, x_4, y_4

The dynamic equations for rotating parts can be written as:

$$C1 : J_1 \dot{\omega}_1 = T_{d1}, \tag{3.26}$$

$$C2 : J_2 + J_3 + J_4 + J_5) \ \dot{\omega}_2 = T_{d2}, \tag{3.27}$$

At the end of the first phase the sliding sleeve start moving axially. Therefore, the axial motion will be transferred to the strut detents. Due the axial motion the sleeve compress the ball and spring. The following equations present the translational dynamic equation for the sliding sleeve and strut detents displacement. In addition, to overcome the geometrical limitation, the condition:

$$C2, C4 : x_2 - x_4 = \frac{\Delta y_4}{\tan\theta} \tag{3.28}$$

should be satisfied [23].

$$C2 : m_2\ddot{x}_2 = f_6 - N_2(sin\theta + \mu_2 cos\theta) \tag{3.29}$$

$$C4 : n_p m_4\ddot{x}_4 = N_2(sin\theta + \mu_4 cos\theta) \tag{3.30}$$

$$C4 : m_4\ddot{y}_4 = f_{sp} - \frac{N_2}{np}(\mu_2 sin\theta - cos\theta), \tag{3.31}$$

where:

$$f_{sp} = k_{sp}(f_{sp} - \sqrt{{l_{sp0}}^2 + {l_{sp}}^2}), \tag{3.32}$$

Phase 2- spline positioning during detent motion

When actuator moves the fork axially, the sliding sleeve starts moving to the synchronizer ring. In the second phase, the balls and springs that are inserted to the struts detents are compressed while they sliding along the hub grooves. Figure 3.10 shows the second phase of the synchronization process.

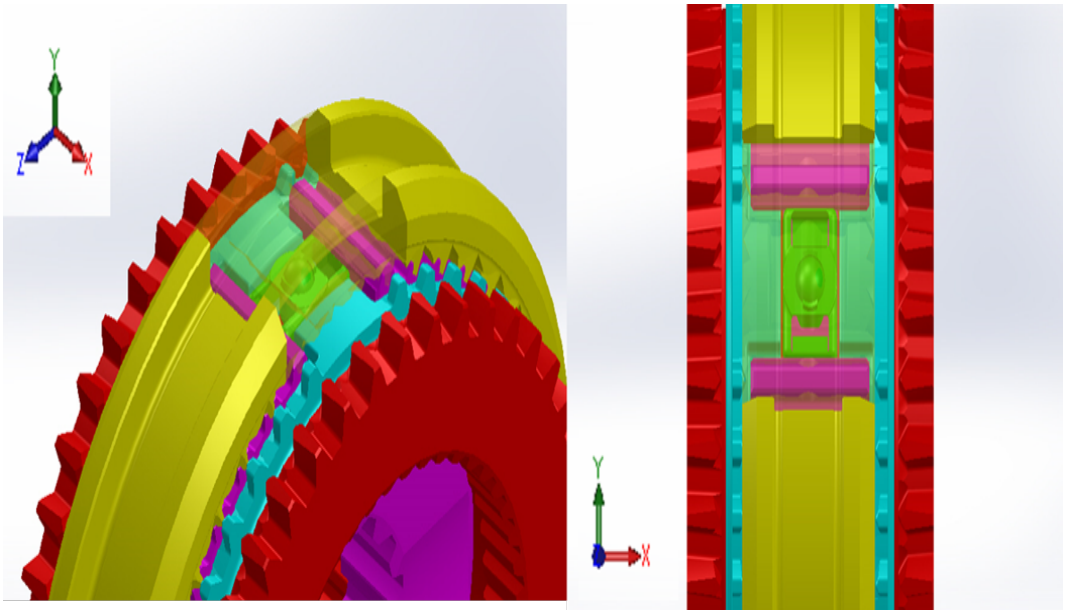

Fig. 3.10 The second phase of the synchronization process.The axial moving of the sliding sleeve to the synchronizer ring.

In this phase the sliding sleeve moves forward to the synchronizer ring. Therefore, the contact between sleeve and strut detents generates an axial force. This force push the outer surface of strut detents to the outer surface of synchronizer ring and subsequently the load will be transferred to the synchronizer ring. At this moment the synchronizer ring, synchronizer hub, strut detents and sliding sleeve have the same angular velocity. The following formulations present the rotational dynamic equations for gear body, sliding sleeve and connected strut detents. Due to lubrication the churning oil between friction surfaces generates a drag torque. The other sources of mechanical drag torques were considered as the constant parameters from previous works [83].

The available degree of freedom for different component is as follow:

$\omega_1, \omega_2 = \omega_3 = \omega_4 = \omega_5, x_2 = x_4, y_4$

The dynamic equations for rotating parts can be written as:

$$C1 : J_1 \dot{\omega}_1 = T_c + T_{d1}, \tag{3.33}$$

$$T_c = 4\pi\mu {R_c}^3 b \frac{\omega_3}{h} \tag{3.34}$$

$$h = h_0 - (x_3 - x_{3@t_0}) \sin\alpha_c \tag{3.35}$$

$$C2, C4 : (J_2 + J_4 + J_5)\ \dot{\omega}_2 = N_2\mu_4 R_4 - N_4 R_5 + T_{d3} \tag{3.36}$$

When there is no relative motion between C3 and C5, we have:

$$(J_2 + J_3 + J_4 + J_5)\ \dot{\omega}_3 = |T_c| + T_{d2} \tag{3.37}$$

Through an upshifting, due to higher speed of clutch gear than the hub synchronizer the frictional torque has a negative sign in order to brake the rotation of the gear.

The translational dynamic equations for the second phase of synchronization can be presented as below. The reaction force from viscosity of oil film between friction cones also can be calculated as:

$$C2 : m_2\ddot{x}_2 = f_6 - N_2(\sin\theta\ + \mu_2 \cos\ \theta\ ) \tag{3.38}$$

$$C3 : (m_2 + m_3 + n_p m_4)\,\ddot{x}_4 = f_6 - N_c(1 + \mu_c \cot\alpha_c) \tag{3.39}$$

$$N_c = \begin{cases} 0 & if\ \ h_1 < h < h_0 \\ k_{NC} 16\pi\mu\dot{x}_3 sin^2_\alpha R_c (\frac{b}{h})^3 & if\ \ h_{min} < h < h_1 \end{cases}$$

$$k_{NC} = \frac{1}{n^2}[1 + (1-n)\frac{a}{b_i}]^3 \tag{3.40}$$

$$b_i = b - \frac{na}{2} \tag{3.41}$$

where h_1 is the initial normal oil, film thickness between friction cones. hmin is the normal distance of minimum oil film thickness between the friction cones and it could be considered as the surface roughness. K_{NC} is the geometrical factor for introducing the circumferential groove on the inner surface of friction cones. The negative effect of axial load on transferring torque can be removed rapidly by increasing the number of circumferential grooves [84, 85]. a is the half width of a

groove on the friction cone and b is the half length of the friction surface. Also, n is the number of circumferential grooves.

$$C3,C4 : (\ m_3 + n_p m_4)\ddot{x}_4 = N_2 - (\sin\theta\ + \mu_2 \cos\theta\ ) - N_c(1 + \mu_c \cot\theta\ ) \tag{3.42}$$

$$C4 : m_4 \ddot{y}_4 = f_{sp} + \frac{N_2}{n_p}(\mu \sin\theta\ - \cos\theta\ ) \tag{3.43}$$

Phase 3-final position of synchronizer ring

By increasing the axial force, the meshing between sliding sleeve and the synchronizer teeth occurs (indexing phase). Figure 3.11 indicates the first indexing phase of the synchronization process.

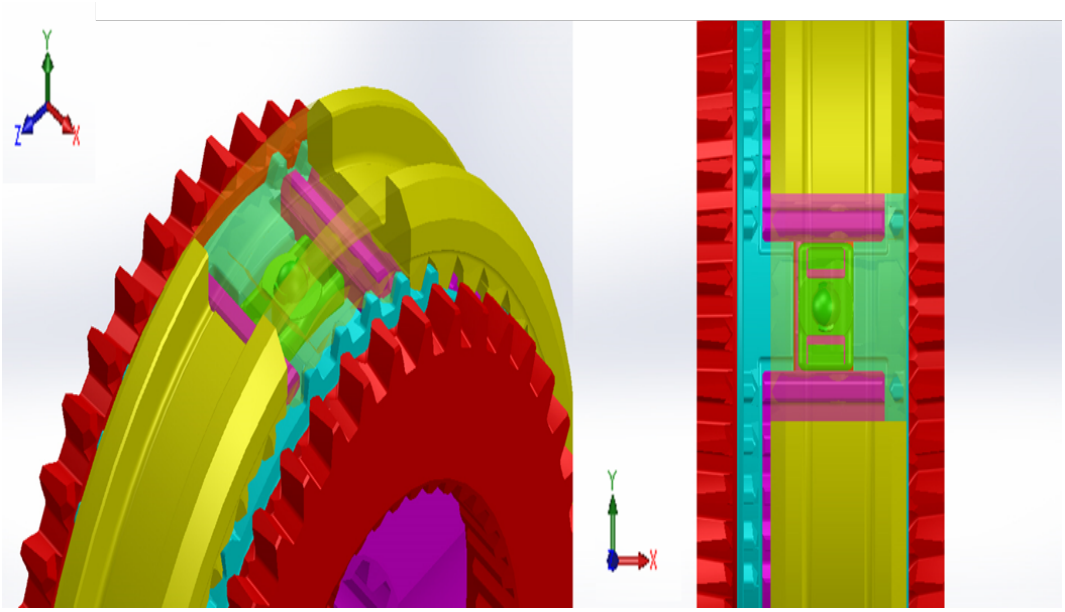

Fig. 3.11 the third phase of synchronization process (first indexing).

In this phase we have only rotational motion and gear clutch sleeve and synchronizer ring have the same angular velocity. It means that the degree of freedom for the system become one. Available DOF in this phase: $\omega_1 = \omega_2 = \omega_3$. In this phase, the friction coefficient for the friction cones is

$$C1; J_1\ \dot{\omega}_1 = \frac{-\mu_c f_6 R_c}{\sin\alpha}\ (1 + 1/3\left(\frac{b}{Rc}\right)^2\ sin^2_\alpha\Big) + T_{d1} \tag{3.44}$$

$$\mu_c\,(t) = \mu_{solid} - \frac{\mu_{solid} - \mu_v}{s_2 - s_1}(s - s_1) \tag{3.45}$$

where $S1$ is the final value of Stribeck's number for the mixed (stick and slip) friction conditions. $S2$ is the initial value of Stribeck's number for the mixed friction conditions. μ_{solid} is the limiting value of the coefficient of friction at the end of the mixed stage [87].

$$\mu_c\,(t) = \mu_{solid} - \left[\frac{\mu_{solid}}{s_2 - s_1}\,(s_1) - \frac{\mu_{solid} - \mu_v}{s_2 - s_1}.\frac{\mu\,(\omega_1 - \omega_3)\,R_c}{f_6\,(t)} 4\pi R_c \mathrm{b} sin\ \alpha_c\right] \tag{3.46}$$

$$\begin{aligned} C3 : J_3\dot{\omega}_3 = &\left[\frac{\mu_c f(t)_6 R_c}{sin_\alpha}\ \left(1 + \frac{1}{3}\left(\frac{b}{Rc}\right)^2 sin^2_\alpha\right)\right. \\ -N_5R_5 - R_2\left(\frac{1 - \mu\tan\beta}{\tan\beta + \mu_s}\right).&\left.[f_6 - N_6\,(\sin\theta\ + \mu\cos\theta\ )]\right] + T_{d2} \end{aligned} \tag{3.47}$$

$$\begin{aligned} C2, C4 : (J_2{+}J_4{+}J_5)\,\dot{\omega}_2 = R_2\frac{(1 - \mu_s\tan\beta\ )}{\tan\beta\ + \mu_s}[f(t)_6 \\ -N_2\,(\sin\theta\ + \mu_2\cos\theta\ ] + N_5R_5 + T_{d3} \end{aligned} \tag{3.48}$$

$$\begin{aligned} C2, C3, C4 : (J_2 + J_3{+}J_4{+}J_5)\ \dot{\omega}_2 = \\ \frac{\mu_c f(t)_6 R_c}{sin_\alpha}\ \left(1 + \frac{1}{3}\left(\frac{b}{Rc}\right)^2 sin^2_\alpha\right) +\ T_{d2} \end{aligned} \tag{3.49}$$

Phase 4- sleeve motion for engagement

Due to stick contact between the clutch cone and synchronizer cone, the axial force raises to the maximum level at the synchronization phase (Figure 3.12). When multiple cone synchronizers are used, the rotational speed difference between the

synchronizer ring and all friction cones should be zero. Therefore, the synchronization process can be completed.

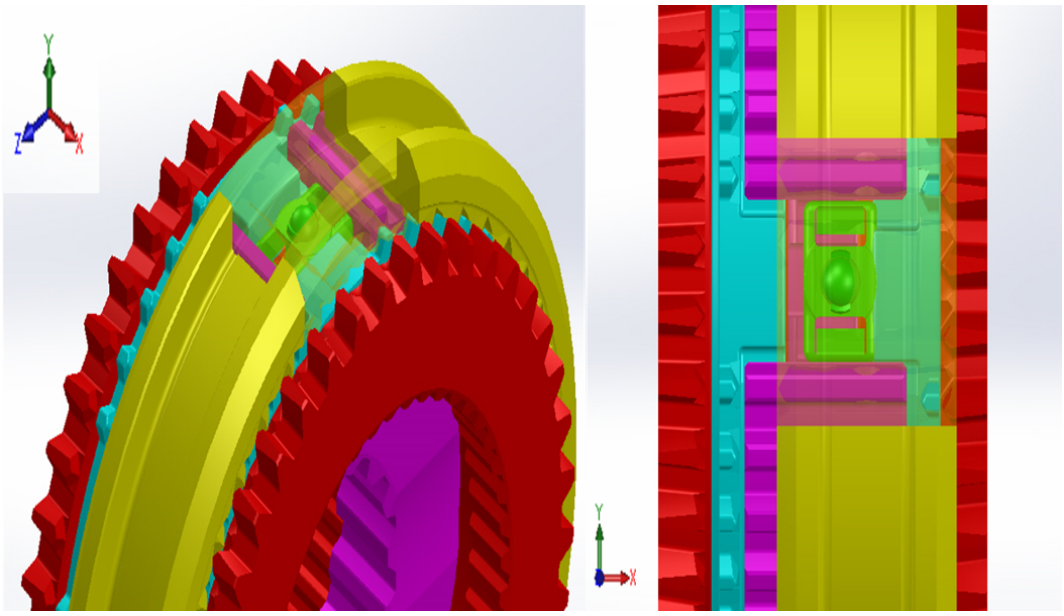

Fig. 3.12 The fourth synchronization phase (synchronization phase).

In this phase the rotational speed of all components are the same. However, the strut detents will be transferred to the final axial position. When the strut detents reach the final position, the locking mechanism will be released and the sliding sleeve can move freely towards to the gear clutch for final indexing. Available DOF in this phase: $\omega_1 = \omega_2 = \omega_3 = \omega_4,\ x_2\ , y_4$

The dynamic equations for rotating parts can be written as:

$$C2 : m_2\ddot{x}_2 = f_6 - N_2\,(\sin\theta\ + \mu_2\cos\,\theta\ ) - N_3\,(\sin\beta\ + \mu_2\cos\,\beta\ ) \tag{3.50}$$

$$C4 : m_4\ddot{y}_4 = f_{sp} + \frac{N_2}{n_p}(\cos\theta\ - \mu_2\sin\theta\ \ \ ) \tag{3.51}$$

In addition the translational dynamic equation for different components can be formulated as:

$$C1,C3 : (J_1 + J_3)\,\dot{\omega}_1 = f_6 R_2 \left(\frac{1-\mu_s \tan\beta}{\tan\beta + \mu_s}\right) - N_2 R_2 \,(\sin\theta \; + \mu_2 \cos\theta \;) \left(\frac{1-\mu_s \tan\beta}{\tan\beta \; + \mu_s}\right) - N_4 R_4 \mu_4 + T_{d1} \tag{3.52}$$

$$C2,C4 : (J_2 + J_4 + J_5)\,\dot{\omega}_2 = N_3 R_2 \,(\cos\theta \; - \mu_2 \sin\theta \;) - R_4 N_4 \mu_4 + T_{d3} \tag{3.53}$$

Phase 5- engagement and final free flying

The final indexing is occurred between sliding sleeve and clutch body teeth when the input and output velocities are same (Figure 3.13).

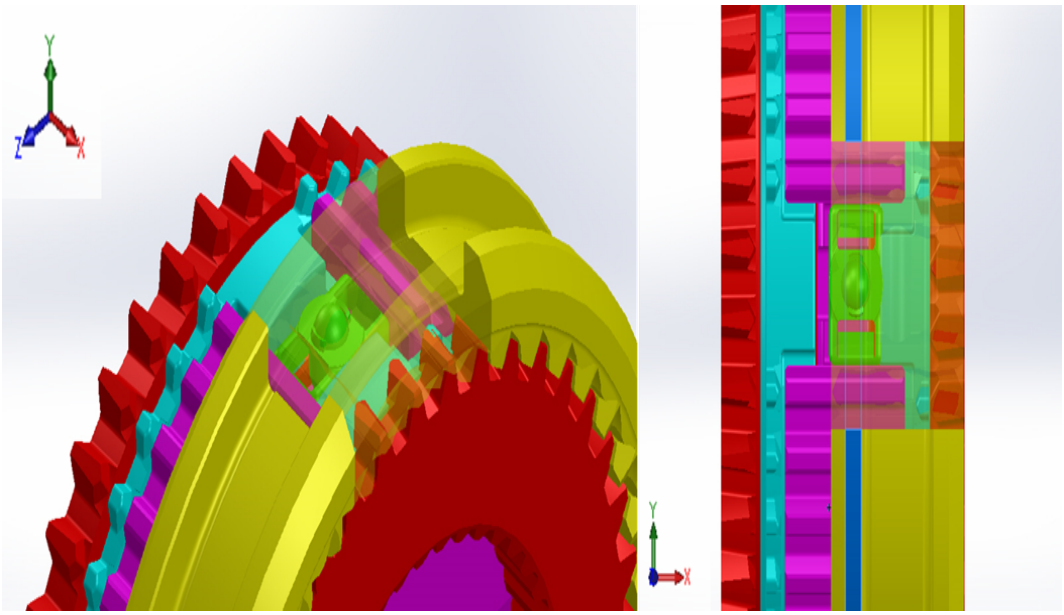

Fig. 3.13 The fifth phase of synchronization second indexing and final engagement.

In this phase, the only degree of freedom of the system is rotational DOF i.e. $\omega_1, \omega_2, \omega_3, \omega_4 \,, \omega_5$. Furthermore, in order to rotate in free fling phase, the only resistant torque is related to the mechanical drag toques of rotational components that can be seen in the following formulation.

$$C1-C5:(J_1+J_2+J_3+J_4+J_5)\,\dot{\omega}_1 = T_{d1}+T_{d2} \tag{3.54}$$

3.4 Numerical approach

3.4.1 Geometry preparation and CAD model

In order to generate a numerical model, the first step is creating a CAD model. Models for different synchronizer mechanism were generated via Pro Engineering software based on the real part dimensions which are used in the experimental test. After creating every single part of each synchronizer set, they were assembled as a final product regarding nominal clearance between different parts. The final model were converted to the *.STP file in order to be imported into the FE software. In this study the commercial code ABAQUS was utilized. However, after importing a CAD model to the FE software, some round surfaces or sharp corners will face with errors. This kind of errors reduce the quality of mesh for the next steps. Therefore this problems should be solved by using improvement tools to obtain smooth surfaces. The other reason for repairing the surfaces is to control the seed size of element for creating a uniform mesh distribution over the geometry. Figure 3.14 shows an imported geometry (a) with error surface and (b) after improvement. Figure 3.15 (a), (b) and (c) depicts the final assemblies for SC-74, DC-170 and TC-100, respectively.

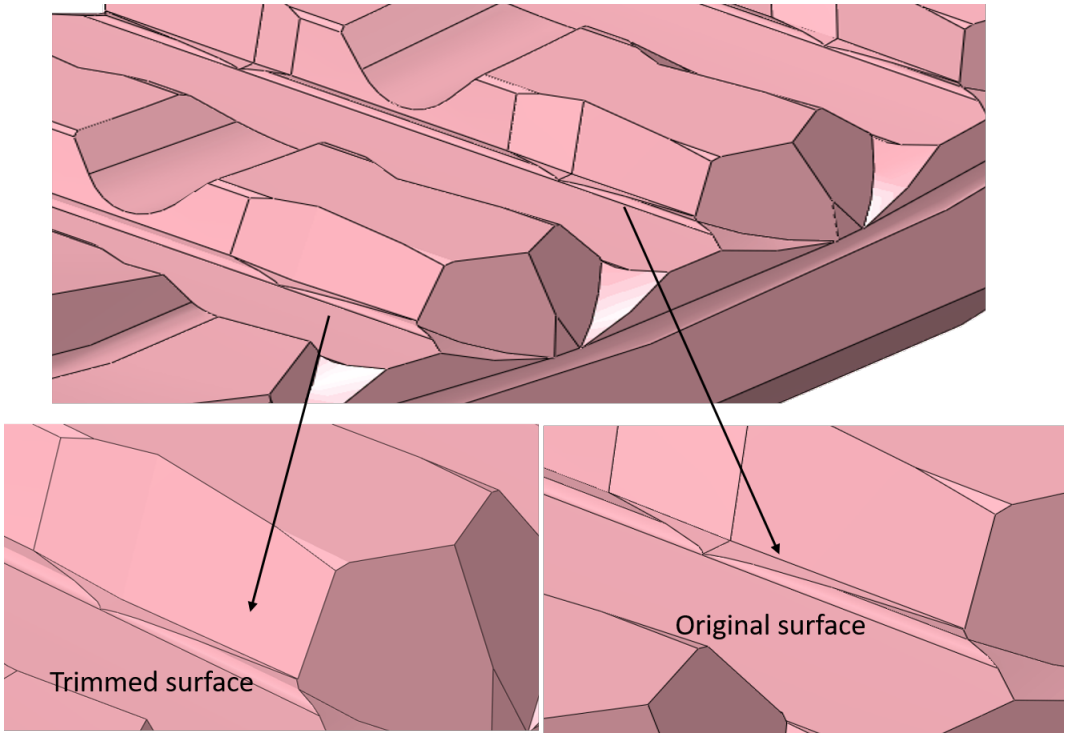

Fig. 3.14 An imported geometry (a) with error surface and (b) after improvement.

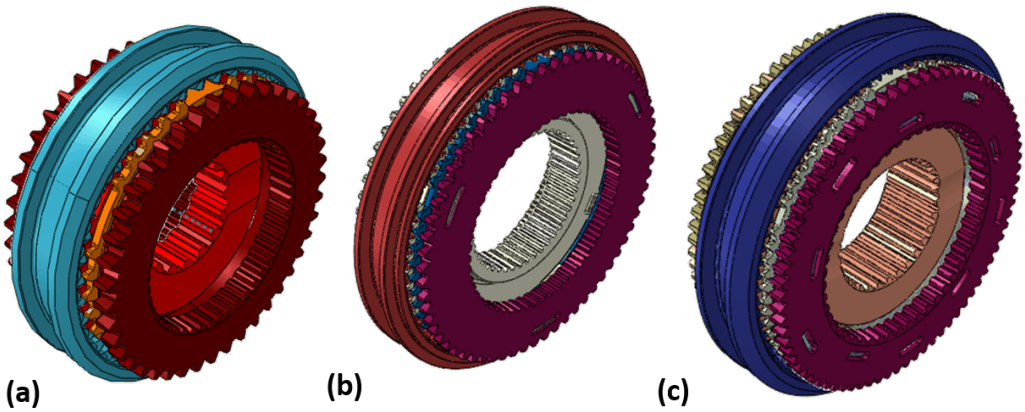

Fig. 3.15 The final assemblies of (a) SC-74, (b) DC-170 and (c) TC-100 were used for FE modeling.

3.4.2 Physical condition and applied loading and boundary condition

Based on the test condition, data from Table 3.1 are taken into account to create the model for different synchronizer models. In addition, based on the experimental data, the mass and inertial properties of each component were applied to the MBD model. Furthermore, the moment of inertia will generate a drag torque to the rotational part. Table 3.3 lists the inertial and mass properties of SC-74, DC-170 and TC-100.

Table 3.3 The inertial and mass properties of SC-74, DC-170 and TC-100.

		SC-74				DC-170				TC-100			
			Inertia ($kg.mm^2$)				Inertia ($kg.mm^2$)				Inertia ($kg.mm^2$)		
Part name	Code	Mass (kg)	I_{xx}	I_{yy}	I_{zz}	Mass (kg)	I_{xx}	I_{yy}	I_{zz}	Mass (kg)	I_{xx}	I_{yy}	I_{zz}
Sliding sleeve	A	0.28	0.61	0.32	0.32	1.3	13.44	6.88	6.88	0.4	1.47	0.76	0.76
Hub	B	0.47	0.51	0.26	0.26	2.02	11.76	5.95	5.95	0.69	0.98	0.64	0.64
Strut detents	C	0.07	1.46e-4	1.67e-4	8.9e-5	0.022	0.001	9.24e-4	7.77e-4	0.035	5.9e-5	8.31e-5	3.14e-5
Friction cone 1	D	0.089	0.14	0.07	0.07	0.41	3.1	1.55	1.55	0.13	0.36	0.18	0.18
Friction cone 2	D	—	—	—	—	0.2	1.27	0.6	0.6	0.2	0.09	0.046	0.046
Friction cone 3	D	—	—	—	—	—	—	—	—	0.035	0.082	0.041	0.041
Clutch body ring	E	0.212	0.278	0.142	0.142	0.91	5.55	2.76	2.76	0.29	0.48	0.24	0.24

3.4.3 Connector element implementation

In this study, to provide the degree of freedom for different parts two different type of kinematic joints were exploited. The revolute and cylindrical joints bring one and two DOF to the system respectively. Table 3.4 indicates the applied joints between different parts. Part i represent the reference part and part j is the follower part when the kinematic joints will be applied. Also, the bodies' coordinates have been addressed in Table 3.4.

Table 3.4 The applied joints between different parts and their bodies' coordinates.

		SC-74							DC-170							TC-100						
			Cordinate (mm)							Cordinate (mm)							Cordinate (mm)					
part i	part j	joint type	X	Y	Z	constraints	part i	part j	joint type	X	Y	Z	constraints	part i	part j	joint type	X	Y	Z	constraints		
ground	hub	revoloute	-0.1	0	0	5	ground	hub	revoloute	-0.1	0	0	5	ground	hub	revoloute	-0.1	0	0	5		
hub	sleeve	cylindrical	0	0	0	4	hub	sleeve	cylindrical	0	0	0	4	hub	sleeve	cylindrical	0	0	0	4		
hub	detent 1	cylindrical	0	32	0	4	hub	detent 1	cylindrical	0	72	0	4	hub	detent 1	cylindrical	0	43	0	4		
hub	detent2	cylindrical	0	-16	-27.7	4	hub	detent2	cylindrical	0	-36	-62	4	hub	detent2	cylindrical	0	-21.8	-37.7	4		
hub	detent 3	cylindrical	0	-16	22.7	4	hub	detent 3	cylindrical	0	-36	62	4	hub	detent 3	cylindrical	0	-21.8	37.7	4		
detent 1	ball 1	cylindrical	0	39.76	0	4	detent 1	ball 1	cylindrical	0	87.2	0	4	detent 1	ball 1	cylindrical	0	52.11	0	4		
detent 2	ball 2	cylindrical	0	-20	-34.6	4	detent 2	ball 2	cylindrical	0	-43.6	-75.5	4	detent 2	ball 2	cylindrical	0	-26.1	-45.05	4		
detent 3	ball 3	cylindrical	0	-20	34.6	4	detent 3	ball 3	cylindrical	0	-43.6	75.5	4	detent 3	ball 3	cylindrical	0	-26.1	45.05	4		
sleeve	Cone 1	cylindrical	9.72	0	0	4	sleeve	Cone 1	cylindrical	12.5	0	0	4	sleeve	Cone 1	cylindrical	9.14	0	0	4		
Cone 1	CBR	cylindrical	15.69	0	0	4	Cone 1	Cone 2	cylindrical	15.42	0	0	4	Cone 1	Cone 2	cylindrical	10.24	0	0	4		
CBR	Ground	revoloute	16	0	0	4	Cone 2	CBR	cylindrical	24.02	0	0	4	Cone 2	Cone 3	cylindrical	11.43	0	0	4		
–	–	–	–	–	–	–	CBR	Ground	revoloute	24.5	0	0	5	Cone 3	CBR	cylindrical	18.23	0	0	4		
–	–	–	–	–	–	–	–	–	–	–	–	–	–	CBR	Ground	revoloute	18.5	0	0	5		

In ABAQUS software, to provide the kinematic joints and global or local coordinates, the connector elements are implemented. Figure 2.20 describes the connector configuration in the ABAQUS library. Moreover to control the axial displacement

of the different bodies, the stop condition was applied to sliding sleeve cylindrical connector. The strut detent have relative displacement inside the synchronizer hub's grooves. Therefore a local coordinate was allocated to each strut detent mechanism. In order to model the spring stiffness, an elastic properties was considered for cylindrical connector between ball and spring inside the strut detents. Figure 3.16depicts the applied connector to the strut detent mechanism regarding coordinate system.

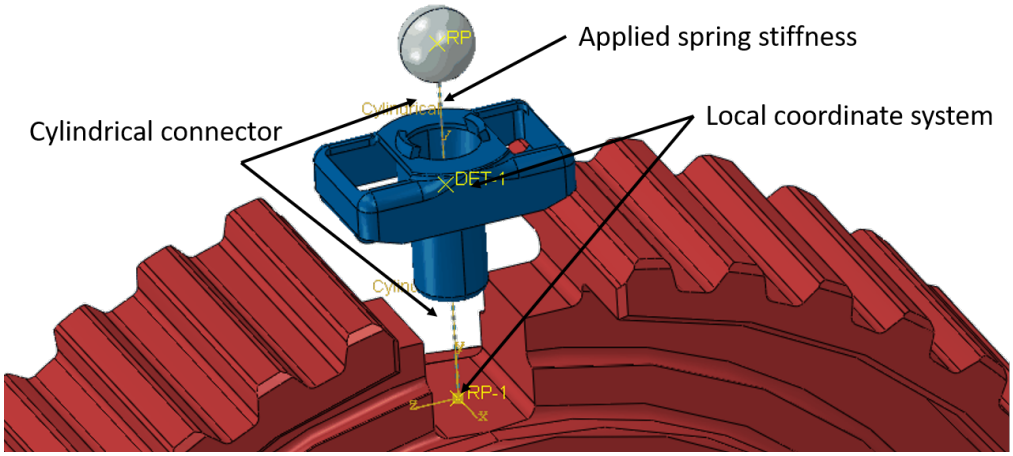

Fig. 3.16 The applied connector to the strut detent mechanism regarding coordinate system.

3.4.4 Dynamic Friction Coefficient

To calculate the friction coefficient between friction cones, the applied force and torque are extracted in every time increment of the test. Substituting the experimental data into equation 3.55,the friction coefficient of each time increment of the test can be calculated as:

$$\mu_c = \frac{M \sin \alpha}{R_c F_{max}}, \tag{3.55}$$

where M is the applied torque, F_{max} is the axial load, α and R_c are the mean angle and the radius of the synchronizer cone, respectively. To confirm the validity of the results, each test was repeated ten times. The extracted data have a transient and steady state region. The steady-state region was assumed as the friction coefficient of the cones and the standard deviation was used to calculate the mean value of friction coefficient for each product. The mean values of friction coefficients for SC-74,

DC-170, and TC-100 were 0.06, 0.1 and 0.1, respectively. The standard deviation of different tests were 0.0078, 0.008 and 0.0082 for SC-74, DC- 170 and TC-100, respectively.

3.4.5 Contact modeling

In order to model the contact between surface pairs, the penalty contact method was implemented. The contact properties of each contact pairs consists of two main characteristics, tangential and normal behavior. The hard contact was considered between different surfaces when two surfaces or two set of nodes have normal interaction. The tangential behavior was applied to the different surfaces regarding dynamic friction coefficient of different material. The procedure of obtaining the friction coefficient for the friction cones is explained in the section of design of experiment. Data extracted from experimental setup were used in FE model for different types of synchronizers. Figure 3.17 illustrates the procedure of contact modeling in ABAQUS. To identify the contact between different surfaces, definition of the master and slave surface to avoid overclosure should be considered. Generally, the surface with higher stiffness is considered as the master surface. It is worth mentioning that one master surface can be in contact with several slave surfaces simultaneously. Therefore, selecting contact surfaces for complex systems is not easy and after finishing contact definition all contact pairs should be checked precisely. Due to the high rotational speed at the onset of simulation, the high impact can occur between contact surfaces. Therefore, the initial contact stabilization option is a good solution to resolve this issue. In this study, to avoid penetration of components in each other and to perform contact models 284, 312 and 364 contact pairs were selected for SC-74, DC-170 and TC-100 respectively. Moreover, the contact model for rigid elements is different with deformable elements. The rigid element is converted to the shell rigid element with two dimensional formulation. Therefore, in order to define contact surface the normal direction of surface should be identified.

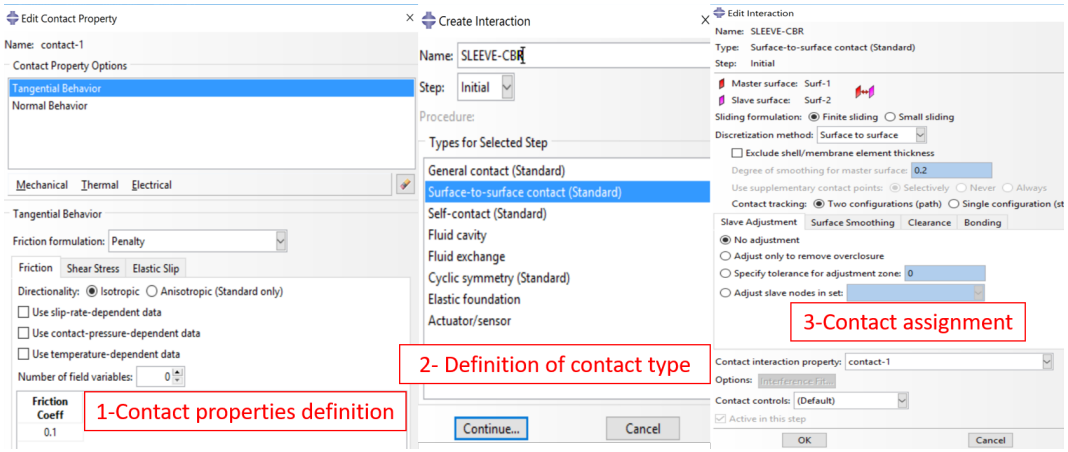

Fig. 3.17 The procedure of contact modeling in ABAQUS.

3.4.6 Material properties

In this study the elastic behavior of different materials was taken into account. The stiffness of all the parts due to heat treatment is high and in normal condition there is no plastic deformation observed in experimental tests. Table 3.5 demonstrates the material properties of different materials used for different models.

Table 3.5 The material properties of different materials were used for different models.

material	Density (kg/m3)	Elastic modulus (GPa)	Poisson's Ratio	Friction Coeficient
Steel	7800	210	0.3	0.05
carbon	1600	70	0.29	0.1
Molybdenum	10300	330	0.32	0.09
Sintered brass	8950	118	0.3	0.08

3.4.7 Modal dynamic analysis

Mesh convergence study

To investigate the dynamic response of the synchronizer mechanism, the three dimensional CAD geometries of different synchronizer (SC-74, DC-170 and TC-100) were imported to the ABAQUS commercial software. The element type of all

the parts was the continuum solid element with 4 nodes and reduced integration (C3D4R) ability. All the elements were considered as the second order finite element formulation. The first step of modal analysis of the synchronizer mechanism is to study the natural frequency of system's components. The first simulation was run with coarse mesh and in the next try the size of Lagrangian mesh was reduced. When the natural frequency of system converged to the stable value, it can be said that the element size is appropriate for the next simulations. As mentioned previously the eigensolver in this study was AMS solver. The main reason to choose this solver was the complexity for geometries. The conventional eigensolvers are not suitable to solve the eigenproblems with complex geometries or high number of contact areas. After mesh convergence study, the element quality assessment was performed on the important parameters such as aspect ratio, element warpage and shape factor of elements. When the meshes for every parts are verified, the final assembly will be generated. This process for different synchronizer (SC-74, DC-170 and TC-100) were repeated. The final meshed parts were used in every simulations with deformable elements.

Extraction of natural frequencies

In order to extract the natural frequencies of each synchronizer set, the connecting shafts should be added to the FE model. Adding the input and output shafts to the synchronizer assembly will change the frequency modes of synchronizers. However, in reality the synchronizers always are connected to these shafts and the study of the dynamic response of the system regardless of the role of the shafts is not correct. To reduce the time of calculation, the 3D beam element (B31) with size of 0.5 mm was used to model the shafts. One side of each shafts was connected to the clutch gear by tie constraint. The other side of the shaft is used to apply the boundary conditions. Figure3.18 shows the schematic of connecting shafts to the synchronizer.

Table 3.6 The dimension of connecting shafts of synchronizer mechanism.

Boundary conditions	Shaft diameter(mm)		Shaft length (mm)	
	Internal diameter	External diameter	Left side	Right side
Lmax-Dmin	12	34	172	69
Lmax-Dmax	18	47	172	69
Lmin-Dmin	12	34	56	75
Lmin-Dmax	18	47	56	75

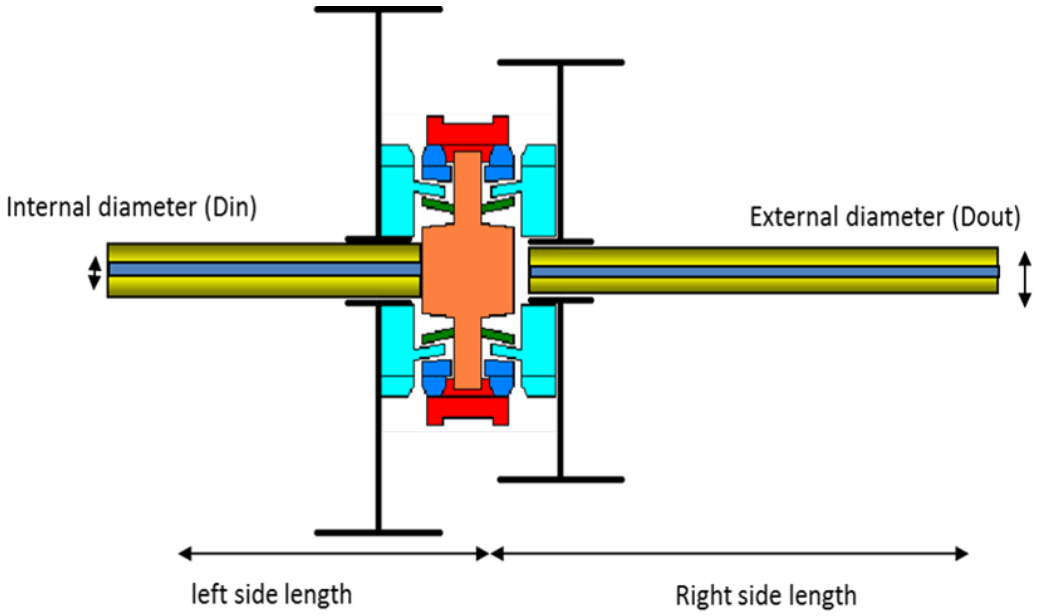

Fig. 3.18 The schematic of connecting shafts to the synchronizer.

In this study, four different configurations of shafts were used for all types of synchronizers. Table3.6 shows the dimensions of connecting shafts to the synchronizer mechanism.

To apply the boundary conditions, one end of shaft is only free to rotate and the other side is free to rotate and free to move axially. To apply the contact between different parts, the surface to surface contact method was performed. The details of contact modeling were mentioned in previous sections. To provide rotational ability and apply the boundary condition, the connector element was allocated to the different parts. As mentioned in Table 3.4, the cylindrical connectors were used to provide axial and rotational degree of freedom for synchronizer ring, sliding sleeve and strut detent. The revolute joint was assigned to the synchronizer hub and clutch

gear. Figures 3.19,3.20 and3.21 show the applied boundary conditions to the FE model for three different synchronizers.

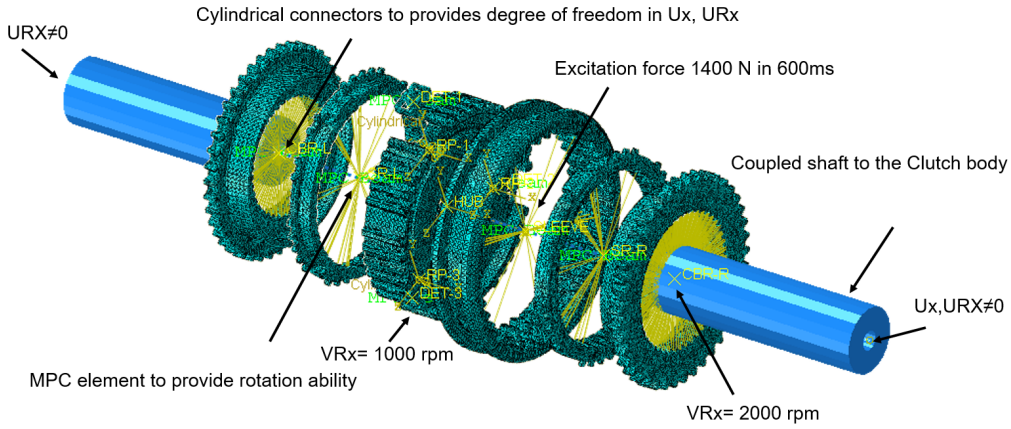

Fig. 3.19 The applied boundary conditions to the FE model (modal dynamic) of SC-74.

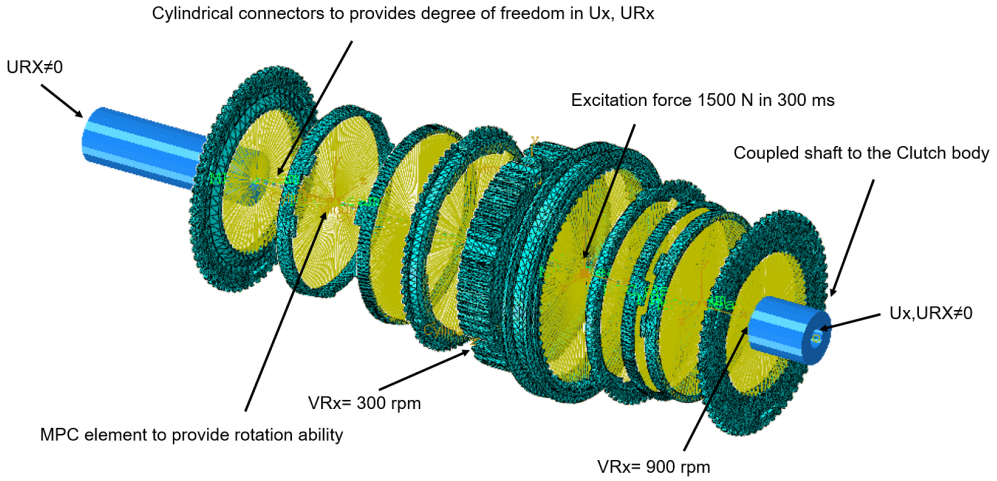

Fig. 3.20 The applied boundary conditions to the FE model (modal dynamic) of DC-170.

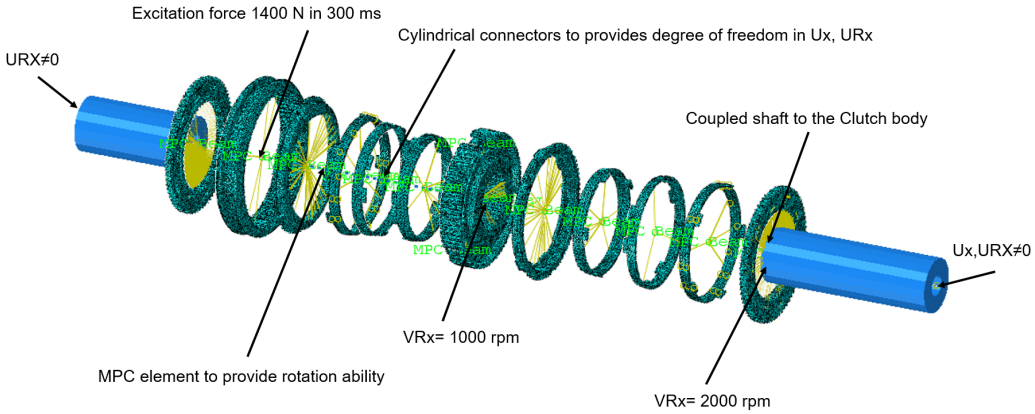

Fig. 3.21 The applied boundary conditions to the FE model (modal dynamic) of TC-100.

In this study, 10 frequency modes were extracted from every different shaft configuration. This method can be used to identify the range of interest for the system frequencies. Therefore, after finishing the natural frequency extraction, only the modes of interest will be used for further analysis. For instance, if we have only three modes of frequency in range of interest, it is not necessary to evaluate all the modes for modal dynamic analysis. In this case it is better to consider the range of frequency 1.5 times bigger than the operational frequency range [87, 88].Moreover, the natural frequency of the system in two different conditions, i.e. neutral position of sleeve and engaged sleeve with clutch body, were investigated.

Transient modal dynamic

The extracted natural frequency will be used to study modal dynamic behavior of the system. Due to the nature of synchronizer as a mechanism with transient behavior, the "Transient Modal Dynamic" solver was chosen to study the dynamic behavior of the system. To perform the transient modal dynamic analysis, the previous model is extended. The boundary conditions applied to the shafts and different shaft configurations were remain as previous section. The FE model consists of two different steps. The first step is the same as for the previous model and is used for natural frequency extraction. In the second step, a time response analysis was performed and the FE results are converted to the frequency domain by using Fast Fourier Transform (FFT). The clutch body ring and the hub are free to rotate $(UR_x \neq 0)$ and synchronizer rings and sliding sleeve are free to rotate and move

axially (U_x, ($UR_x \neq 0$)). The base motion technique from ABAQUS was used to provide the effect of rotational speed on the rotating parts. The surface to surface penalty contact method was applied to the contact pairs of different synchronizers (for more detail see section contact modeling). The different friction coefficients were taken from experimental test and based on experimental data from Table 2.1, the different angular velocities were assigned to the input and output shafts. In the second step the system was excited with a ramp force in a short period of time and after excitation of the system the load was removed. This kind of loading has an impulsive effect on the system. Figure3.22 shows the applied load as the excitation force in a short period of time. The loading time was taken from experimental test rig for different type of synchronizers. The damping ratio in this study was set to 2% while the critical damping of the system was 3% [88]. Figure 3.23 demonstrates the different steps of FE modeling in ABAQUS.

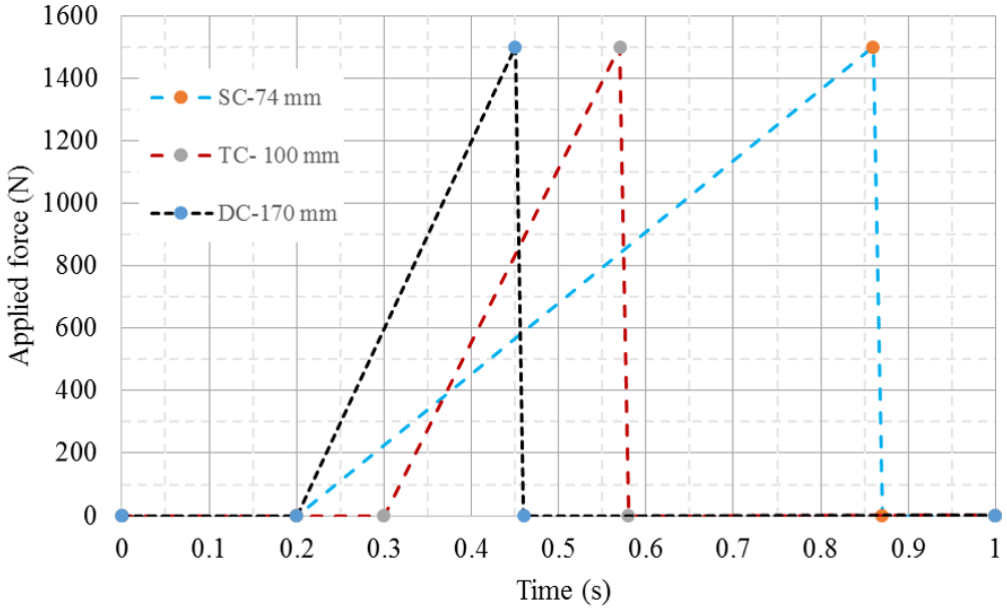

Fig. 3.22 The applied load as the excitation force in a short period of time.

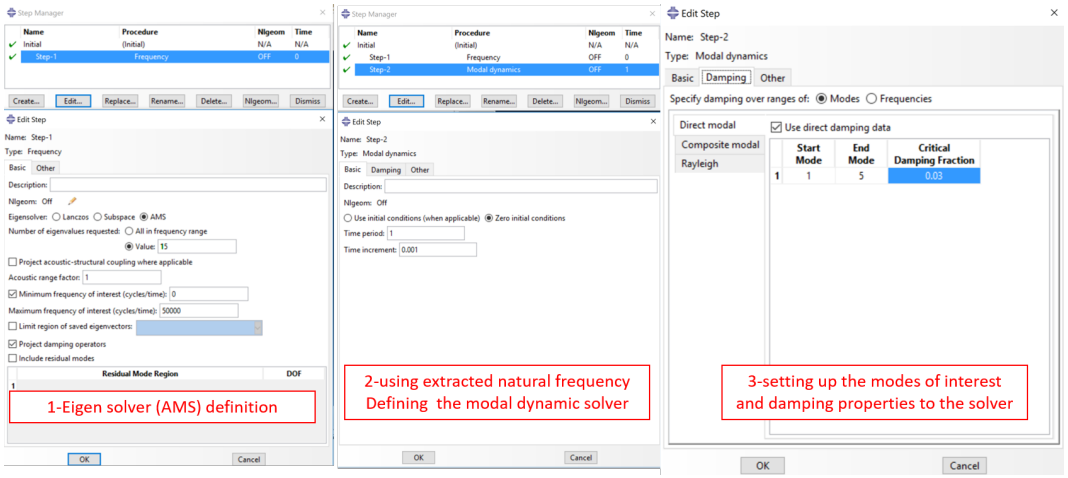

Fig. 3.23 The different steps for setting up the modal dynamic solver in ABAQUS.

3.4.8 Rigid MBD model

Rigid MBD model with nominal dimensions

To assess the overall dynamic behavior of a multibody mechanism regardless the stress- strain behavior, the rigid multibody dynamic analysis was proposed [69]. To generate the rigid bodies, the geometry should be converted to the shell body. After converting solid to shell geometries, all components should be meshed again. Figure3.24 demonstrates the converted solid geometry of synchronizer hub to the shell body.

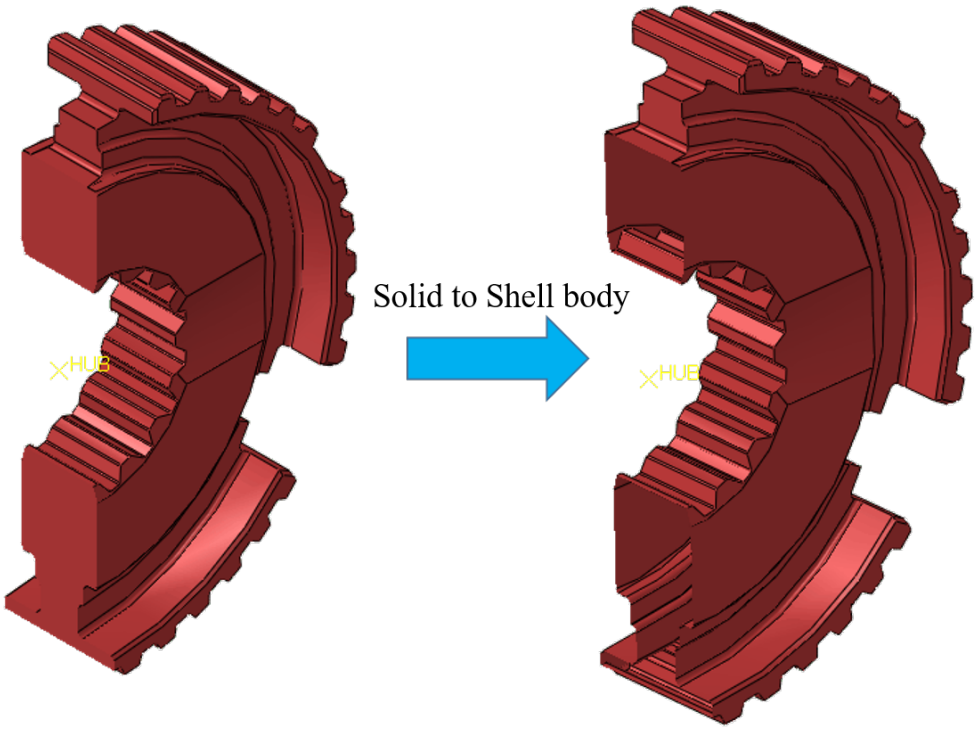

Fig. 3.24 The converted solid geometry of synchronizer hub to the rigid shell body.

In this section, all parts of the SC-74, DC-170 and TC-100 synchronizers were meshed with four node rigid shell (RS4) elements. The size of meshes were based on the previous mesh convergence study. However, the size of meshes are not effective in rigid body analysis. The surface-to-surface pair contact method between components was implemented considering the penalty method for the purpose of the friction coefficient modeling. The dynamic friction coefficient of the friction cones was taken from experiment and applied for each type of synchronizer. The ABAQUS connector element library explained before was used to provide the available degree of freedom based on Table 3.3 information. Gruebler-Kutzbach equation calculates possible DOF for different type of synchronizers as it is introduced in Chapter 2.The available degree of freedom for SC-74, DC-170 and TC-100 were 14, 16 and 18 respectively. The Dynamic/Implicit solver was utilized to solve the rigid MBD model. The total time of simulation was same with experimental time and each increment was assumed 1E-6 s. As mentioned previously, only cylindrical and revolute joints were used in this simulations. The reference points of the sliding sleeves were subjected to ramp axial load within 180-220 ms for different synchronizers (see Table 2.1). Figures 3.25 (a), (b) and (c) indicate the applied boundary conditions on

the different synchronizer models. In these models, due to the element stiffness, only one side of synchronizer with single stroke is simulated. Table 2.1 shows the physical characteristics of different components for the three different types of synchronizers that were used in MBD model.

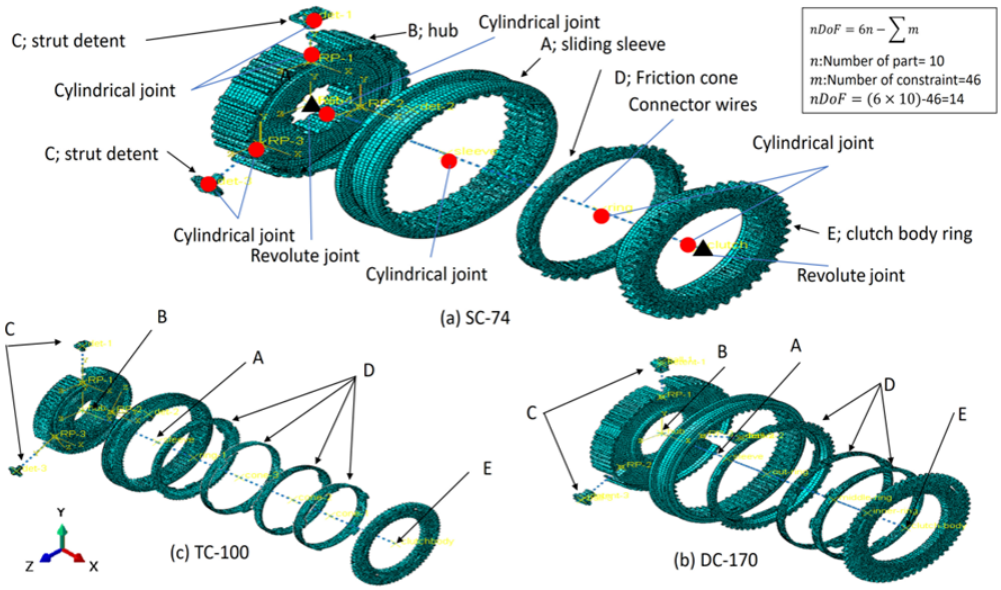

Fig. 3.25 The applied boundary conditions for rigid MBD analysis of (a) SC-74, (b) DC-170 and (c) TC-100 synchronizer models.

MBD model with dimensional tolerance (sensitivity analysis)

Given the manufacturing process, a tolerance dimension will be applied to all synchronizer components. The applied dimension on the friction cones influences the performance of the synchronizer mechanism. To investigate the effect of this phenomena on the overall behavior of single cone synchronizer (SC-74), three different tolerance levels were considered in this step. The nominal dimension, the upper bound tolerance for the cone's clutch body and the lower bound tolerance for the synchronizer cone were the three scenarios that are used in this study. Figure 3.26 shows the three geometry configurations that are used for rigid MBD model. The size of elements, applied load and boundary conditions, applied constraints and DOFs were the same as the model with nominal dimensions.

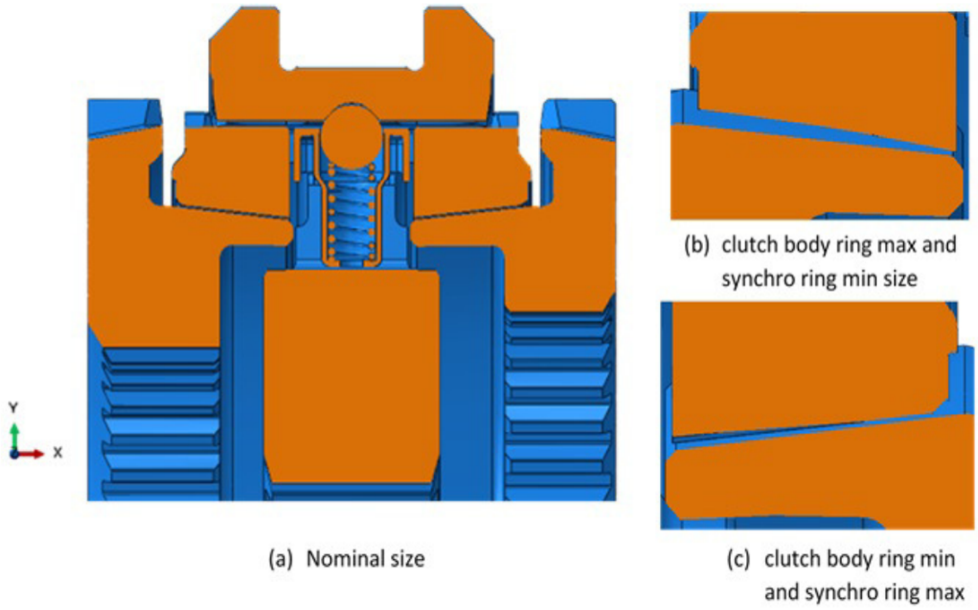

Fig. 3.26 The three friction cones configurations for sensitivity model.

To study the effect of geometry, the ratio between applied force and reaction force of the MBD model in synchronization process can be introduced (force ratio error). The force ratio error can be written as:

$$F_{err} = 1 - \frac{F_{app}}{F_{RA}} \tag{3.56}$$

where F_{app} is the actuating force over simulation and F_{RA} is the reaction force from synchronizer hub. By plotting this factor over the time a fluctuated curve can be obtained. Applying a linear interpolation on this curve gives a linear straight line. Calculating the slope of this line will show the effect of different geometries on the dissipated force of the system. As much as the slope of this line is close to zero, which means that less force was dissipated inside the system and, with increasing the slope of the line, the effect of geometry changes can be observed.

3.4.9 Flexible MBD model

Flexible MBD – Full model

To better understand the dynamic behavior of a synchronizer, a deformable FE model was proposed in this section. The major difference between this model and the rigid model is the type of used elements. In this step the deformable solid element (C3D4R) with second order FE formulation were used. In fact, the model is same with FE model that was used for modal analysis. The solver of this model also was the Dynamic/Implicit. The total time was the same with rigid MBD model however the time increment assumed with smaller time seed (1E-9 s). All the operational and applied loading condition (see Figure 3.25)) were repeated same as the rigid MBD model and the data were taken from Tables 2.1, 3.3 and 3.4. All the connector elements, material properties and frictional properties were similar to the previous MBD models for different synchronizers.

The surface to surface penalty contact method were applied on the models. Moreover, to avoid instability in contact areas, the contact initialization and contact stabilization options were activated for flexible MBD model. In the start of simulation (start of rotation) all the parts experiences a high acceleration with a negative effect on the corresponding stress. Using contact initialization helps to relieve the stress value in normal range. In other word this option decrease the impulsive impact between two contact surfaces. After starting the rotation of the system, the contact stabilization will control the contact surfaces in a stable condition. It helps to avoid numerical convergence problem over the simulation. After finishing the simulations, the balance of energy for each simulation should be performed. This procedure can be a good tool to verify the numerical simulation for a dynamic problem. The full expression of energy balance for a FE model can be written as follow [11]:

$$\begin{aligned} ExternalWork = {} & KineticEnergy + InternalEnergy + ViscousDissipation \\ & + StaticDissipation + FrictionDissipation + HeatDissipation \\ & + ContactElasticEnergy - ContactDiscontinuityWork - TotalEnergy \end{aligned} \quad (3.57)$$

Flexible MBD – Sub model

In order to reduce the calculation time, a sub model for each synchronizer was proposed. In this section, the only parts involved in the synchronization phase are considered and the synchronizer hub, sliding sleeve and strut detents were neglected. The axial load as equal as the experiment was applied to the synchronizer ring and the time of synchronization, friction dissipation energy and contact pressure on friction cones were investigated. These factors are the main factors that can be identified as the dynamic characters of the system. It means that these three factors (synchronization time, friction dissipation energy and contact pressure on friction cones) can be investigated as the responses of a synchronizer mechanism. All the physical conditions, element size and element types were same with previous model. However the degree of freedom and number of elements of this model is lower than previous model. Figure 3.27 compare the full and sub model for flexible MBD analysis.

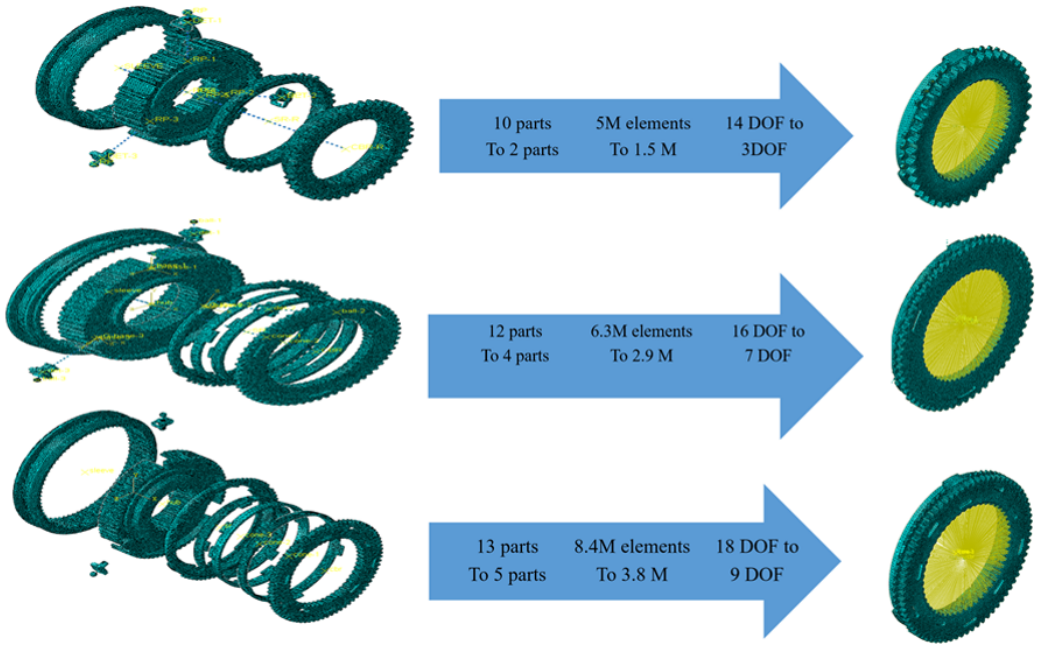

Fig. 3.27 Comparison between the full and sub model for flexible MBD analysis.

The main purpose of this methodology is to collect data for optimization process. Although the results of the sub-models are less accurate than the full models, considering that the overall behavior of the system is close to the experiments, it

is possible to rely on the results of these models to calculate the synchronization time and energy loss of the system. On the other hand the time of calculation can be increased 100 times faster. Therefore, this method is acceptable for providing the data for optimization technique. For the number of components were reduced from 10 to 2, 12 to 4 and 13 to 5 for SC-74, DC-170 and TC-100 respectively. In addition, the DOFs of the system are reduced from 14 to 3, 16 to 7 and 18 to 9.

3.5 DOE technique

To analysis the data and examine the effective variables affecting synchronization process, the DOE technique was utilized in this study. The first step of DOE method is to define the influential main factors, those affecting synchronizers and evaluation of the system response is the next step of design of experiments. In this study, two levels have been taken into account for all the main factors. The half central composition regarding the response surface methodology (RSM) method was considered as the DOE method to examine the numerical data. The reason to choose half central composition was reducing the number of runs. In addition, the RSM was selected to generate the quadratic response surface in order to achieve more accurate results. Six main factors are friction coefficient (mu), Applied force (Fapp), time of applied force (Tapp), the difference of angular velocities between input and output shafts (d-omega), applied inertia and drag torque (Td). Tables 3.7, 3.8 and 3.9 10 show the main factors for three different synchronizers (SC-74, DC-170 and TC-100) which were used for DOE analysis. The upper and lower thresholds were considered based on the operational conditions of each synchronizer. These values were converted to the coded value by normalizing between -1 to 1. Three different responses for all cases were defined i.e. synchronization time (T_s), friction dissipated energy (ALLFD), and the maximum contact pressure between friction cones (C_p).In this study due to numerical run no replication were considered. Moreover the number of center points for each case were assumed as one. In other word the results of a numerical simulation has no fluctuation and the results repeatability can be achieved for every single simulation.

Considering half central composition (quadratic) method with 6 continues factors, 3 different responses and 1 center point generates 45 randomized trials for every synchronizer type. The design tables for SC-74, DC-170 and TC-100 are available

Table 3.7 The main factors for SC-74 synchronizers were used for DOE analysis.

Factor	Name	Units	Min	Max	Coded	Values	Mean	Std. Dev.
A	Mu	–	0.035	0.114127	-1.000=0.05	1.000=0.1	0.075	0.0212
B	Fapp	N	473.966	1726.03	-1.000=700	1.000=1500	1100	340.23
C	Tapp	s	0.07174	0.228254	-1.000=0.1	1.000=0.2	0.15	0.0425
D	d-Omega	rad/s	558.729	1341.27	-1.000=700	1.000=1200	950	212.648
E	Inertia	kg/m^2	0.1217	0.278254	-1.000=0.15	1.000=0.25	0.2	0.04252
F	Td	N.m	0	12.8254	-1.000=0	1.000=10	5.054	4.1682

Table 3.8 The main factors for DC-170 synchronizers were used for DOE analysis.

Factor	Name	Units	Min	Max	Coded	Values	Mean	Std. Dev.
A	Mu	–	0.0558	0.1341	-1.000=0.07	1.000=0.12	0.095	0.0212
B	Fapp	N	473.96	1726.03	-1.000=700	1.000=1500	1100	340.237
C	Tapp	s	0.0717	0.2282	-1.000=0.1	1.000=0.2	0.15	0.0425
D	d-Omega	rad/s	302.22	1397.78	-1.000=500	1.000=1200	850	297.708
E	Inertia	kg/m^2	0.0022	1.0977	-1.000=0.2	1.000=0.9	0.55	0.2977
F	Td	N.m	0	12.825	-1.000=0	1.000=10	5.0543	4.168

in Appendix 1. After generating the design tables, each simulation with different randomized conditions (different main factor values) was performed. The responses of each simulation will be imported to the design table. After finishing every 45 trails for each synchronizer type, the statistical analysis will be implemented on the extracted data. In this study the effects of main factors and their interaction were considered. Therefore, the ANOVA analysis were performed to analyze the data statistically. To evaluate the accuracy of the result, four main tools such as normal distribution, residual error, run vs. predicted error and Box-Cox transformation were used. Implementation of these four criteria verify the accuracy of the results. Furthermore, the outcome of the ANOVA analysis leads the empirical models to predict all responses. Using these empirical models helps to predict the system responses over the upper and lower thresholds without performing additional simulation.

3.5.1 Sensitivity analysis through DOE method

As mentioned in the previous sections, changing the tolerance dimension of the friction cone can influences on the dynamic responses of the synchronizer. In order to evaluate the significant parameters by changing the geometry of the friction cones, a new design table was generated. In this step, the effect of drag torque was

Table 3.9 The main factors for TC-100 synchronizers were used for DOE analysis.

Factor	Name	Units	Min	Max	Coded	Values	Mean	Std. Dev.
A	Mu	–	0.0586	0.1213	-1.000=0.07	1.000=0.11	0.09	0.0170
B	Fapp	N	473.966	1726.03	-1.000=700	1.000=1500	1100	340.237
C	Tapp	s	0.0717	0.2282	-1.000=0.1	1.000=0.2	0.15	0.04252
D	d-Omega	rad/s	558.729	1341.27	-1.000=700	1.000=1200	950	212.648
E	Inertia	kg/m^2	0.3304	1.26953	-1.000=0.5	1.000=1.1	0.8	0.2551
F	Td	N.m	-2.8254	12.825	-1.000=0	1.000=10	5	4.252

neglected and cone angle were considered in three different levels namely: nominal, minimum and maximum tolerance range. Therefore, the cone angle with three levels is a categorical factor and it is not like previous DOE analysis. However the other factors and all responses are same with previous section. Table3.10 shows the design table for SC-74 synchronizer. Due to complexity of the problem this analysis was performed only on the single cone synchronizer.

Table 3.10 The main factors for SC-74 with different geometries were used for DOE analysis.

Factor	Name	Units	Min	Max	Coded	Values	Mean	Std. Dev.
A	Mu	–	0.035	0.114127	-1.000=0.05	1.000=0.1	0.075	0.0212
B	Fapp	N	473.966	1726.03	-1.000=700	1.000=1500	1100	340.23
C	Tapp	s	0.07174	0.228254	-1.000=0.1	1.000=0.2	0.15	0.0425
D	d-Omega	rad/s	558.729	1341.27	-1.000=700	1.000=1200	950	212.648
E	Inertia	kg/m^2	0.1217	0.278254	-1.000=0.15	1.000=0.25	0.2	0.04252
F	alpha	—	min	max	—-	—-	nominal	—-

Similarly, regarding the half central composition with 5 continues factors, 1 categorical factor, 3 responses, 1 center point and no replicate, the table of experiments were generated. In this case 82 experiments have been performed. The completed design table with extracted responses are available in appendix 1. After filling up the corresponding responses to the related tabs the ANOVA analysis were implemented and verification procedure was performed. At the end of this step the empirical models for different responses are available to illustrate the response of the system with different tolerance dimensions.

3.6 Summary of this chapter

This chapter presents the research methodology implemented to perform this research that includes analytical models, development of different MBD models and carrying out experimental and validation trials. The next chapter will discuss the outcome results through presented methodology.

Chapter 4

Results and Discussion

4.1 Introduction

The results of an integrated FE model are presented in this chapter. At the first step, the natural frequencies of different synchronizer mechanisms were extracted. Extracted natural frequencies of a system were used to evaluate the modal dynamic behavior of synchronizers with different boundary conditions. By changing the solver of the FE model, an MBD model with two different approaches, namely the rigid model and flexible model, were introduced. The results of the rigid model are appropriate for evaluating the overall behavior of the system regarding computational time. Moreover, the result of a sensitivity analysis based on the rigid MBD model was presented and the effect of the geometrical error on the performance of synchronization was addressed. Furthermore, the results of the flexible MBD model demonstrate much accuracy compared with rigid model. The results of the analytical model in terms of estimation of synchronization time were compared with experimental and numerical results. The results of the flexible model were used for statistical analysis through the DOE method. Performing several FE trials leads to complete the DOE design table and by carrying out the ANOVA analysis the main factors of different synchronizers were identified. In every section of this chapter, a discussion was carried out to clarify the validity of the results.

4.2 Numerical approach

4.2.1 Natural frequency of synchronizer mechanism

In order to perform FE analysis, the size of the mesh is the most important factor that has some effects on the numerical results. Therefore, a mesh convergence study was carried out on synchronizer's components. After reaching the stable numerical result for each component, the size of the mesh remained the same for all the following FE simulations. Figure 4.1, 4.2 and 4.3 show the natural frequency of every separate part of SC-74, DC-170, and TC-100, respectively (after mesh convergence study).

Figure 4.1 shows that all components have six rigid modes. The maximum natural frequency is for strut detents due to the weight of these parts. The minimum frequency is related to the synchronizer ring. It can be interpreted that the stiffness of the synchronizer ring is lower than the other components: hence the natural frequency of this component is lower than other parts.

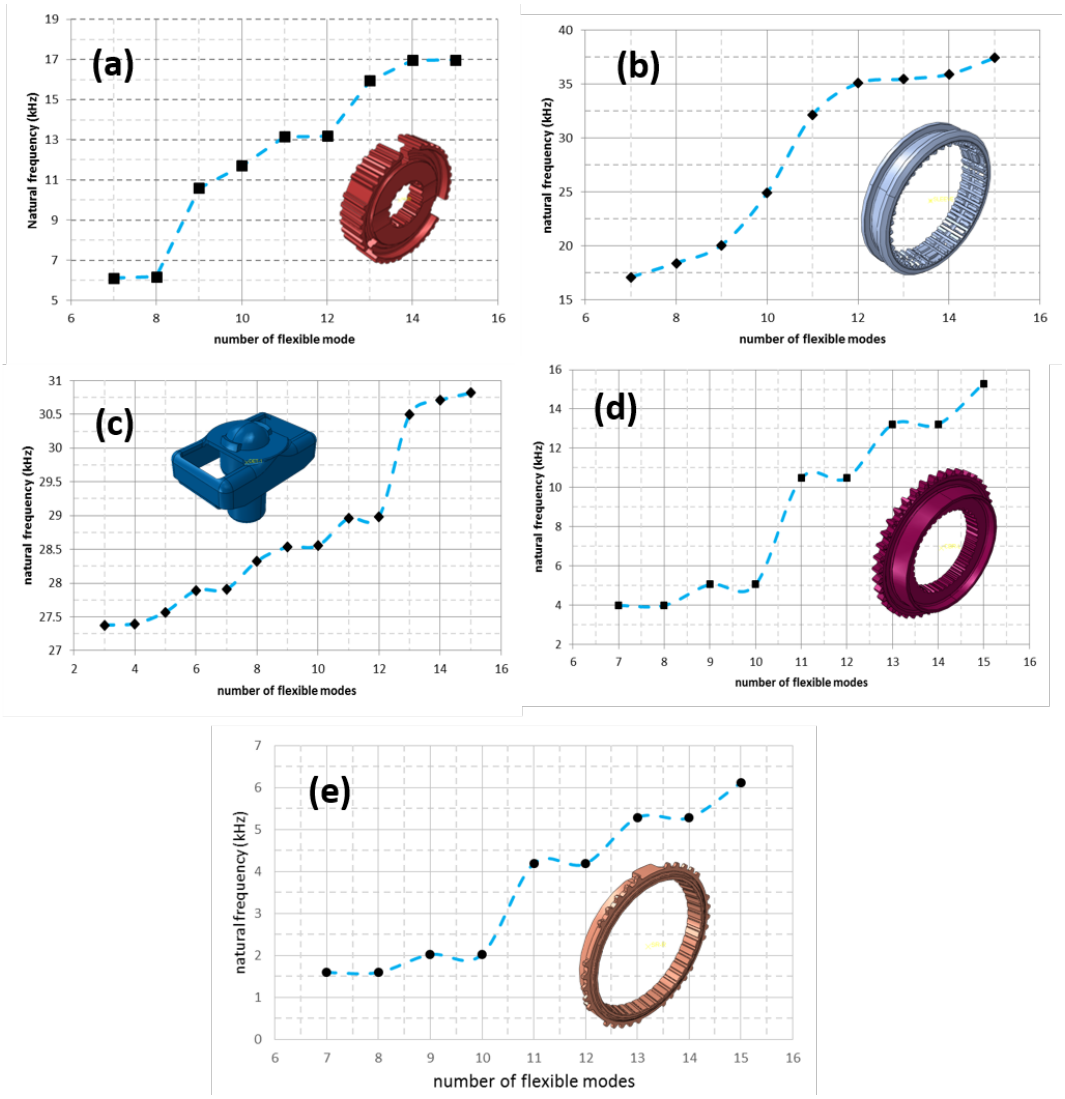

Fig. 4.1 The natural frequency of separate parts of SC-74 after mesh convergence study.

Unlike SC-74, the results of natural frequencies for DC-170 show that the number of rigid modes decreased. Figure 4.2 shows the mesh converged results of natural frequencies for different parts of the double-cone synchronizer. The maximum frequency in this synchronizer is for the strut detent and the minimum frequency is related to the friction cone with minimum stiffness among all synchronizer parts. The comparison of results of same components between the single-cone and double-cone synchronizers shows the effect of the size of each component on the natural frequency of that part. For example, by comparing the natural frequency of the hub from two different synchronizers (SC-74 and DC-170), it can be said that, by

increasing the outer diameter of the hub, the first mode of frequency decreased more than two times. The significant difference between these two parts is the value of outer diameter. Therefore, the effect of the size of the component on the extracted natural frequency can be observed.

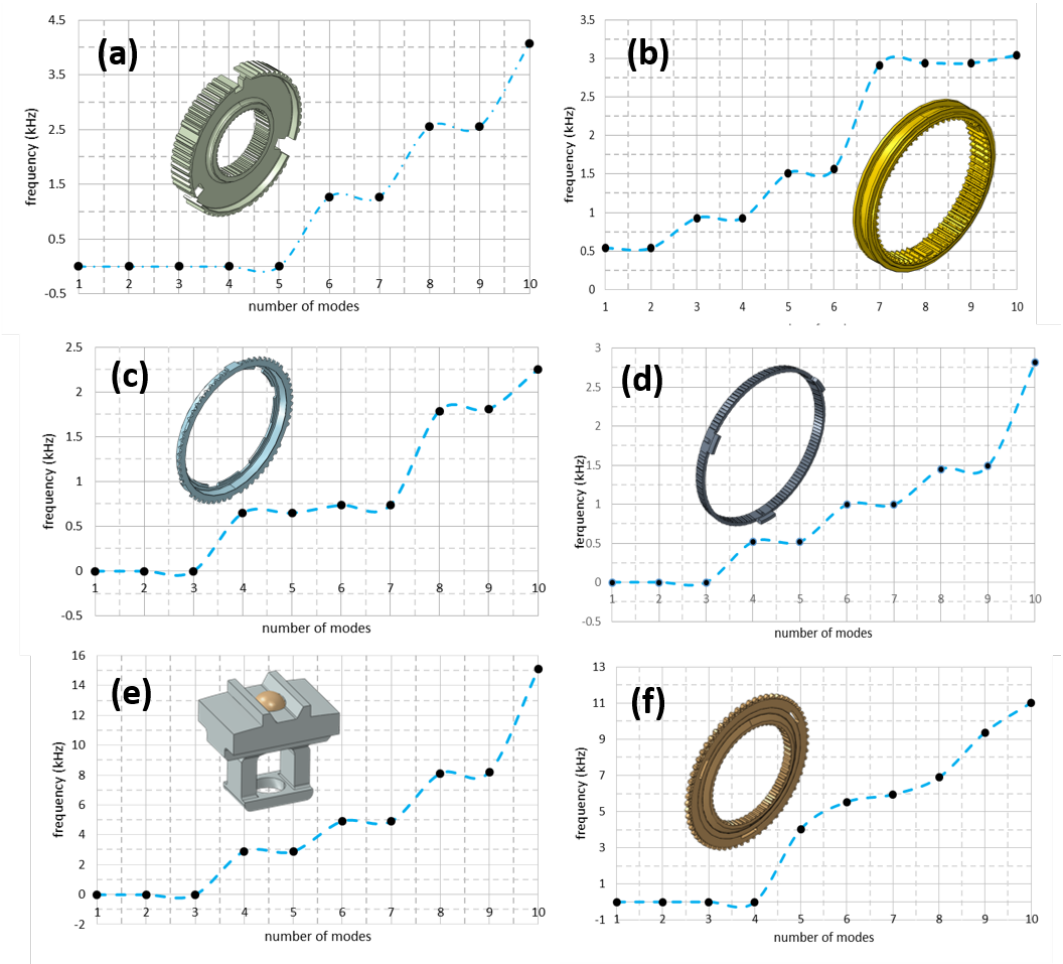

Fig. 4.2 The natural frequency of separate parts of DC-170 after mesh convergence study.

In both single-cone and double-cone synchronizers, the maximum frequency range is related to the strut detent and the minimum natural frequency is for the third friction cone. Comparing the first natural frequency of the hub between SC-74 and DC-170 proves that by increasing the size of the component, the natural frequency will decrease.

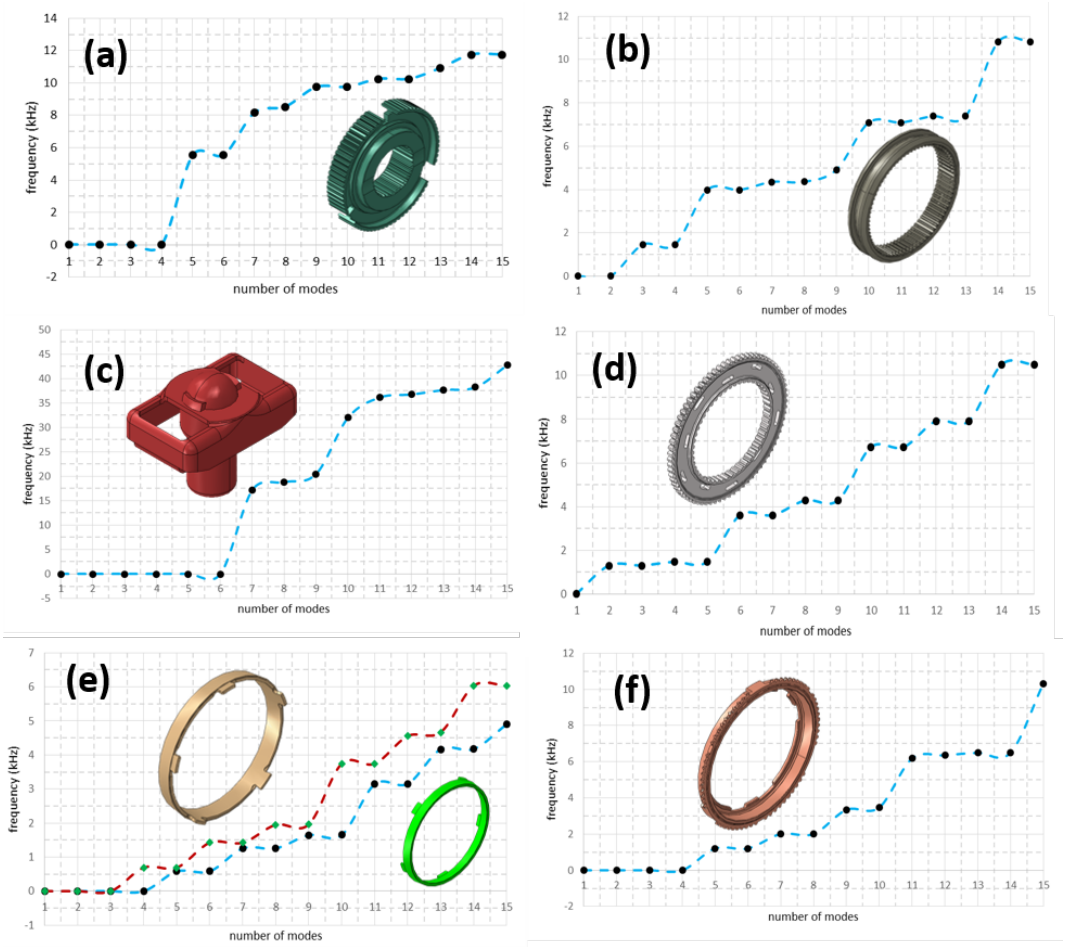

Fig. 4.3 The natural frequency of separate parts of TC-100 after mesh convergence study.

After natural frequency's extraction of different components and obtaining the best mesh quality, the full synchronizer models were assembled, and the natural frequency of the whole system with the free-free boundary condition was examined. Figure 4.4 shows the first ten mode shapes for SC-74. In this model, the four initial modes are rigid modes and the flexible modes start from the fifth mode of frequency.

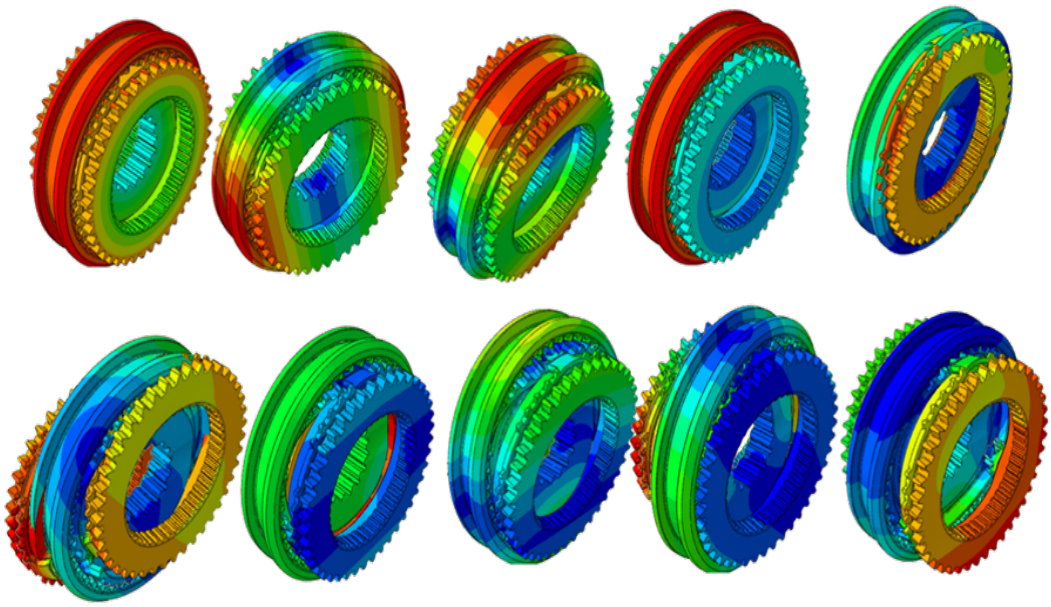

Fig. 4.4 The first ten mode shapes of frequency with free-free condition for SC-74.

Changing the position of the sleeve in two main conditions (neutral and engaged) can have some effects on the natural frequency of the system. Figure 4.5 (a), (b) and (c) presents the effect of sleeve position on the natural frequency of the system for the different types of synchronizers. The first flexible mode for SC-74 was at the fourth mode of frequency and it was 1 kHz in the neutral state and increased to 4.9 kHz when it was engaged. For the next mode, the increasing of a natural frequency from the neutral to engaged state can be observed. The critical damping ratio of the system also can be extracted from the eigensolver. In this case, the critical damping ratio was 3.125%. The natural frequency at the neutral state for DC-170 and TC-100 was 980 and 490 Hz, respectively. It should be mentioned that the first flexible mode for DC-170 was at the third mode whereas the fifth mode was the first flexible mode for TC-100. In all synchronizer mechanism, by changing the position of the sleeve from the neutral to engaged condition, the natural frequency of all modes will increase. Increasing the stiffness of the system is the reason of the higher frequency at the engaged conditions. However, adding the input and output shafts to the system will have an effect the system's natural frequency. Therefore, in the next step, the connected shafts were considered as system components.

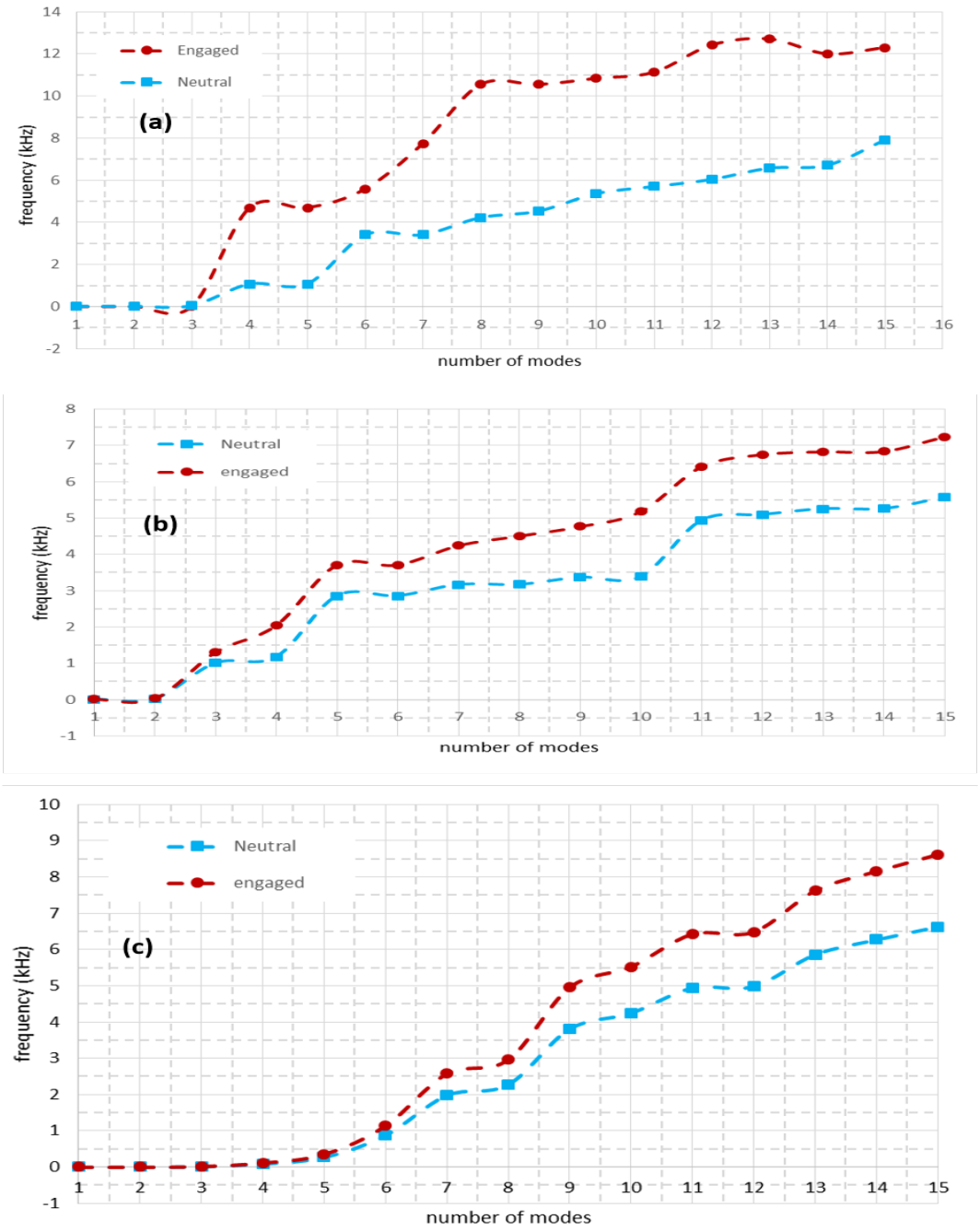

Fig. 4.5 The effect of sleeve position on the natural frequency of the system for (a) SC-74, (b) DC-170 and (c) TC-100.

4.2.2 Transient modal dynamic analysis of synchronizer mechanism

In this study, four different shaft configurations were used to provide input and output rotational speeds. The detail of shaft size was discussed in chapter three. Adding different shafts to the system changes the natural frequency of the system. The extracted natural frequencies were used to evaluate the transient modal dynamic behavior of the synchronizer. Figure 4.6 shows modal responses of SC-74 with different shaft size configurations. The results show that the maximum amplitude is related to the longest shaft length with the minimum shaft diameter, and the minimum deflection of the system is for the shortest shaft length with the maximum shaft diameter. The resonance frequency for different cases was varied between 30 to 35 Hz. The critical resonance frequency occurred at 35 Hz on the $L_{max} - D_{min}$ conditions. Since the range of interest in this mechanism is lower than 100 Hz the next frequency amplitudes were neglected.

The same shaft configurations were considered for double-cone and triple-cone synchronizers. Figure 4.7 illustrates the modal responses of DC-170 with different shaft configurations. Similarly, the critical resonance occurred when the DC-170 was connected to the shaft with the maximum length and minimum diameter $(L_{max} - D_{min})$. Surprisingly, the resonance frequency in DC-170 happened in a low-frequency range. The critical condition in all cases will happen at around 8 Hz.

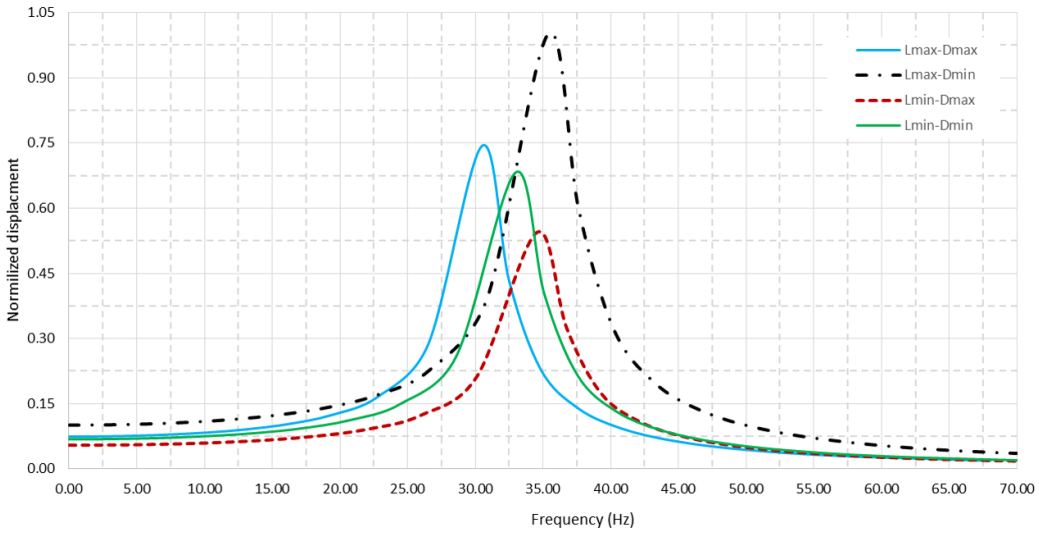

Fig. 4.6 The modal responses of SC-74 with different shaft size configuration.

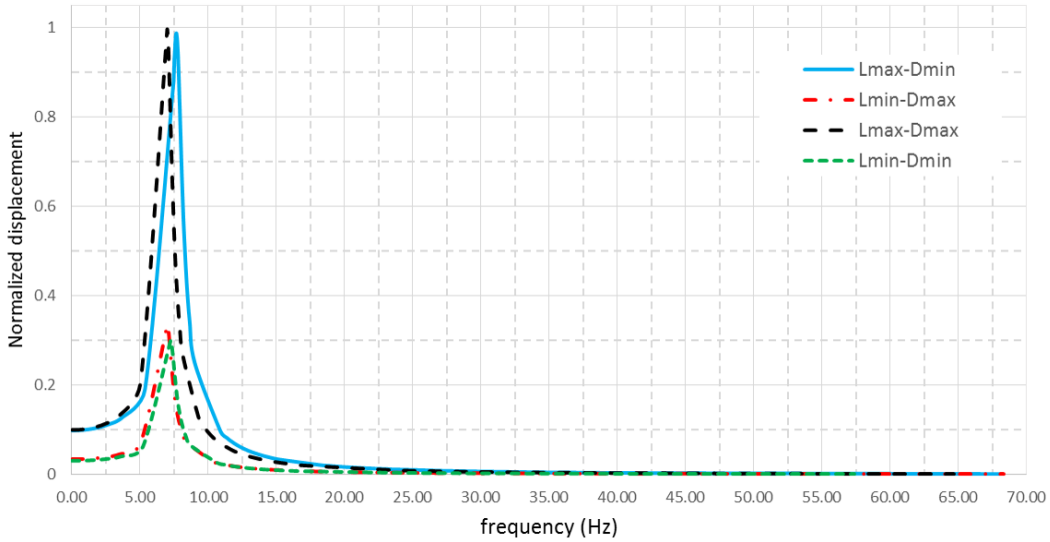

Fig. 4.7 The modal responses of DC-170 with different shaft configurations.

Figure 4.8 depicts the frequency responses of transient modal analysis of TC-100 with different shaft size configurations. It can be seen that the critical condition is related to the shaft with maximum length and minimum diameter $(L_{max} - D_{min})$.The resonance frequency for TC-100 was around 15 Hz. It shows that the size and mass of the synchronizer mechanism will shift the resonance frequency in the transient frequency region. Moreover, comparing the results of different synchronizers show that the size and mass of the synchronizer were effective on the modal responses of the system. The results show that in all synchronizers, the shaft configuration has an effect on the modal responses of the synchronizer. Figure 4.9 shows the maximum amplitude of each synchronizer on the critical condition. The results show that the maximum deflection is related to DC-170 with 250 $\mu m$and TC-100 was in the middle range with 112 μm and SC-74 with 50 μm has the minimum amplitude. In all cases, the connecting shafts were the same, however, the type of synchronizer has the dominant effect on the modal response of the system and it is highly dependent on the mass and size of mechanisms.

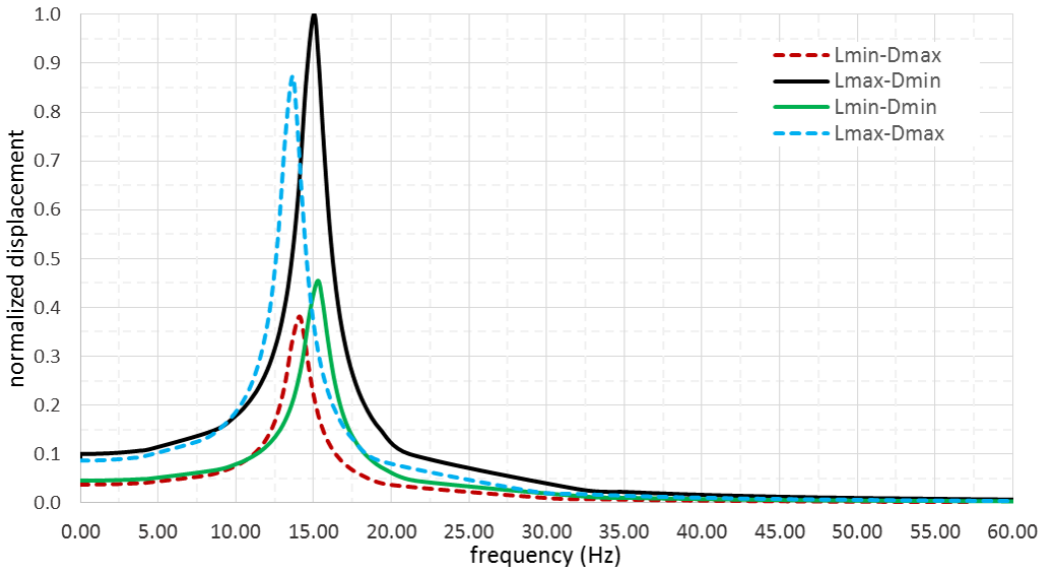

Fig. 4.8 The modal responses of DC-170 with different shaft configurations.

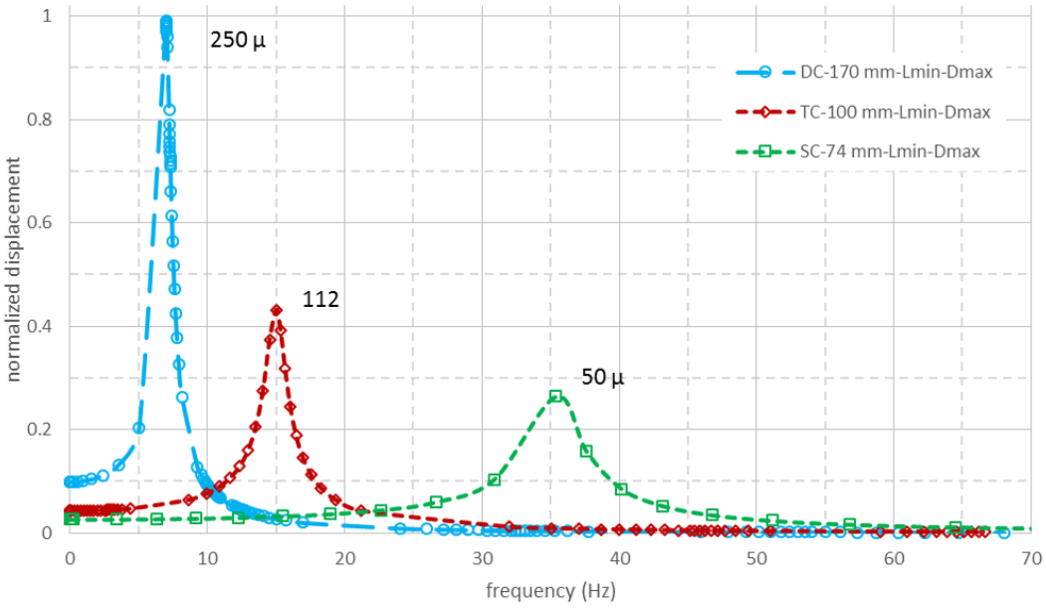

Fig. 4.9 The maximum modal responses of different synchronizers (SC-74, DC-170 and TC-100).

Effect of Sleeve position on the modal response of system

The geometrical tolerances in the manufacturing process of all assemblies should be considered. Therefore, the effect of this issue will be discussed in this section. In this case, the sleeve position can be varied in three conditions, namely: nominal, minimum and maximum backlash between the sleeve and synchronizer ring. In other words, the clearance between the fork and sleeve can be varied in three states. Figure 4.10 compares different sleeve positions in different shaft configurations for SC-74. The results show that the critical situation is related to the $L_{max} - D_{max}$ condition. It shows that the critical condition changed from $L_{max} - D_{min}$ to $L_{max} - D_{max}$. Moreover, the minimum backlash, in this case, increases the maximum amplitude more than 1.8 times higher than the nominal condition. In other cases, the minimum backlash increased significantly. It can be said that, in all shaft configurations minimum, maximum, and nominal backlash were the critical conditions, respectively. In addition, by changing the nominal position of the sleeve, the modal frequency of synchronizer will be shifted. However, the resonance frequencies in all cases were around 25-40 Hz.

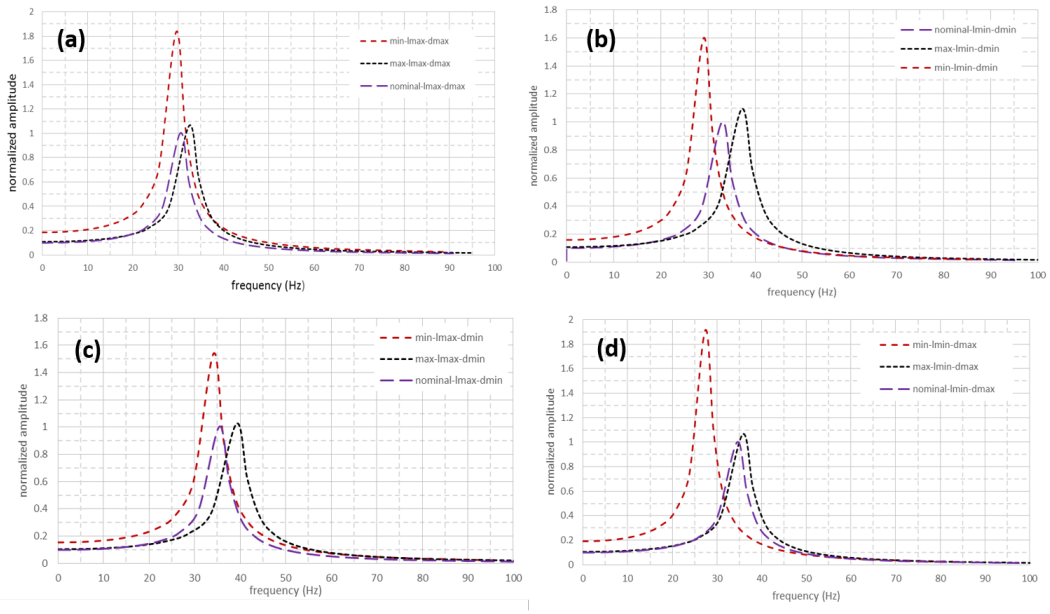

Fig. 4.10 Different sleeve positions in different shaft configurations for SC-74.

Figure 4.11 shows the transient modal responses of DC-170 with different sleeve positions and different shafts size configurations. The critical conditions are related

to $L_{max} - D_{min}$ when the sleeve's position is in the minimum state. Changing the sleeve position from a nominal state to the minimum position increases the amplitude 1.8 times higher. In the other cases, changing the position of the sleeve from nominal position increased the amplitude up to 1.9 times higher than nominal conditions. The range of frequencies in all cases were varied between 6-9 Hz.

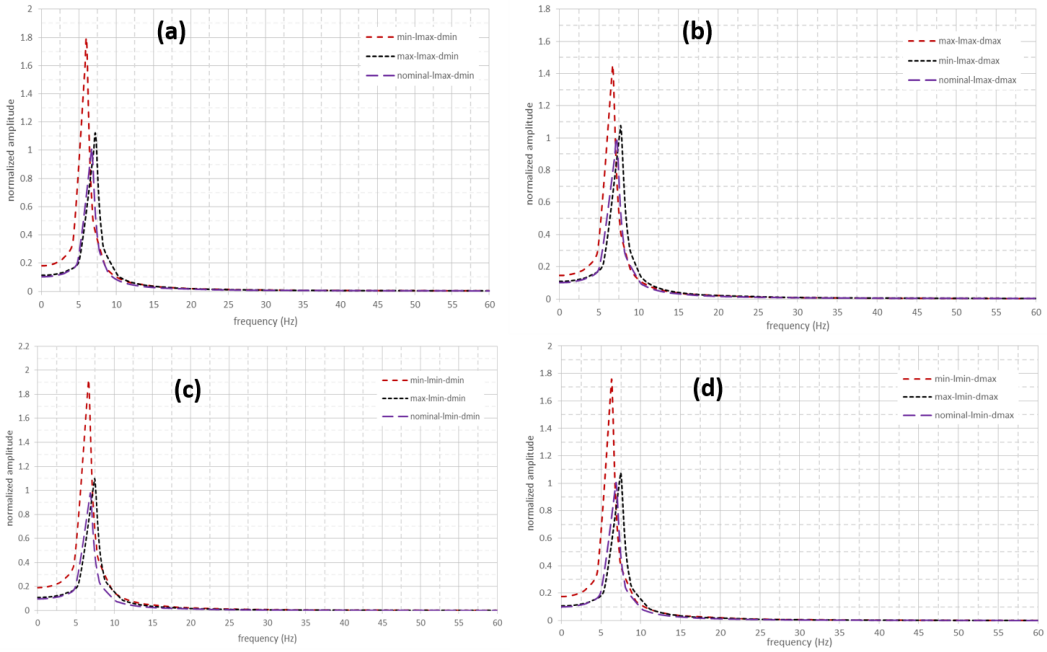

Fig. 4.11 Different sleeve positions in different shaft configurations for DC-170.

The results of the modal dynamic analysis for TC-100 show that the critical amplitude can be observed on $L_{max} - D_{min}$ when the sleeve's position is in the minimum state. Figure 4.12 shows that changing the position of the sleeve from nominal condition to the minimum position can increase the maximum amplitude more than 1.4 times. The range of frequencies were varied between 13.5-16.5 Hz. In both single and double cone synchronizers, changing the position of the sleeve from nominal conditions will increase the maximum amplitude in all shaft configurations.

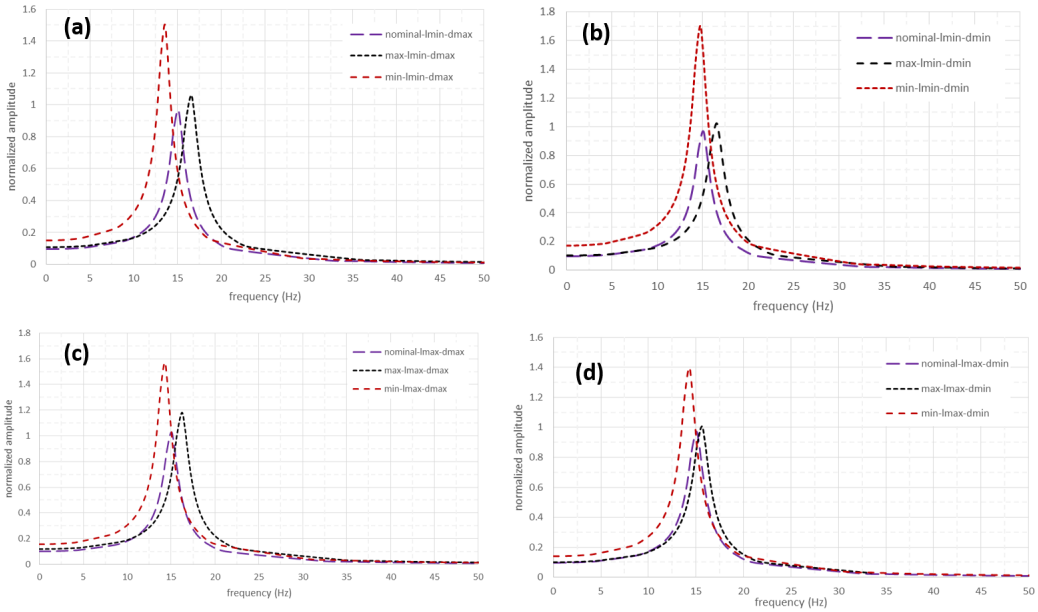

Fig. 4.12 Different sleeve positions in different shaft configurations for TC-100.

Figure 4.13 compares the critical condition of modal responses of different synchronizers when the sleeve position changed from nominal conditions to the minimum backlash of the system. It can be seen that by decreasing the clearance between the sleeve and the synchronizer ring, the maximum amplitude increases from 50 μm to 92 μm, 100 μm to 141 μm and 250 $\mu m$to 436 μm in SC-74, DC-170 and TC100 respectively. Table 4.1 demonstrates all modal dynamic results of SC-74, DC-170, and TC 100 regarding the shaft configurations and backlash conditions.

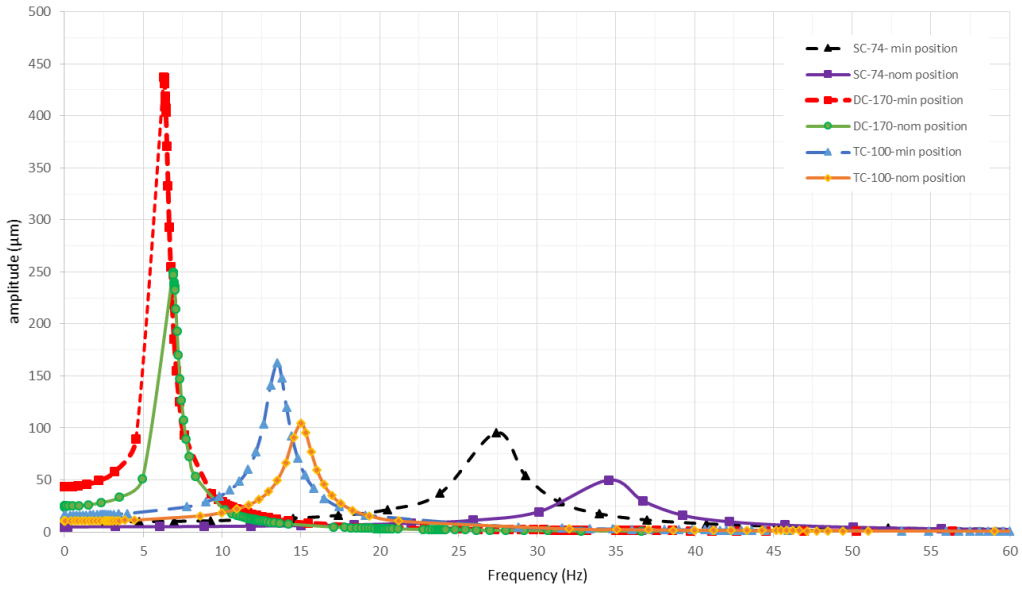

Fig. 4.13 The modal responses of different synchronizers regarding nominal and minimum backlash.

Table 4.1 The modal dynamic characteristics of SC-74, DC-170 and TC 100 under different operational conditions.

	Backlash state	Lmin-Dmax		Lmin-Dmin		Lmax-Dmax		Lmax-Dmin	
		FREQ (Hz)	AMP (µ)	FREQ (Hz)	AMP (µ)	FREQ (Hz)	AMP (µ)	FREQ (Hz)	AMP (µ)
SC-74	min	27	51.952	29.1	54.56	29.6	92	34.1	57.75
	nom	34.6	27.2	33	34.1	35.4	50	30.5	37.5
	max	35.8	28.832	37.2	37.169	32.5	53	39.2	38.625
DC-170	min	6.32	137.456	6.6	144.576	6.76	357.5	5.96	436.48
	nom	7.11	78.1	7.35	75.3	7.03	250	7.75	248
	max	7.5	83.567	7.57	78.312	7.76	265	7.14	275.28
TC-100	min	13.5	64.175	14.7	74.256	14.3	175.84	14.32	141.12
	nom	14.01	42.5	15.4	43.68	15	112	14.1	100.8
	max	16.5	45.05	16.45	44.5536	16.2	132.16	15.6	101.808

4.2.3 Rigid MBD model

The results of rigid MBD model for different synchronizers are presented in this section. Figure 4.14 depicts the difference between angular velocities of input and output shafts for SC-74. Comparing the results of MBD model and experimental

results shows a good agreement between experimental and numerical data. Due to the stiffness of element in this model at the first indexing phase of synchronization, some error can be observed. However, the overall behavior can be useful to evaluate the dynamic behavior of the model. The time of synchronization in this model was estimated around 0.69 ms. After this time, the difference between velocities of input and output shafts becomes null.

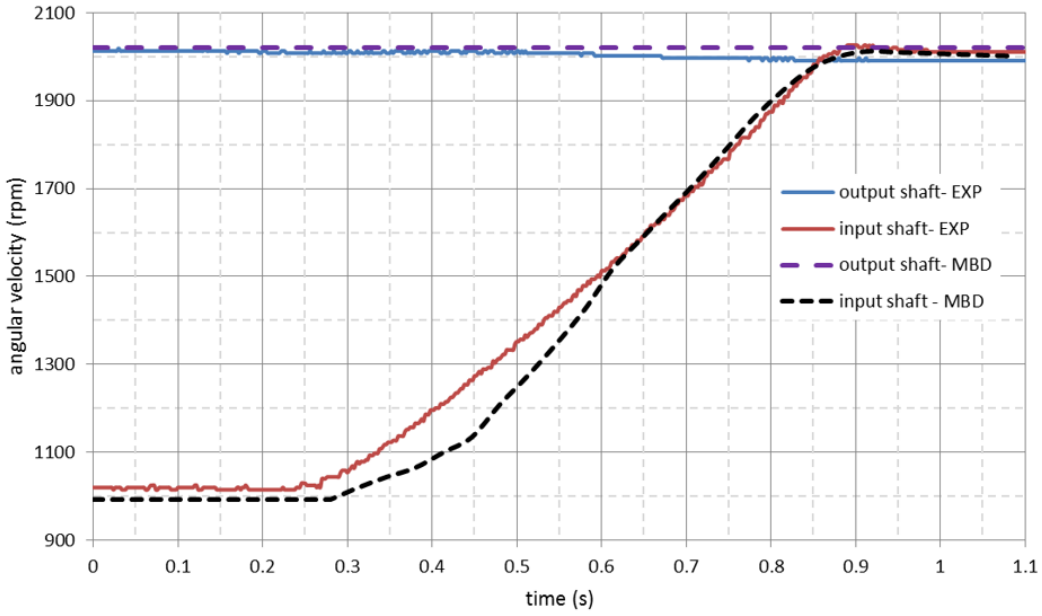

Fig. 4.14 The difference between angular velocities of input and output shafts for SC-74.

Figure4.15 illustrates the results of sleeve motion of SC-74 from experimental and rigid MBD model. The results show that the rigid model is not able to show the detail of sleeve displacement, however, the overall motion of sleeve from the rigid model is close to the overall behavior of experimental data. In other words, the rigid model has problems to simulate the sleeve motion during the third phase of synchronization. This problem can be related to the element stiffness and absence of dissipated strain energy between elements. Therefore, a deformable element can be proposed when more accurate results are needed.

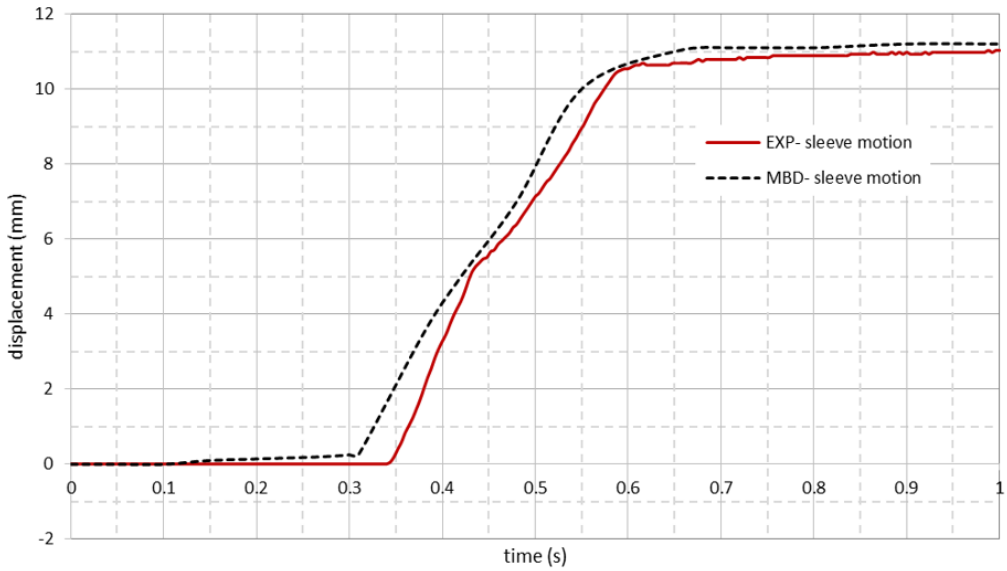

Fig. 4.15 Comparison the results of experimental and rigid MBD model for sleeve motion of SC-74.

The results of rigid MBD model DC-170 were compared with experimental data that is shown figure 4.16. In this case, the difference between input and output shafts was around 600 rpm. The applied inertia on the DC-170 was also lower than the test of SC-74. These two factors decrease the time of synchronization significantly. The estimated time for experimental and simulation was 279 and 290 ms, respectively. The overall dynamic behavior of numerical and experimental results are in agreement. The fluctuation during synchronization in both cases can be observed. The size of the synchronizer and the design of friction cones are the main reasons for this issue.

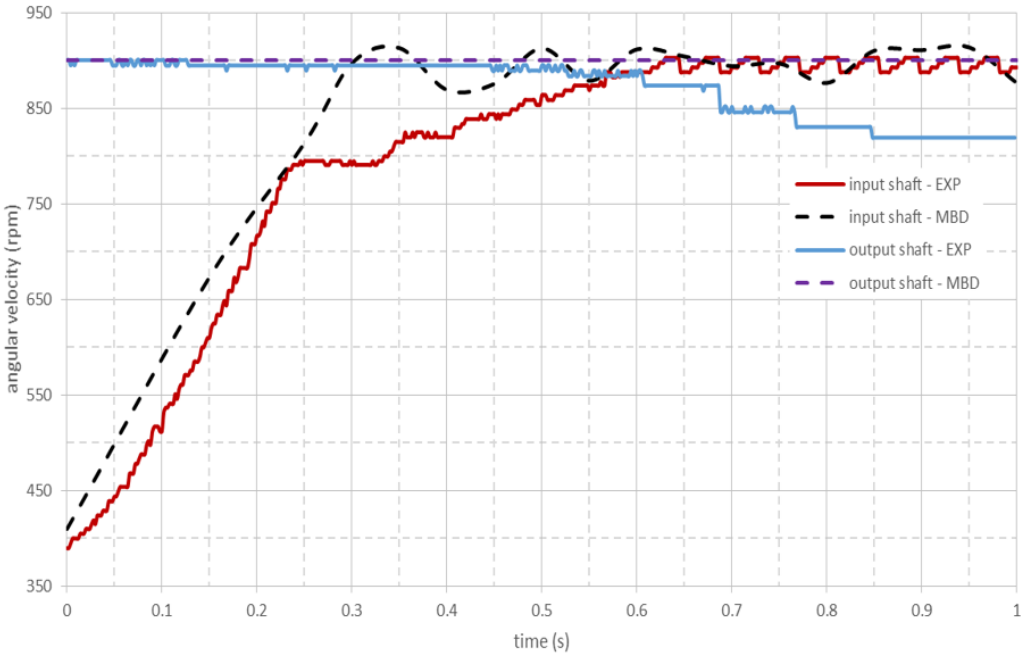

Fig. 4.16 The difference between angular velocities of input and output shafts for DC-170.

Figure 4.17 compares the results of rigid MBD model and experimental data to show the sliding sleeve motion over the synchronization process. It can be seen that at 420 and 570 ms of the test, the slope of displacement curve has changed. It shows the synchronization of the first and second friction cones with the clutch body ring in two steps. The results of sleeve motion of rigid MBD model has good agreement with the experimental dynamic behavior of the system. The numerical results show that the synchronization process initiates earlier than experimental results. The time gap between numerical and experimental results is related to the stiffness of the components. For example, the friction cones in experimental tests can be expanded radially which cannot be shown in rigid MBD model.

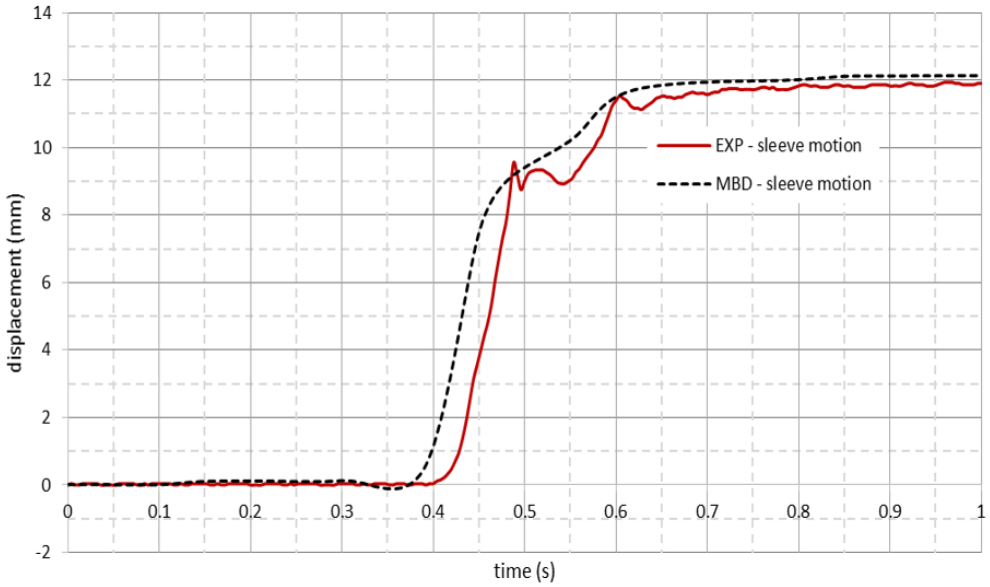

Fig. 4.17 Comparison the results of experimental and rigid MBD model for sleeve motion of DC-170.

Figure 4.18illustrates the results of rigid MBD model compared with TC-100 experimental data. It can be seen that the results of the MBD model are in good agreement with experimental results. The time of synchronization of TC-100 was 289 and 290 ms for experimental and MBD model, respectively. The fluctuation in this model due to stiffness also can be observed. However, the overall dynamic behavior shows a good contribution between experimental and MBD results.

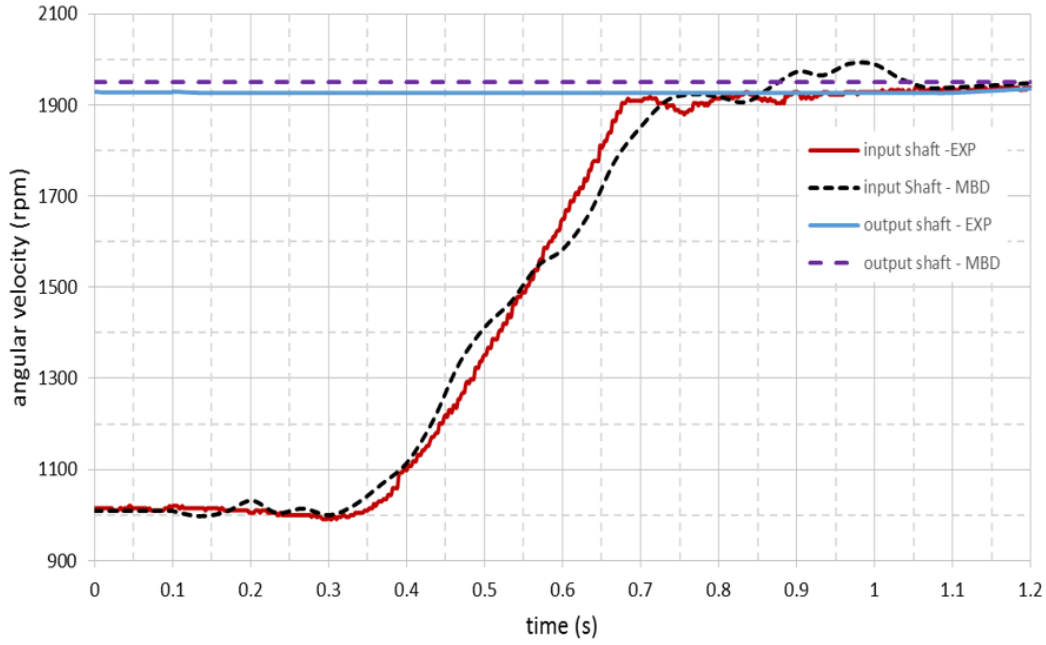

Fig. 4.18 The difference between angular velocities of input and output shafts for TC-100.

For TC-100 synchronizer also, the oscillation can be observed over the synchronization. However, the amount of the instabilities are lower than DC-170. The size of synchronizer can be a reason for this behavior. It can be interpreted that the size of synchronizer has a dominant effect on the dynamic behavior of the synchronization in comparison with increasing of the number of friction cones. Figure 4.19 presents the displacement of the sleeve over time for the TC-100. By moving the sliding sleeve, friction cones will be attached together one by one. Synchronization of each friction cone to the next one will change the slope of sleeve motion or the axial velocity of the sliding sleeve. Furthermore, the impulsive dynamic behavior between the synchronizer ring and the other friction cones could introduce some transient effect for multiple-cone synchronizers.

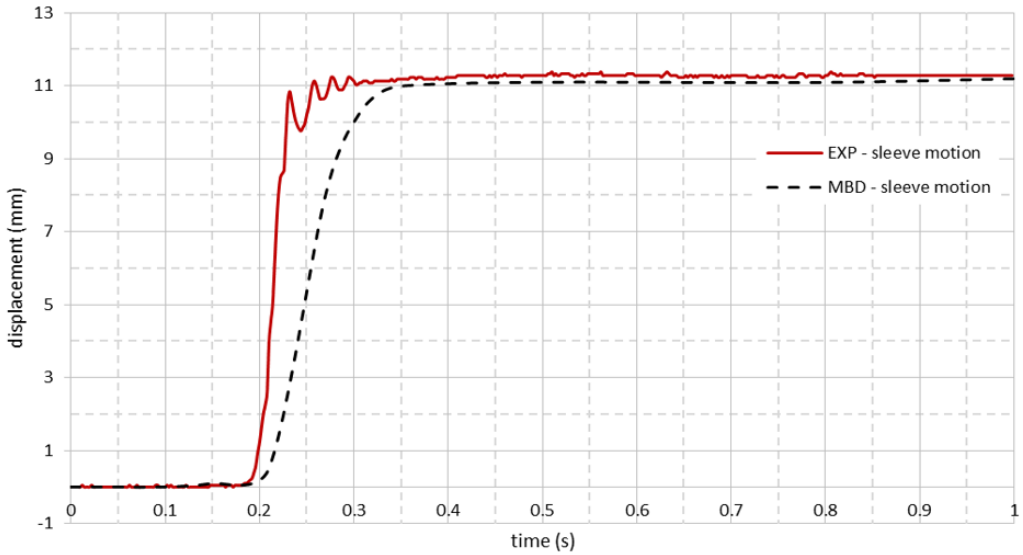

Fig. 4.19 Comparison the results of experimental and rigid MBD model for sleeve motion of TC-100.

By increasing the number of cones, the output torque and the shifting time can be improved, but a possible transient dynamic effect can be introduced. In order to verify the numerical solution, the dissipated energy balance has been evaluated. Since rigid elements are used in this study, the terms of internal energy dissipation, contact elastic energy, heat dissipation, and contact discontinuity work can be neglected. Figures 4.20(a), (b) and (c) represents the balance of dissipated energies for the SC-74, DC-170, and TC-100 synchronizers, respectively. The value of total energy in all cases was less than 2% of the energy balance equation and it means that the results of MBD models are satisfactory.

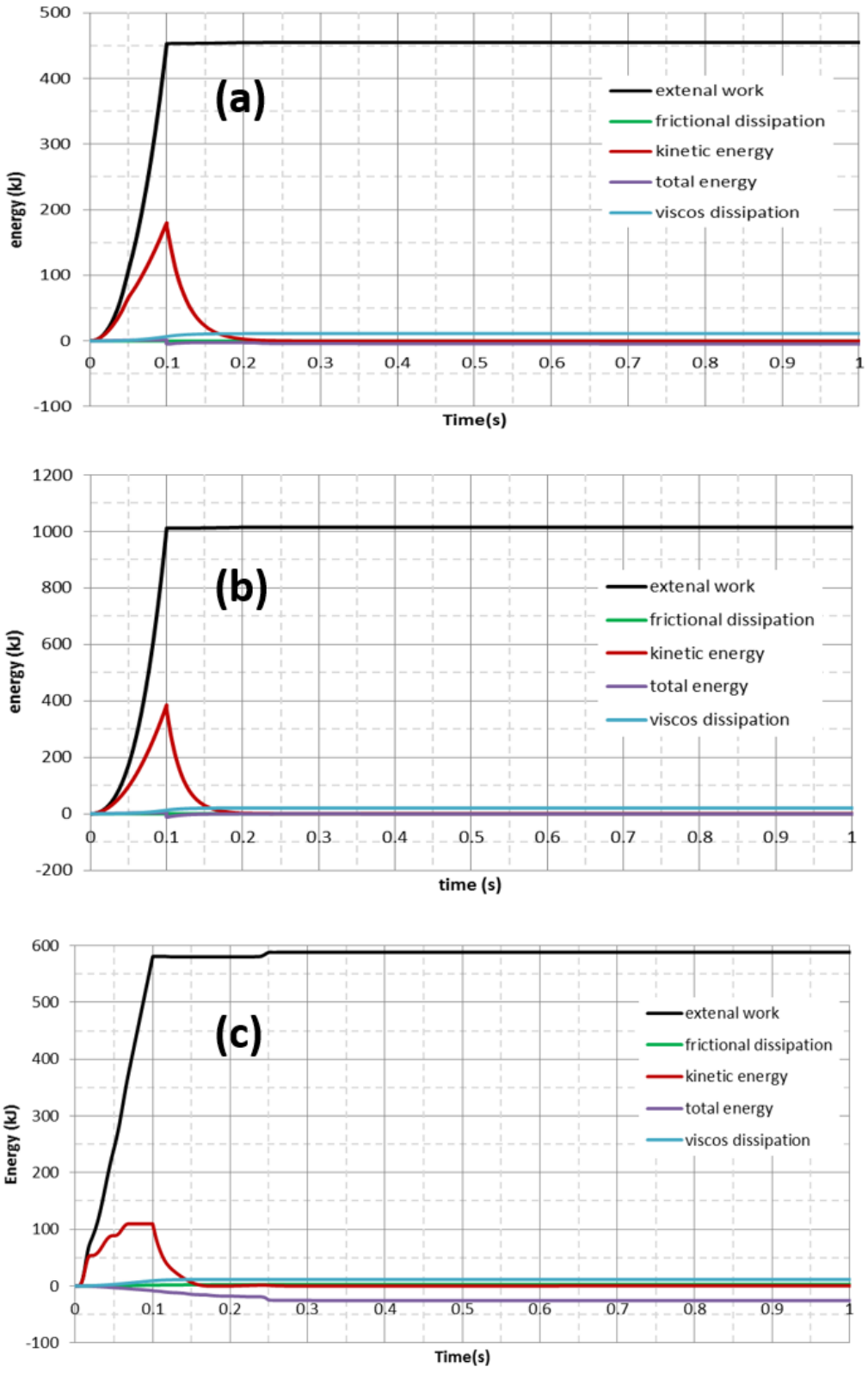

Fig. 4.20 Energy balance through simulation for (a) SC-74, (b)DC-170 and (c) TC-100 synchronizers.

4.2.4 Sensitivity analysis through rigid MBD

To understand the effect of dimensional tolerance on the friction cones of the single-cone synchronizer, a sensitivity analysis with three different scenarios was carried out. The nominal size was the first case study. The second case study was the minimum tolerance threshold at clutch body ring (CBR) and maximum tolerance threshold at the synchronizer ring. The third case study was the maximum dimensional tolerance at CBR and the minimum dimensional tolerance at the synchronizer ring. Figure 4.21 depicts the dynamic behavior between the input and output shafts for different cases in comparison with the experimental data. The overall trend of the synchronization process in all cases is the same, however, the synchronization time changes. When the synchronizer is working with the minimum size in CBR and the maximum size at synchronizer ring, the synchronization time decreases from 670 milliseconds (with nominal size) to 550 milliseconds. On the other hand, when the synchronizer has the maximum size in CBR and minimum size at synchronizer ring, the synchronization time increases to 700 milliseconds.

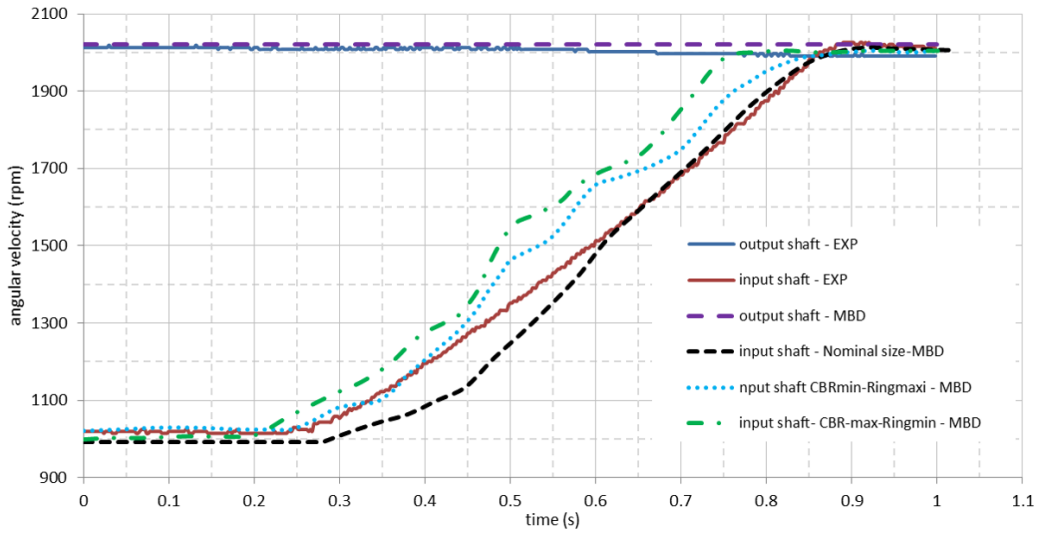

Fig. 4.21 Effect of tolerance dimension on the performance of the SC-74 during synchronization process.

Figure4.22 (a), (b) and (c) shows the contact pressure for the nominal size, $CBR_{max} - Ring_{min}$ and $CBR_{min} - Ring_{max}$, respectively. When the synchronizer has the nominal size, the contact pressure in the synchronizer ring is 0.68 MPa, while in case CBRmax- Ringmin the contact pressure increases to 1.06 MPa at the previous

region. However, in the other case with $CBR_{min} - Ring_{max}$,, the maximum contact pressure area changes from the synchronizer ring to the clutch body ring with 1.66 MPa. The maximum allowable contact stress for the friction material is 4 MPa, and in all cases, the contact pressure was in the allowable range but by changing the tolerance dimension, the critical contact area will change.

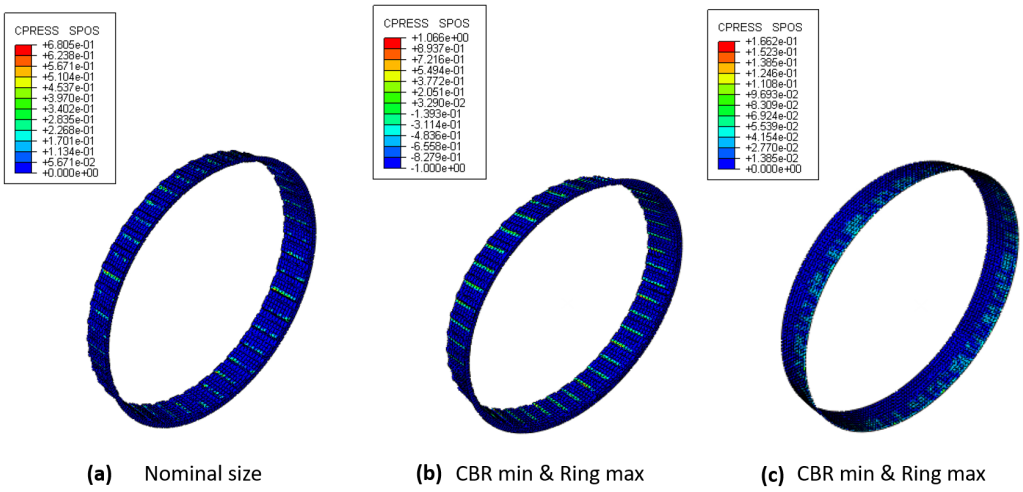

Fig. 4.22 The maximum contact pressure for SC-74 with different tolerance dimension.

The force ratio error is a criteria to evaluate the effect of geometrical tolerance on the performance of synchronization. Figure 4.23 shows the force ratio error during time with linear interpolated curves. When the components are working with the nominal dimension, the slope of the curve is near zero while by applying dimensional tolerance to the components, the force ratio error becomes higher. The results show that CBR with maximum size and synchronizer with the minimum size has the higher force ratio error that it would be the reason for friction dissipated energy enhancement during the synchronization process.

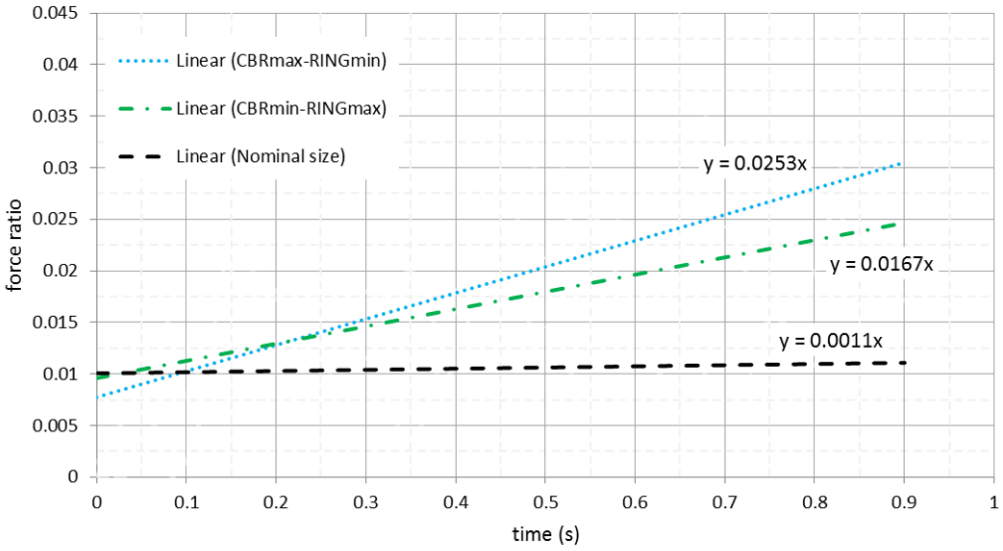

Fig. 4.23 Effect of tolerance dimension on the force ratio error.

4.2.5 Flexible MBD model

To better understanding the dynamic behavior of the synchronizer mechanism, the flexible MBD model is an appropriate tool. The detailed and precise results of flexible models can help to predict all possible conditions that may happen during operational conditions. The weakest point of flexible MBD model is heavy calculation time. In this study, three flexible MBD models are presented to validate the models through experimental data. In order to reduce the time of calculation, a sub-model was proposed. The advantages of sub-model in terms of the number of elements and the number of DOF were discussed in chapter 3.

Figure 4.24 (a) presents the results of two flexible MBD models (full model and sub-model). The results show that there is a good agreement between the MBD and experimental data. The time of synchronization were 670 and 675 ms for the full model and sub-model, respectively. The difference between the rigid and flexible model is that the MBD results were fitted on the experimental data over the full process of synchronization while this cannot be reached in the rigid MBD model. In order to simulate a single full model MBD model for SC-74 16 days, a computer should be run while the time for a sub-model is less than 4 hours. Therefore, for the optimization process in the next step, using the results of sub-model is much

sophisticated. Moreover, the results of sub-model can predict the synchronization process properly. The negative point for sub-model is that this model neglected the effect of the sleeve motion and strut detents.

Furthermore, Figure 4.24(b) shows the sleeve motion of SC-74 synchronizer from the full model FMBD and experimental results. This figure also shows more accurate results from FMBD model rather than rigid MBD model. The flexible model is able to show the fluctuations during teeth indexing and synchronization properly. The material deformability and elements energy absorption due to the contact between different parts is the reason to show more detailed dynamic behavior than the rigid model.

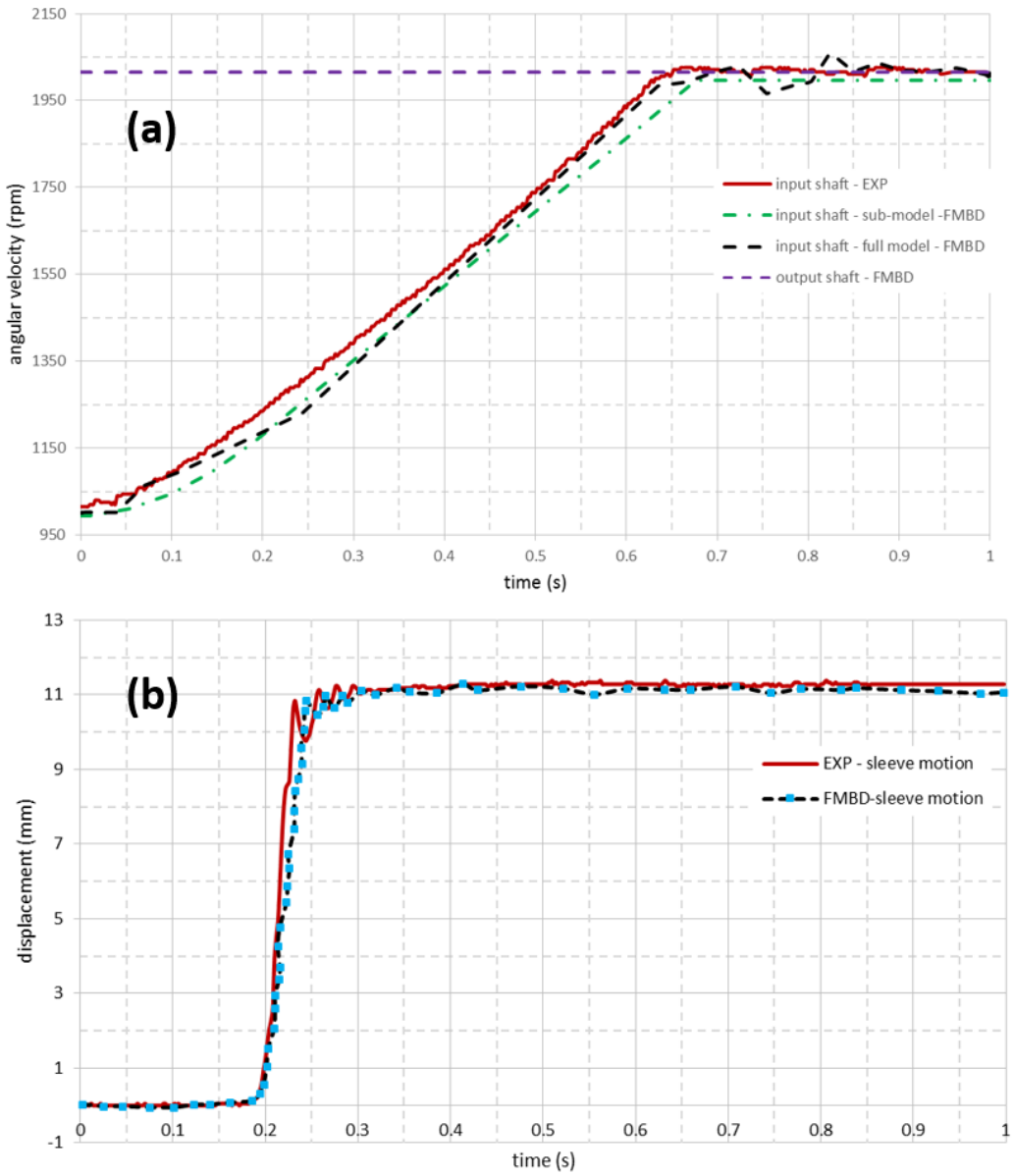

Fig. 4.24 (a) The difference between angular velocities of input and output shafts and (b) representation of sleeve motion for SC-74.

Figure 4.25 (a) compares the results of flexible MBD model in full and sub-model with experimental data. It can be seen that the results of FMBD model show an acceptable presentation of dynamic behavior for DC-170 synchronizer. The estimated synchronization time for the full model and sub-model were 292 and 295 ms, respectively. The fluctuations after synchronization are related to the axial motion of sleeve. In sub-model results due to the absence of sleeve and strut detents,

this effect cannot be seen. The axial displacement of the sleeve is shown in Figure 4.25 (b).The results are validated through experimental data and it can be said that the FMBD model is an appropriate approach when accurate results in detail are needed. The dissipated energy over the simulation can be considered as the system energy loss. However, due to reducing the computational time, the drag torque was neglected in the full model. For the purpose of optimization in the next section, the drag torque was applied in sub-model as a system variable.

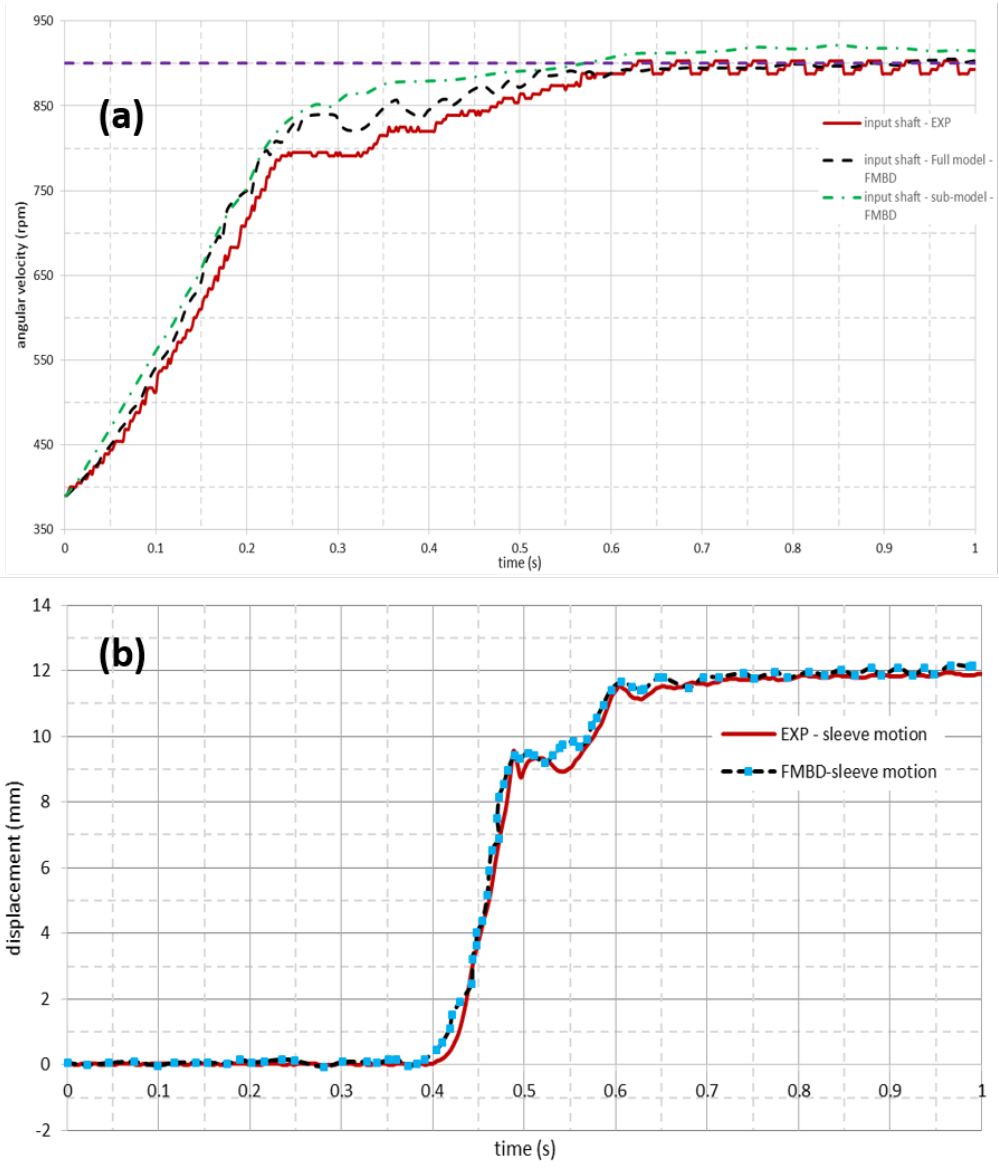

Fig. 4.25 (a) The difference between angular velocities of input and output shafts and (b) representation of sleeve motion for DC-170.

Figure 4.26(a) illustrates the angular velocities of input and output shafts of TC-100 synchronizer. The results of FMBD model were compared with experimental data and show an acceptable trend for both full and sub-FMBD models. It can be seen that after 290 ms, the difference in velocities between input and output shafts become infinitesimal. The sleeve motion of TC-100 is shown in Figure 4.26(b).The motion path is completely fitted on the experimental curve. The results of different simulations show that the FMBD models are able to predict the dynamic behavior of synchronizer mechanisms. The results of TC-100 demonstrate high similarity to experimental data. This similarity can be related to the generated drag torque in the experimental procedure. As mentioned in chapter 2, drag torque will generate a negative effect on the synchronization process. In this study, the drag torque was neglected and if during the experimental testing, the generated drag torque is in a minimum range, the FMBD and test data can be fitted closely.

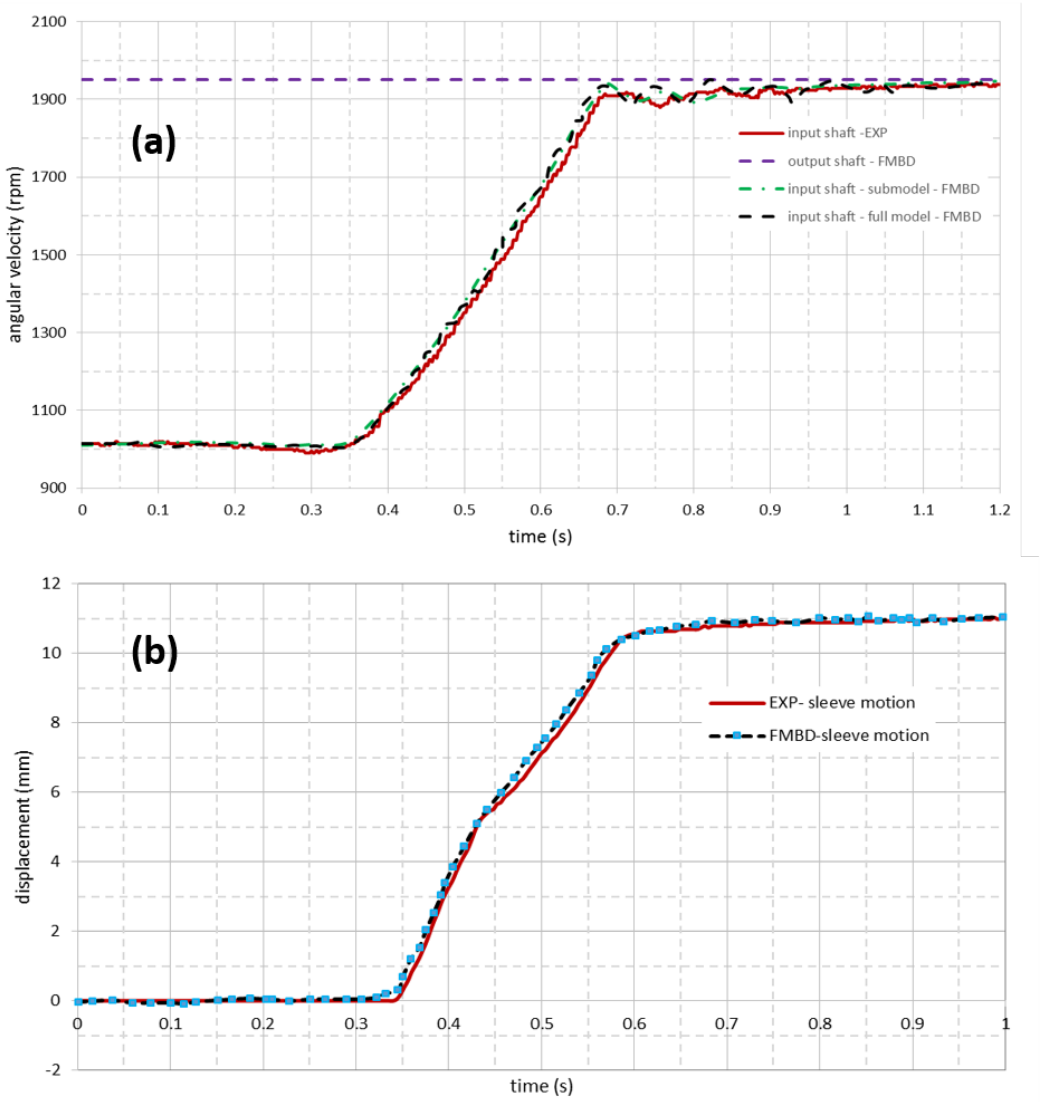

Fig. 4.26 (a) The difference between angular velocities of input and output shafts and (b) representation of sleeve motion for TC-100.

In order to verify numerical solution, a balance of energy for all terms of energy was carried out. Unlike rigid MBD model, the flexible MBD model contains all terms of dissipated energy especially dissipated strain energy. Comparing between different terms of energy shows that the value of Total energy is lower than 2% of internal and kinetic energies. It means that the numerical solutions have acceptable accuracy.

4.3 Results of analytical model

4.3.1 Dynamic behavior of analytical model

In this study, two different analytical models were presented. The first model is only able to predict the time of synchronization regarding time-dependent applied force. The second model can solve the rotational and translational dynamic equation of each phase of synchronization. At the end of each phase, by using MATLAB solver (ODE45) as a set of equations were solved and the results can be presented as the dynamic motion of different parts. The computer code can be found in Appendix 2. Figure 4.27 (a), (b) and (c) presents the synchronization process from the second analytical model and experimental results for SC-74, DC-170, and TC-100 synchronizers, respectively. The time of synchronization was 675,260, and 270 ms for SC-74, DC-170, and TC-100, respectively. The results show a smooth curve from first indexing until synchronization phases (third phase of shifting process). This difference between the analytical model and MBD models is due to the contact between parts. However, the analytical model can be a fast response solution in comparison with numerical methods.

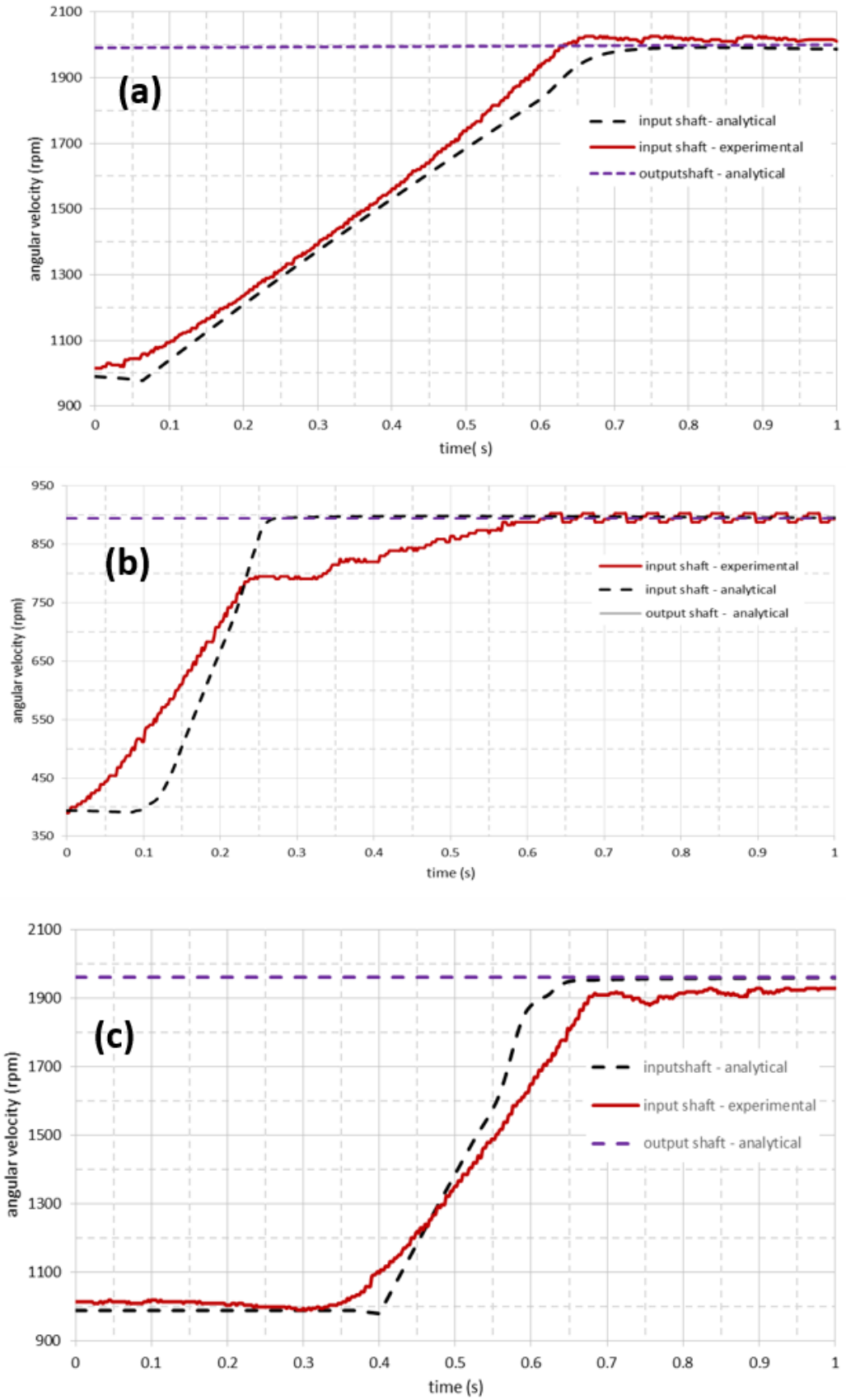

Fig. 4.27 The difference between angular velocities of input and output shafts from analytical solution and experimental test for (a) SC-74, (b) DC-170 and (c) TC-100.

4.3.2 Comparison between Analytical and Numerical approaches

Solving analytical models which are presented in chapter 3 estimates the time of synchronization as the most important factor in the synchronization process. Figure 4.28 (a), (b) and (c) compares the estimated synchronization time from FMBD model and analytical model with experimental data for SC-74, DC-170, and TC-100, respectively.

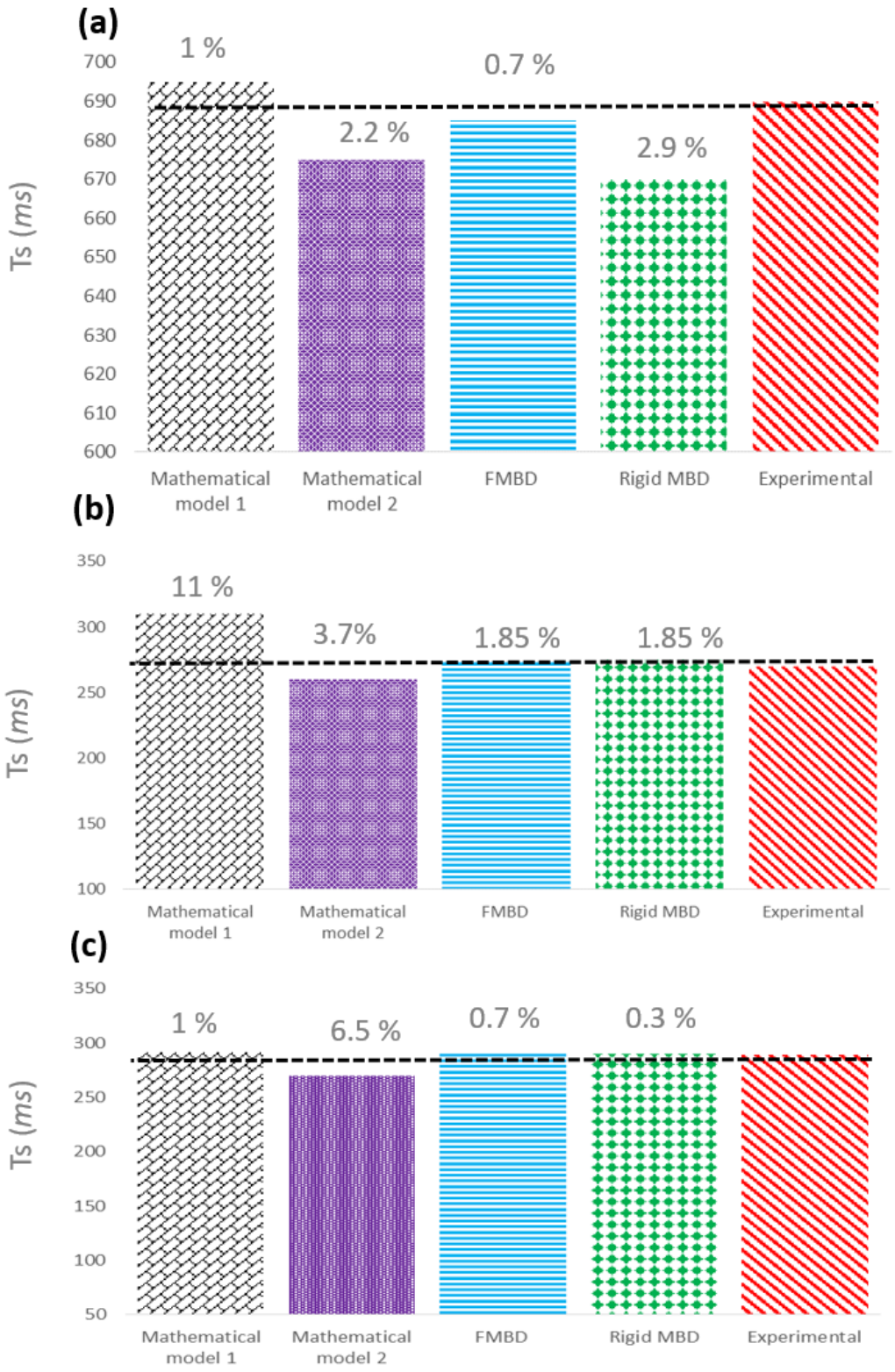

Fig. 4.28 Comparison between different models for synchronization time estimation of (a) SC-74, (b) DC-170 and (c) TC-100.

It can be seen that the most accurate method for all types of the synchronizer, was FMBD model. However, the time of calculation of this method is too much. On the other hand, the accuracy of analytical methods is lower than the MBD model but the calculation time is much affordable. As a result, it can be said that, to estimate the synchronization time, using the analytical model is recommended and for extraction of other dynamic characteristics of the system, MBD models are strongly recommended.

4.4 DOE analysis

4.4.1 Results of DOE method for SC-74

In this study, six variables such as friction coefficient (A-mu), applied force $(B - F_{app})$, time of applying force $(C - T_{app})$, angular velocity difference $(D - d_{omega})$, applied inertia $(E - Inertia)$, and drag torque $(F - T_d)$ were considered as the control factors. Moreover, synchronization time (T_s), the maximum contact pressure (C_p), and friction dissipated energy $(ALLFD)$ as the objective responses were considered. After running all tests the design table that is mentioned in chapter 3 was filled and DOE analysis regarding RSM method was performed. Table 4.2 demonstrates the filled design table for SC-74 synchronizer.

Table 4.2 Design of Experiment's table for SC-74

		Factor 1	Factor 2	Factor 3	Factor 4	Factor 5	Factor 6	Response 1	Response 2	Response 3
Std	Run	A:Mu	B:Fapp	C:Tapp	D:d-Omega	E:Inertia	F:Td	T_s	C_p	ALLFD
		–	N	s	rad/s	kg/m^2	N.m			
1	45	0.05	700	0.1	700	0.15	0	0.998369	6.00163	4.05135
2	27	0.1	700	0.1	700	0.15	10	0.548701	19.286	17.0441
3	12	0.05	1500	0.1	700	0.15	10	0.499054	19.4637	16.9282
4	48	0.1	1500	0.1	700	0.15	0	0.26586	8.68615	4.71802
5	41	0.05	700	0.2	700	0.15	10	1.0974	18.393	17.0441
6	7	0.1	700	0.2	700	0.15	0	0.562701	6.7416	4.66004
7	16	0.05	1500	0.2	700	0.15	0	0.531721	6.84307	4.71802
8	43	0.1	1500	0.2	700	0.15	10	0.347527	20.3199	18.6673
9	5	0.05	700	0.1	1200	0.15	10	1.48126	18.0843	24.406
10	49	0.1	700	0.1	1200	0.15	0	0.84563	6.1589	12.0054
11	36	0.05	1500	0.1	1200	0.15	0	0.792521	6.23656	12.0551
12	11	0.1	1500	0.1	1200	0.15	10	0.437094	19.7421	25.7973
13	19	0.05	700	0.2	1200	0.15	0	1.69126	5.57945	12.0054
14	31	0.1	700	0.2	1200	0.15	10	0.96463	18.5159	26.1948
15	20	0.05	1500	0.2	1200	0.15	10	0.874188	18.621	25.7973
16	2	0.1	1500	0.2	1200	0.15	0	0.469761	7.08617	14.2911
17	18	0.05	700	0.1	700	0.25	10	1.437	18.1001	19.2619
18	46	0.1	700	0.1	700	0.25	0	0.823501	6.19004	6.81988
19	52	0.05	1500	0.1	700	0.25	0	0.771868	6.26965	6.84887
20	38	0.1	1500	0.1	700	0.25	10	0.426767	19.7963	20.0735
21	15	0.05	700	0.2	700	0.25	0	1.647	5.59502	6.81988
22	47	0.1	700	0.2	700	0.25	10	0.942501	18.5398	20.3054
23	17	0.05	1500	0.2	700	0.25	10	0.853535	18.6482	20.0735
24	3	0.1	1500	0.2	700	0.25	0	0.459434	7.13306	8.15321
25	28	0.05	700	0.1	1200	0.25	0	1.53464	5.36237	19.1974
26	21	0.1	700	0.1	1200	0.25	10	1.41172	18.1942	32.5421
27	26	0.05	1500	0.1	1200	0.25	10	1.30454	18.2512	32.3433
28	30	0.1	1500	0.1	1200	0.25	0	0.668601	6.46575	20.3402
29	14	0.05	700	0.2	1200	0.25	10	1.74543	17.8471	32.5421
30	4	0.1	700	0.2	1200	0.25	0	1.42572	5.68737	20.2409
31	33	0.05	1500	0.2	1200	0.25	0	1.3372	5.73287	20.3402
32	44	0.1	1500	0.2	1200	0.25	10	0.750268	18.8062	35.3247
33	37	0.0358729	1100	0.15	950	0.2	5	1.58189	11.8695	16.2725
34	29	0.114127	1100	0.15	950	0.2	5	0.559077	13.0029	17.5192
35	22	0.075	473.966	0.15	950	0.2	5	1.76814	11.8043	16.3417
36	25	0.075	1726.03	0.15	950	0.2	5	0.538846	13.0687	17.4499
37	32	0.075	1100	0.0717458	950	0.2	5	0.756625	12.5452	16.2725
38	34	0.075	1100	0.228254	950	0.2	5	0.850744	12.4019	17.5192
39	50	0.075	1100	0.15	558.729	0.2	5	0.509828	13.1722	10.2219
40	42	0.075	1100	0.15	1341.27	0.2	5	1.09754	12.1429	26.7762
41	51	0.075	1100	0.15	950	0.121746	5	0.52452	13.1184	13.1979
42	10	0.075	1100	0.15	950	0.278254	5	1.08285	12.155	20.5937
43	39	0.075	1100	0.15	950	0.2	0	0.78698	6.24527	10.4246
44	40	0.075	1100	0.15	950	0.2	12.8254	0.829829	22.2127	27.0239
45	35	0.075	1100	0.15	950	0.2	5	0.803685	12.4694	16.8958

ANOVA analysis of first response; synchronization time

After finishing all simulations and filling up the table in order to analyze the data, analysis of variance (ANOVA) was performed on each set of response data. According to ANOVA analysis in Table 4.3, in order to evaluate the first response (T_s),all main factors are significant with P-value of less than 0.05 for 95% confidence. To apply the RSM on DOE table of T_s, the main factors and their interactions were considered. The R-Squared shows how accurate the model is in predicting the response values. Also, the measurement of the amount of variation around the mean; R-Squared value that is closer to 1.0 is desirable. The value of R-square for T_s response is 0.9826 that shows high accuracy of the model. Moreover, the difference between Predicted R-square of 0.9287 and Adjusted R-square of 0.9704 is less than 0.1 which is desirable. The signal-to-noise ratio is illustrated by Adequate Precision that compares the range of the predicted value at the design points to the average prediction error. A desirable ratio should be greater than 4 while this value for the first response is higher than 43 that shows high confidence on this model. With post ANOVA analysis, the estimated true coefficients at 95% of Confidence Internal (CI) are fitted in the high and low threshold. The results between CIs prove that the single effect of each parameters are significant and will have an effect on the synchronization time. Furthermore, the Variance Inflation Factor (VIF) with a value of 1 indicates an ideal correlation between the regression coefficients. VIFs values more than 10 would raise the alarm that present coefficients are poorly estimated because of multi-co-linearity. [90].

Table 4.3 ANOVA analysis for synchronization time as the first response of DOE method for SC-74.

Source	Sum of Square	DoF	Mean Square	F- Value	p-value		Coefficient	Standard Error	95% CI Low	95% CI High	VIF
Model	3.3	21	0.16	80.73	<0.0001	significant					
A-Mu	0.9	1	0.9	463.78	<0.0001	significant	0.16	7.27E-03	0.14	0.17	1
B-Fapp	1.17	1	1.17	598.97	<0.0001	significant	0.18	7.27E-03	0.16	0.19	1
C-Tapp	0.03	1	0.03	15.45	0.0005	significant	-0.029	7.27E-03	-0.043	-0.014	1
D-d-Omega	0.55	1	0.55	282.78	<0.0001	significant	-0.12	7.27E-03	-0.14	-0.11	1
E-Inertia	0.49	1	0.49	250.64	<0.0001	significant	-0.12	7.27E-03	-0.13	-0.1	1
F-Td	4.79E-03	1	4.79E-03	2.46	0.1274		-0.012	7.42E-03	-0.027	3.52E-03	1
Residual	0.058	30	1.95E-03			Std. Dev.	0.044		R-Squared	0.9826	
Lack of Fit	0.058	23	2.54E-03			Mean	1.13		Adj R-Squared	0.9704	
Pure Error	0	7	0			C.V. %	3.92		Pred R-Squared	0.9287	
Cor Total	3.36	51				PRESS	0.24		Adeq Precision	43.173	

In order to predict the synchronization time, an empirical model in un-coded format from ANOVA analysis was obtained. Based on the un-coded format, the response can be predicted by allocating the factors between the lower and upper bound of each factor which has been defined from Table3.7.

$\frac{1}{\sqrt{T_s}}$ = 0.6+ 11.4*Mu + 7.89E-04*Fapp- 0.9*Tapp - 2.53E-04*d-Omega - 1.1*Inertia - 2.7E-03*Td + 3.6E-03*Mu*Fapp - 5.3*Mu*Tapp- 4.17E-03*Mu* d-Omega - 20.3*Mu*Inertia-0.06*Mu*Td - 3.4E-04*Fapp*Tapp -2.8E-07* Fapp * d-Omega - 1.4E-03 *Fapp*Inertia - 2.3E-06*Fapp*Td + 5.6E-04*Tapp*d-Omega + 2.5 *Tapp* Inertia + 0.01* Tapp * Td + 1.4E-03* d-Omega * Inertia + 3.1E-06* d-Omega * Td + 0.01* Inertia *Td

In order to verify the ANOVA statistical analysis, four main tools can be used. If the normal distribution of residuals follows a straight line, it means that the model is acceptable which is shown in Figure 4.29 (a). Figure 4.29 (b) shows the plot of residuals versus simulation runs that is shown in a randomly scattered run from the analysis. This is the second tool to prove the validity of statistical analysis. The third tool for statistical verification test is controlling the randomly scattered data from residuals versus predicted data between upper and lower CI lines. Figure 4.29 (c)) shows an acceptable distribution between CI lines. The plot in Figure 4.29 (d) provides a guideline to select the correct inverse square root transformation. A recommended transformation is listed, based on the best λ (lambda) value, which is found at the minimum point of the curve generated by the natural log of the sum of squares of the residuals.

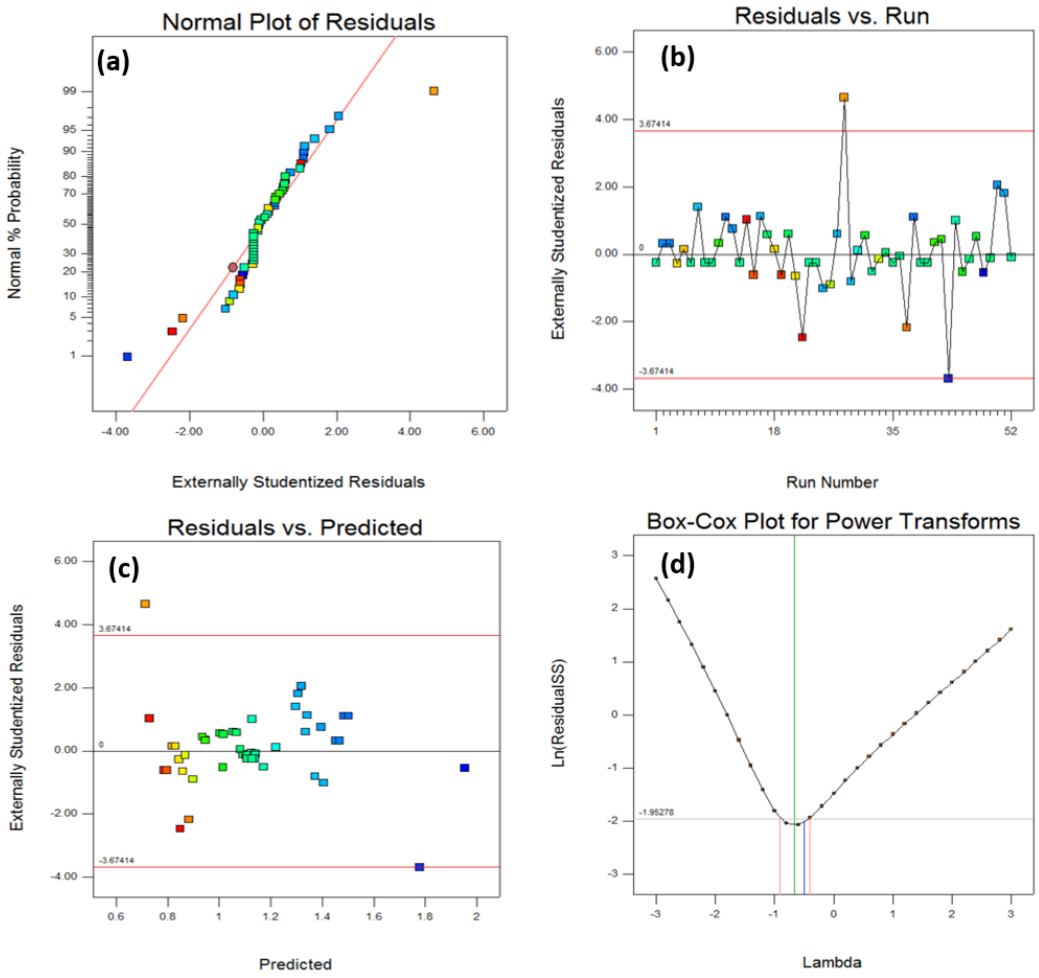

Fig. 4.29 Post ANOVA verification tools for prediction of synchronization time of SC-74.

Figure 4.30 illustrates the effect of all main factors on the synchronization time. This graph shows how changing the value of variables can have some effects on the response time of synchronization. The most effective factors related to the T_s are friction coefficient and rotational velocity, respectively. It can be seen that increasing the friction coefficient reduces the T_s, however, the rotational velocity difference increases T_s. Surprisingly, the drag torque was the lowest effective parameter on the synchronization time.

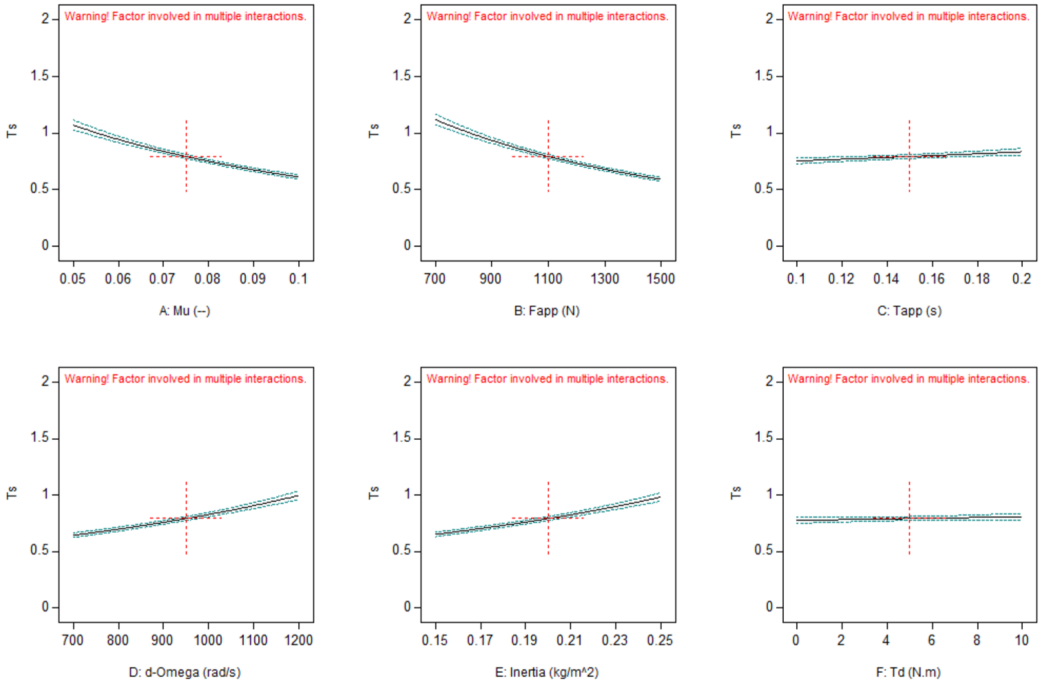

Fig. 4.30 Effect of changing main control factors on the response of the synchronization time for SC-74.

4.4.2 ANOVA analysis of second response; Contact Pressure

In order to evaluate the second response (C_p) based on ANOVA analysis from Table 4.4,all the main factors are significant with P-value of less than 0.05 for 95% confidence. To apply the RSM on DOE table of C_p, a quadratic model was proposed by the Design Expert software. The value of R-square for C_p response is 0.999 that shows high accuracy of the model. Moreover, the difference between Predicted R-square of 0.998 and Adjusted R-square of 0.999 is less than 0.001 which is desirable. The signal-to-noise ratio is illustrated by Adequate Precision which this value for C_p is higher than 583 that shows high confidence in this model. The results between CIs prove that the main factors are significant and will have some effect on the contact pressure. Additionally, VIF with the value of 1 indicates an ideal correlation between the regression coefficients.

Table 4.4 ANOVA analysis for contact pressure as the second response of DOE method for SC-74.

Source	Sum of Square	DoF	Mean Square	F- Value	p-value		Coefficient	Standard Error	95% CI Low	95% CI High	VIF
Model	32334.82	27.00	1197.59	31352.90	<0.0001	significant					
A-Mu	117.60	1.00	117.60	3078.71	<0.0001	significant	1.79	3.20E-02	1.72	1.85	1
B-Fapp	149.31	1.00	149.31	3908.96	<0.0001	significant	2.01	3.20E-02	1.95	2.08	1
C-Tapp	3.94	1.00	3.94	103.21	<0.0001	significant	-0.33	3.20E-02	-0.39	-0.26	1
D-d-Omega	75.12	1.00	75.12	1966.68	<0.0001	significant	-1.43	3.20E-02	-1.49	-1.36	1
E-Inertia	67.28	1.00	67.28	1761.45	<0.0001	significant	-1.35	3.20E-02	-1.42	-1.28	1
F-Td	30423.57	1.00	30423.57	796500.00	<0.0001	significant	29.66	3.30E-02	29.59	2.97E+01	1.03
Residual	0.92	24	3.80E-02			Std. Dev.	0.2		R-Squared	1	
Lack of Fit	0.92	17	5.40E-02			Mean	43.96		Adj R-Squared	0.9999	
Pure Error	0	7	0			C.V. %	0.44		Pred R-Squared	0.9998	
Cor Total	32335.74	51				PRESS	6.27		Adeq Precision	583.794	

An empirical model in un-coded format from ANOVA analysis was obtained to predict the contact pressure. The higher and lower range of variables was taken from Table 3.7.

$(C_p)^{1.47}$= 18.2 + 136.5* Mu + 9.6E-003* Fapp - 8.07* Tap - 0.01* d-Omega - 64.9* Inertia + 4.5* Td + 0.05* Mu * Fapp - 141.8* Mu * Tapp - 0.05* Mu * d-Omega - 273.07* Mu * Inertia + 2.6* Mu * Td - 9.3E-003* Fapp * Tapp - 4.2E-006* Fapp * d-Omega - 0.01* Fapp * Inertia + 2.1E-004* Fapp * Td + 0.01* Tapp * d-Omega + 53.05* Tapp * Inerti - 0.4* Tapp * Td + 0.02* d-Omega * Inertia - 1.9E-004* d-Omega * Td - 0.9* Inertia * Td - 53.3*Mu^2 - 1.8E-007* $Fapp^2$ + 11.3* $Tapp^2$ + 6.4E-006* $d-Omega^2$ +143.2* $Inertia^2$ + 0.1* Td^2

Figure 4.31 (a) presents an acceptable normal distribution of residuals. It can be observed that all runs are fitted on a straight line which means low residual error. Also, Figure 4.31(b) shows the residuals versus simulation runs in a randomly scattered plot. It can be seen that all data are between the CIs region. Figure 4.31 (c) depicts the data from residuals versus predicted that is distributed randomly between upper and lower CI lines. Figure 4.31 (d) shows the power transformation with the best lambda value ($\lambda = 1.47$) that is recommended by the software. It can be seen that applying the power transformation keeps the lambda between CI lines.

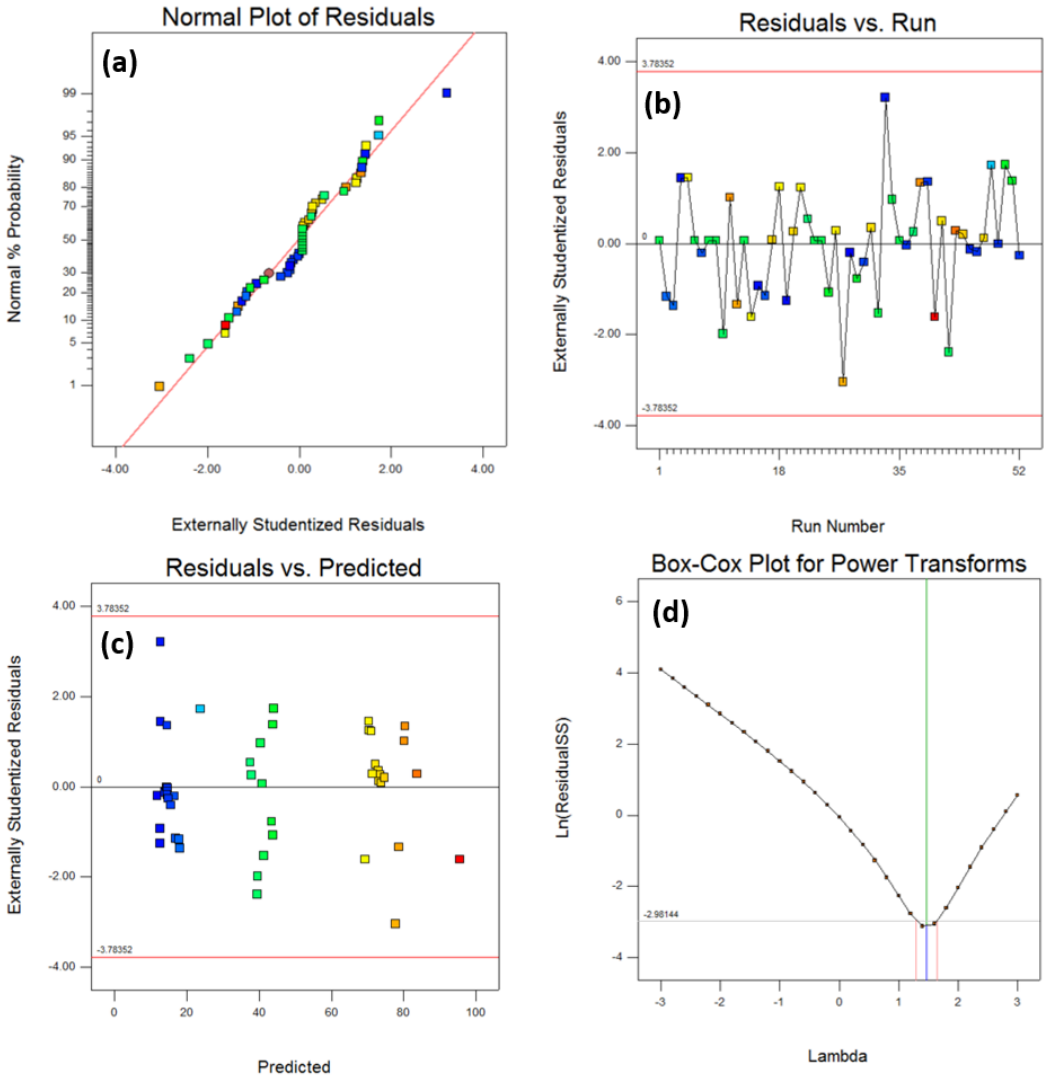

Fig. 4.31 Post ANOVA verification tools for prediction of contact pressure of SC-74.

Figure 4.3279 illustrates the effect of all main factors on maximum contact pressure between friction cones. This graph demonstrates the effect of changing the main factors over design space on the second response C_p. The most effective factors related to the C_p is the drag torque with a sharp slope. In other words, by increasing the drag torque, the contact pressure grows up dramatically.

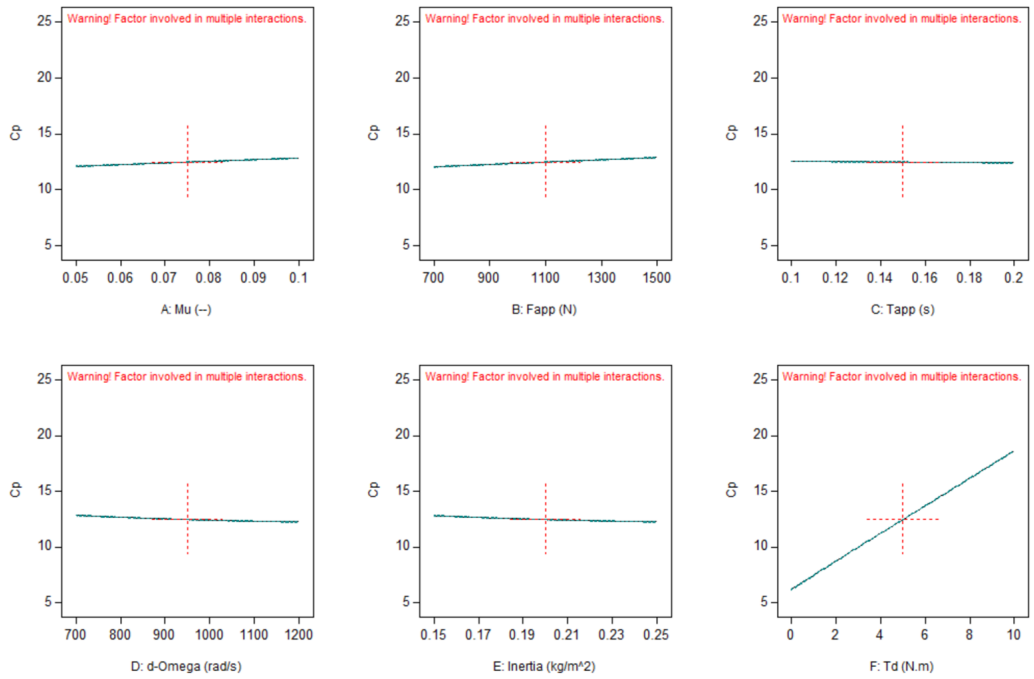

Fig. 4.32 Effect of changing main control factors on the response of the contact pressure for SC-74.

4.4.3 ANOVA analysis of third response; friction dissipated energy

To investigate the effect of the third response of SC-74, as the friction dissipated energy (ALLFD), ANOVA analysis was performed that is shown in Table 4.5.It can be said that all main factors are significant with P-value of less than 0.05 for 95% confidences. To apply the RSM on DOE table of ALLFD, a linear model regarding only main factors was proposed by the Design Expert software. The value of R-square for ALLFD response is 0.983 that shows high accuracy of the model. Moreover, the difference between Predicted R-square of 0.974 and Adjusted R-square of 0.980 is less than 0.05 which is desirable. The signal-to-noise ratio or Adequate Precision value for ALLFD is higher than 81 that show high confidence (much bigger than 4) in this model. Furthermore, the results between CIs prove that main factors are significant and ALLFD can be affected by changing the main factors over the selected region. Additionally, VIF with the value of 1 indicates an ideal correlation between the regression coefficients.

Table 4.5 ANOVA analysis for friction dissipated energy as the third response of DOE method for SC-74.

Source	Sum of Square	DoF	Mean Square	F- Value	p-value		Coefficient	Standard Error	95% CI Low	95% CI High	VIF
Model	420.16	6.00	70.03	432.57	<0.0001	significant					
A-Mu	0.86	1.00	0.86	5.33	0.03	significant	0.15	6.60E-02	0.019	0.29	1
B-Fapp	0.70	1.00	0.70	4.34	0.04	significant	0.14	6.60E-02	0.004624	0.27	1
C-Tapp	0.86	1.00	0.86	5.33	0.03	significant	0.15	6.60E-02	0.019	0.29	1
D-d-Omega	156.94	1.00	156.94	969.47	<0.0001	significant	2.06	6.60E-02	1.93	2.2	1
E-Inertia	34.01	1.00	34.01	210.07	<0.0001	significant	0.96	6.60E-02	0.83	1.09	1
F-Td	226.79	1.00	226.79	1400.89	<0.0001	significant	2.53	6.80E-02	2.39	2.67E+00	1
Residual	7.28	45	1.60E-01			Std. Dev.	0.4		R-Squared	0.983	
Lack of Fit	7.28	38	1.90E-01			Mean	8.62		Adj R-Squared	0.9807	
Pure Error	0	7	0			C.V. %	4.67		Pred R-Squared	0.9748	
Cor Total	427.45	51				PRESS	10.76		Adeq Precision	81.23	

An empirical model in un-coded format from ANOVA analysis were obtained to predict the contact pressure. The higher and lower range of variables were taken from table 3.7.

$(ALLFD)^{0.76}$ = -6.9 + 6.1* Mu + 3.4E-04* Fapp + 3.05* Tapp + 8.2E-003* d-Omega + 19.2* Inertia + 0.5* Td

Figure 4.33 (a) presents a fitted straight line from the normal distribution of residuals with the minimum standard error. Also, Figure 4.33 (b) shows the residuals versus simulation runs in a randomly scattered plot. It can be seen that all data are between the CIs region. Figure 4.33 (c)) depicts the data from residuals versus predicted, that is distributed randomly between upper and lower CI lines. Figure 4.33 (d) shows the power transformation with the best lambda value ($\lambda = 0.76$) that is recommended by the software.

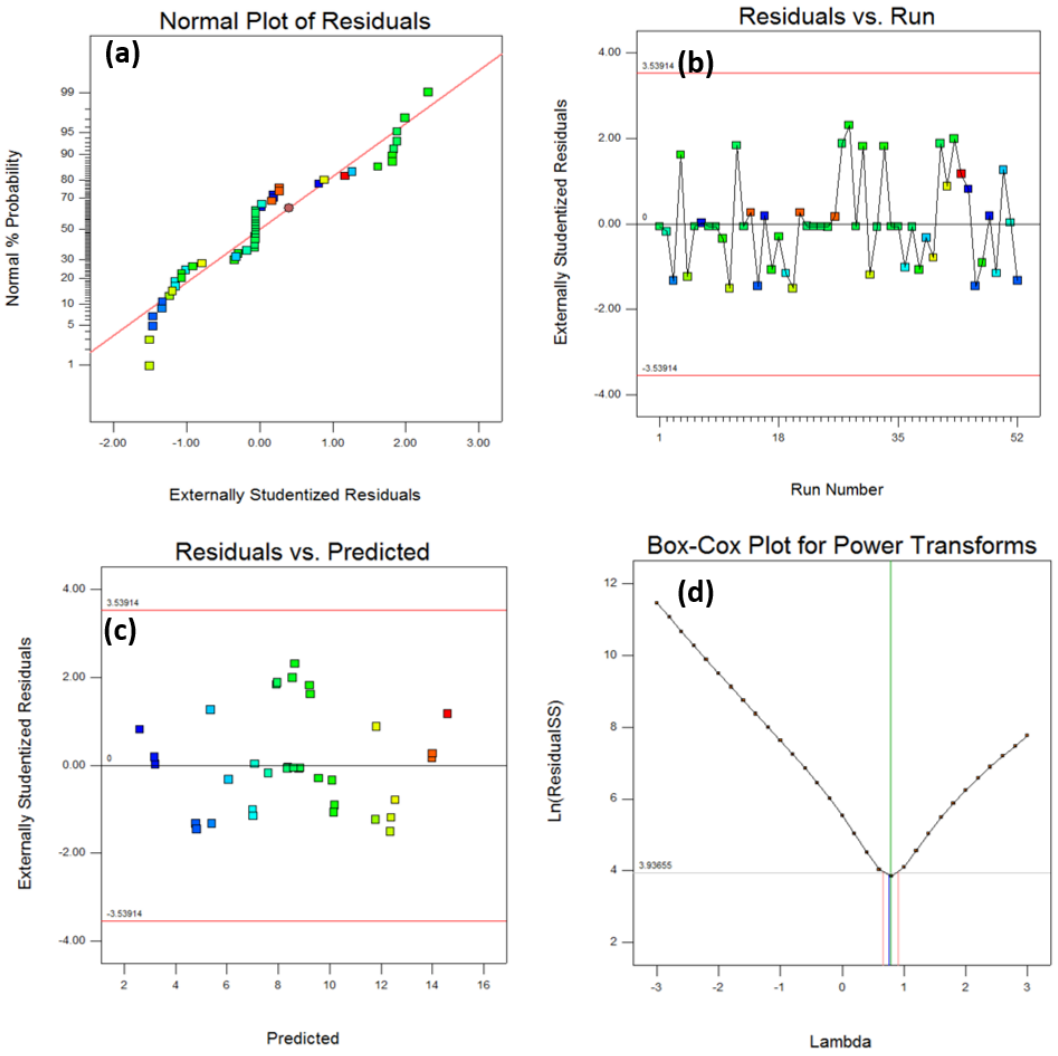

Fig. 4.33 Post ANOVA verification tools to predict the fiction dissipated energy of SC-74.

Figure 4.34 presents the effect of all the main factors on friction dissipated energy during the synchronization process. By changing the variable over the design space the effect of each parameter can be observed from the presented graph. The most effective factors related to the ALLFD are drag torque and rotational velocity, respectively. In addition, increasing the applied inertia will have an effect on the dissipated energy as the third rank.

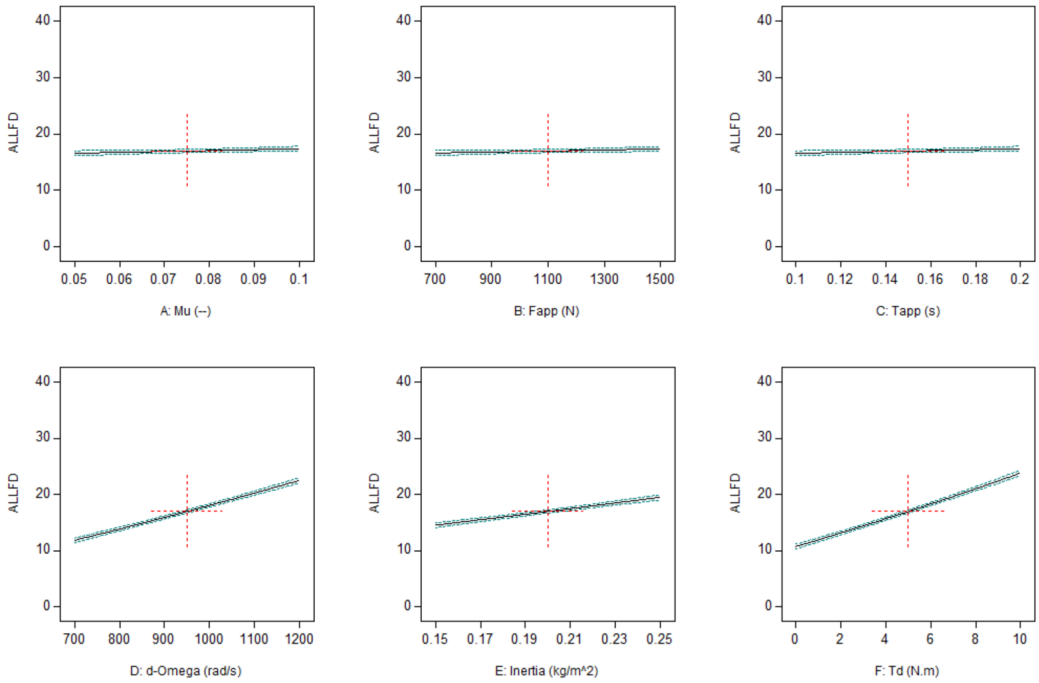

Fig. 4.34 Effect of changing main control factors on the response of the friction dissipated energy for SC-74.

4.4.4 Results of DOE method for DC-170

In order to evaluate the effect of different variables on the performance of DC-170, the same procedure with the same number of factors and the number of runs was carried out. In this section, we also have three responses (T_s, C_p, and ALLFD). The results of the ANOVA table and post ANOVA verification test can be found in Appendix 1. The R-square for T_s, C_p, and ALLFD were 0.983, 0.996, and 0.923, respectively. The models for T_s and C_p were fitted with the quadratic polynomial equation, however, a linear model was suggested by the software for presenting the ALLFD results distribution. The results of the ANOVA table show a significant model and it can be said that the obtained statistical models are valid. Three different empirical models to predict three different responses were achieved. Figures 4.35,4.36 and 4.37 present the effect of each factor on T_s, C_p, and ALLFD, respectively.

From figure 4.35 it can be observed that the most effective factor in T_s is applied inertia and the minimum impact on T_s is related to the drag torque. Increasing of the friction coefficient and applied force have a desirable (positive) effect on the

synchronization time but by increasing other factors the synchro nation time can increase which is not appropriate (negative effect).

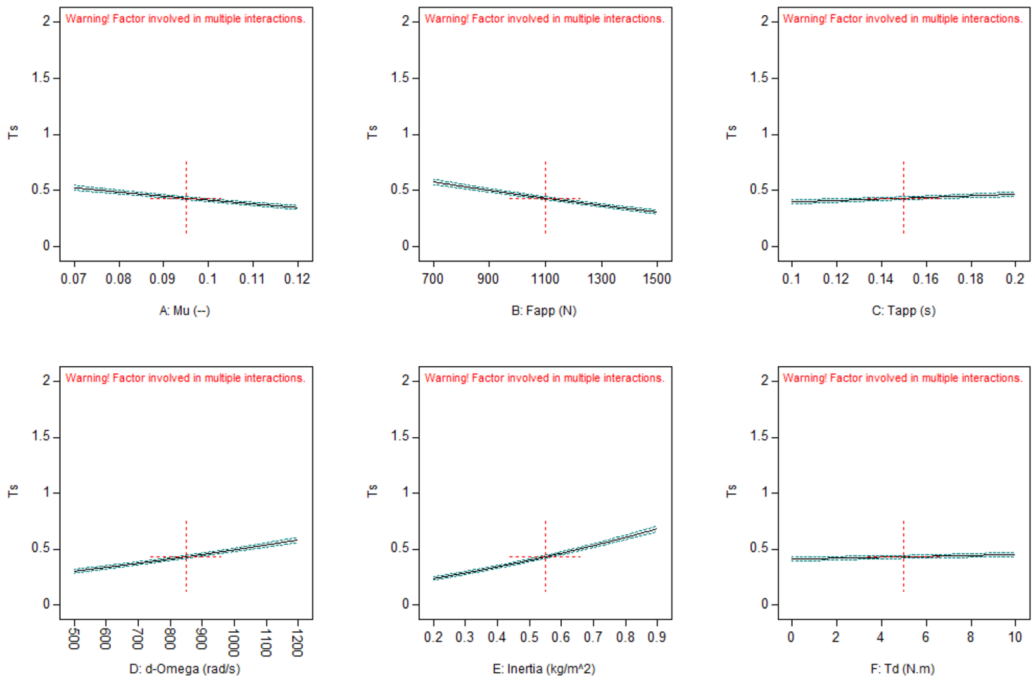

Fig. 4.35 Effect of changing main control factors on the response of the synchronization time for DC-170.

From figures 4.36 and 4.37 it can be interpreted that for the other responses (C_p and ALLFD),the drag torque were the most effective factors in the performance of DC-170 synchronizer. In addition, increasing the applied inertia reduces the contact pressure while the synchronization time and friction dissipated energy increases. To predict ALLFD, the variation of all factors follows higher order polynomial curve that it can be observed clearly.

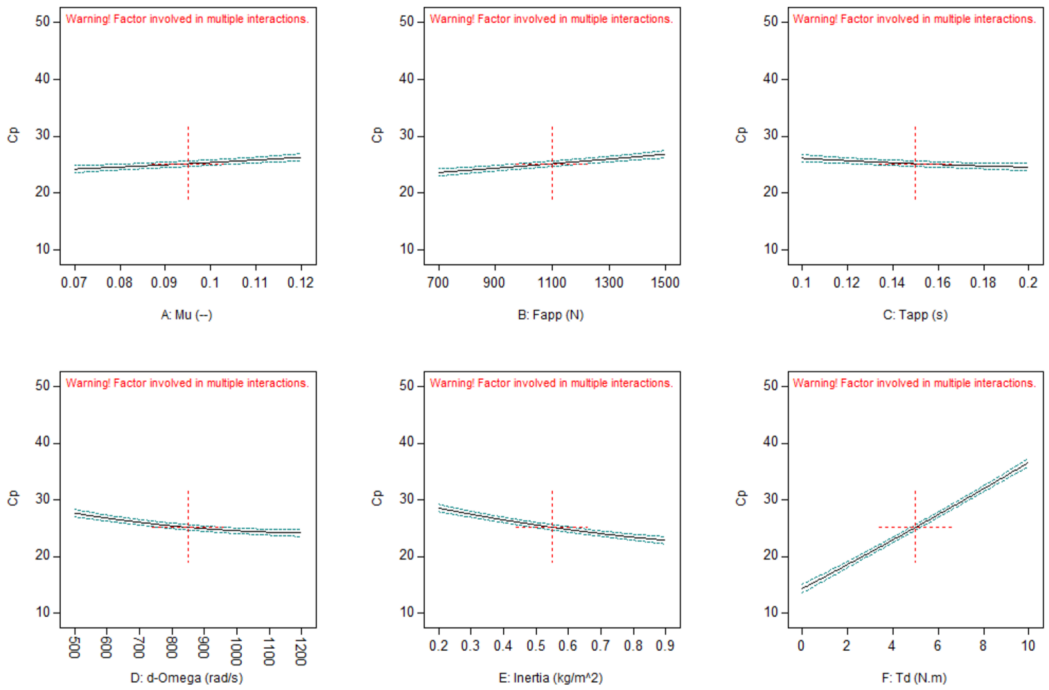

Fig. 4.36 Effect of changing main control factors on the response of contact pressure for DC-170.

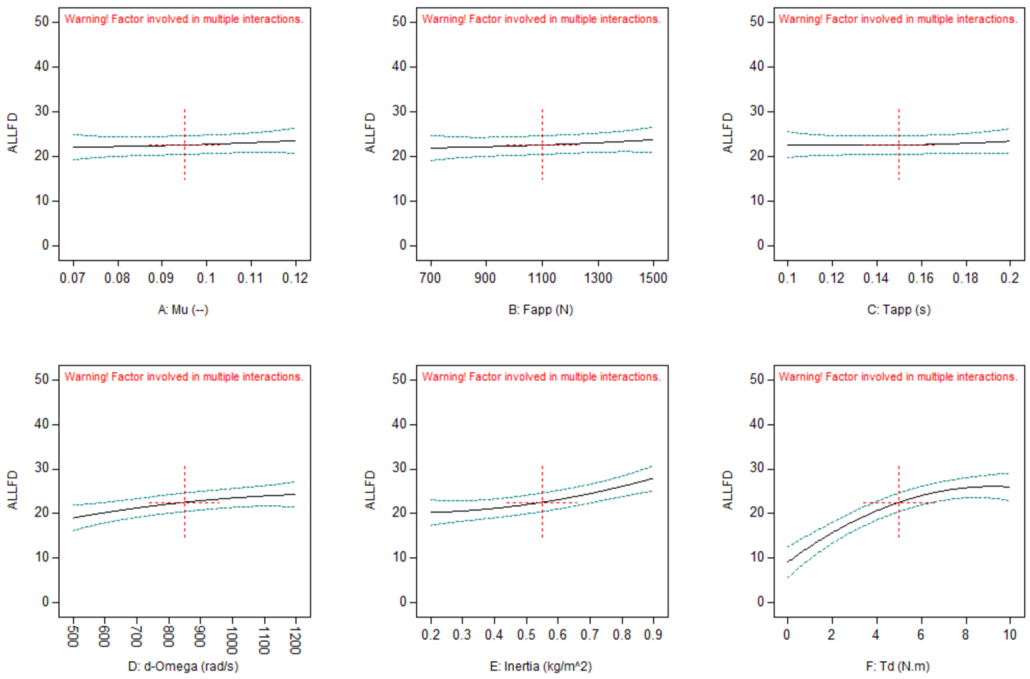

Fig. 4.37 Effect of changing main control factors on the response of friction dissipated energy for DC-170.

4.4.5 Results of DOE method for TC-100

To investigate the effect of different control factors on the performance of TC-100, half central composition RSM method was performed. Similar to SC-74 and DC-170, we have three responses (T_s, C_p, and ALLFD). The results of ANOVA tables and post ANOVA verification tests can be found in Appendix 1. The R-square for T_s, C_p, and ALLFD were 0.998, 0.996, and 0.968, respectively. Adjusted R-square for T_s, C_p, and ALLFD were 0.997, 0.998, and 0.964, respectively which is desirable. The signal-to-noise ratio or Adequate Precision value for T_s, C_p, and ALLFD were higher than 4 that shows high confidence in all three models. The quadratic polynomial models for T_s and C_p were suggested by the software; however, a linear model was applied by the software for presenting the ALLFD results distribution. The results of the ANOVA table show the significant models and it can be said that the obtained statistical models are acceptable. Three different empirical models to predict three different responses were achieved (see Appendix 1). Figures 4.38, 4.39 and 4.40 present the effect of each factor on T_s, C_p, and ALLFD, respectively. Figure 4.38

shows that the only positive factor in T_s is the friction coefficient. It means that by increasing the friction coefficient, the synchronization time decreases as one of objectives of this study. Moreover, the applied inertia, time of applying force and angular velocity were the most effective factors in the synchronization time. Figures 4.38 and 4.39 show similar results with double-cone synchronizer. Also, in this case, the drag torque was the most effective factor in the performance of TC-100 for evaluation of C_p and ALLFD.

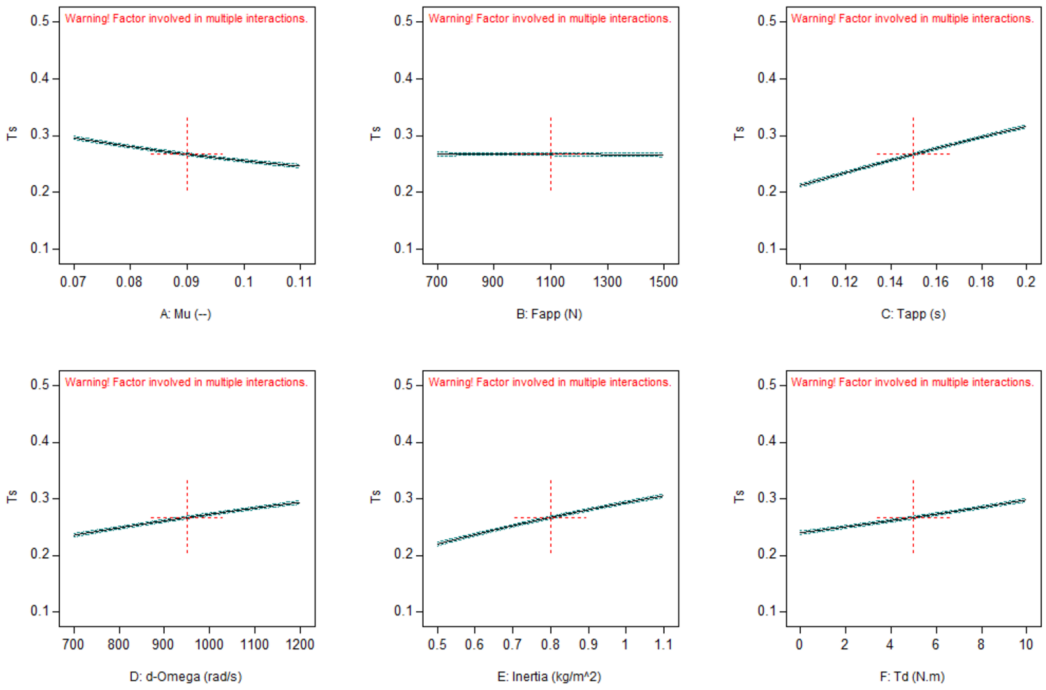

Fig. 4.38 Effect of changing main control factors on the response of the synchronization time for TC-100.

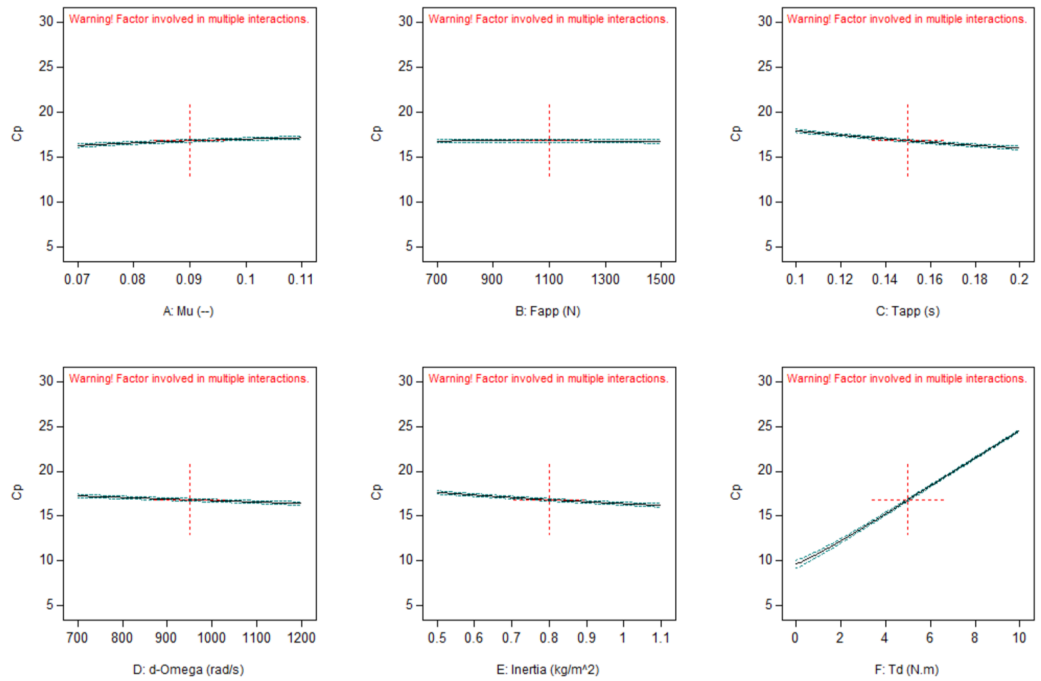

Fig. 4.39 Effect of changing main control factors on the response of contact pressure for TC-100.

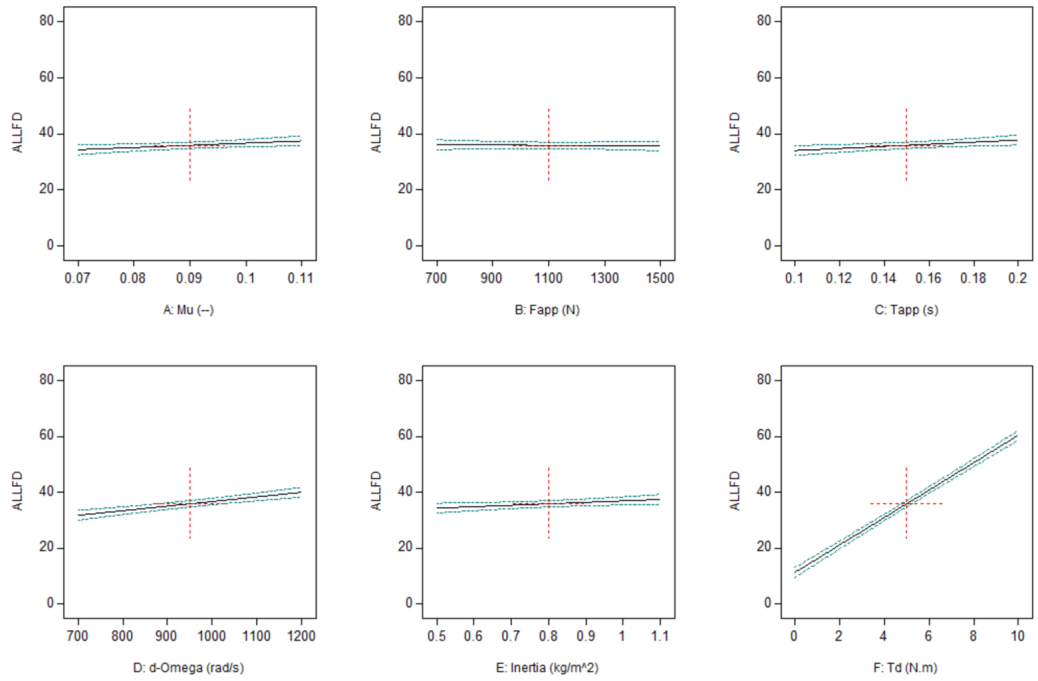

Fig. 4.40 Effect of changing main control factors on the response of friction dissipated energy for TC-100.

4.5 Sensitivity analysis through DOE technique

Three different geometries with different cone angles were used to investigate the effect of tolerance dimension on the performance of single-cone synchronizer. In this study to simplify the model, the effect of drag torque, as a source of noise and disturbance on the system, was neglected. It should be mentioned that in this study five continuous control factors, as well as one categorized control factor, were considered as the main factors of the DOE method. The categorized factor consists of three levels such as minimum threshold, nominal dimension, and maximum threshold. The number and name of responses are the same as previous sections (T_s, C_p, and ALLFD). Based on Table 3.10 from chapter 3 81 simulations were carried out that the full design table is available in Appendix 1. After finishing all simulations, the ANOVA analysis was applied to three responses. In order to evaluate the effect of different factors on T_s,ANOVA analysis was performed that is shown in Table 4.6. Except for applied time (C-T_{app}),all main factors are significant with P-value of less than 0.05 for 95% confidence. To apply the RSM on DOE table of T_s,a quadratic

model was proposed by the Design Expert software. The value of R-square for T_s response is 0.953 that shows high accuracy of the model. Moreover, the difference between Predicted R-square of 0.921 and Adjusted R-square of 0.862 is less than 0.2 which is acceptable. The signal-to-noise ratio is illustrated by Adequate Precision with the value for T_s of higher than 21 which shows high confidence in this model. Additionally, VIF with the value of 1 indicates an ideal correlation between the regression coefficients. Figure 4.41 (a) presents a fitted straight line from the normal distribution of residuals with the minimum standard error. Also, Figure 4.41 (b) shows the residuals versus simulation runs in a randomly scattered plot. It can be seen that all data are between the CIs region. Figure 4.41 (c) depicts the data from residuals versus predicted that is distributed randomly between upper and lower CI lines. Figure 4.41 (d)) shows the inverse sqrt transformation with the best lambda value ($\lambda = -0.5$) that is recommended by the software. Figure 89 shows the effect of every single factor on Ts. The difference between this graph and the previous sections is the upper and lower limit line. In this section, the upper and lower limit lines present the minimum and maximum applied tolerance dimension on the friction cones. From Figure 4.42 it can be observed that the most effective factor on T_s is applied force and the minimum impact on T_s is related to applied time that is shown in ANOVA table as an insignificant factor. Increasing in the friction coefficient and applied force has a positive effect on the synchronization time but by increasing other factors, the synchronization time can be increased which is a negative effect. Moreover, synchronization time is not very sensitive by changing the cone angle.

Table 4.6 ANOVA analysis for synchronization time as the first response of DOE method for SC-74 with varies cone angle.

Source	Sum of Square	DoF	Mean Square	F- Value	p-value		Coefficient	Standard Error	95% CI Low	95% CI High	VIF
Model	5.70	32.00	0.18	30.51	<0.0001	significant					
A-Mu	1.52	1.00	1.52	261.22	<0.0001	significant	0.15	9.00E-03	0.13	0.16	1
B-Fapp	2.21	1.00	2.21	378.55	<0.0001	significant	0.18	9.00E-03	0.16	0.19	1
C-Tapp	0.00	1.00	0.00	0.25	0.62		-0.004544	9.00E-03	-0.023	0.014	1
D-d-Omega	0.79	1.00	0.79	135.36	<0.0001	significant	-0.1	9.00E-03	-0.12	-0.087	1
E-Inertia	0.85	1.00	0.85	145.07	<0.0001	significant	-0.11	9.00E-03	-0.13	-0.09	1
F-Alpha-max	0.02	2.00	0.01	1.29	0.28		0.017	1.20E-02	-0.007332	4.10E-02	
F-Alpha-min							-0.0001512	1.20E-02	-0.024	2.40E-02	
						Std. Dev.	0.076		R-Squared	0.9531	
						Mean	1.06		Adj R-Squared	0.9219	
Residual	0.28	48	5.84E-03			C.V. %	7.22		Pred R-Squared	0.8673	
Cor Total	5.98	80				PRESS	0.79		Adeq Precision	21.32	

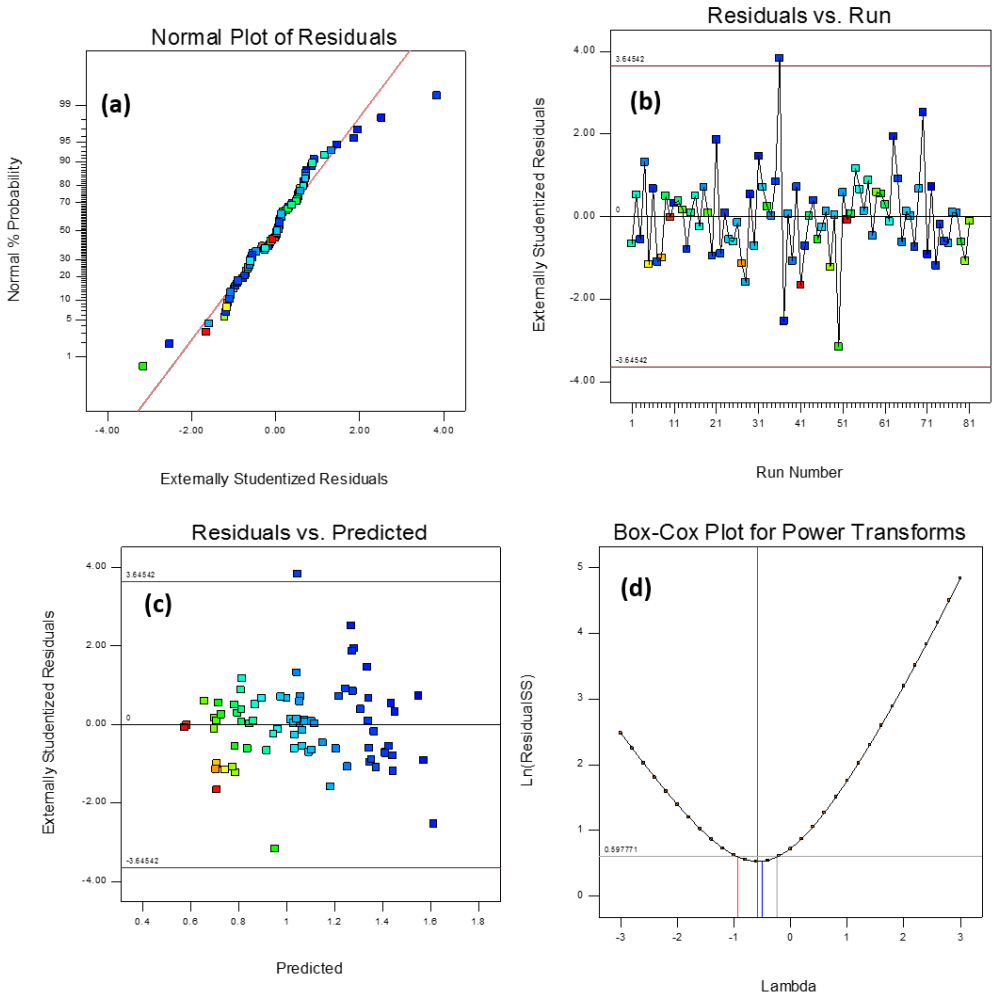

Fig. 4.41 Post ANOVA verification tools for prediction of synchronization time of SC-74 with varies cone angle.

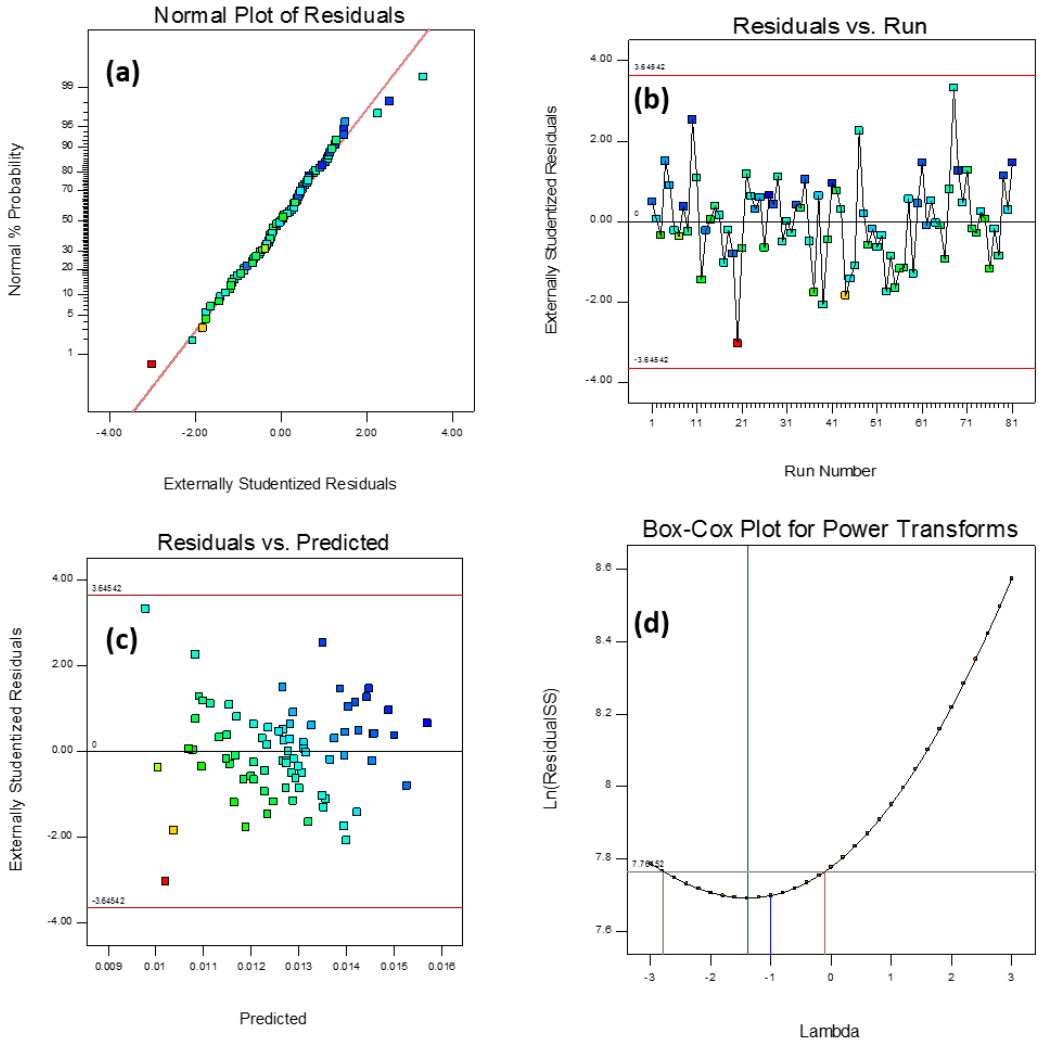

Fig. 4.42 Effect of changing main control factors on the response of synchronization time for SC-74 with varies cone angle.

To assess the effect of different factors on C_p, ANOVA analysis was performed that is shown in Table 4.7.The P-values for all factors are insignificant, however, the model is significant overlay. A linear model was proposed by the Design Expert software to evaluate the response of C_p. The value of R-square for C_pCp response is 0.705 which can be acceptable for this analysis. Furthermore, the difference between Predicted R-square of 0.555 and Adjusted R-square of 0.524 is less than 0.2 which is acceptable. The signal-to-noise ratio is illustrated by Adequate Precision which this value for C_p is higher than 9 that shows the confidence in this model. Additionally, VIF with value of 1 indicates an ideal correlation between the regression coefficients.

Table 4.7 ANOVA analysis for contact pressure as the second response of DOE method for SC-74 with varies cone angle.

Source	Sum of Square	DoF	Mean Square	F- Value	p-value		Coefficient	Standard Error	95% CI Low	95% CI High	VIF
Model	0.0001336	27.00	0.00	4.70	<0.0001	significant					
A-Mu	9.741E-07	1.00	0.00	0.93	0.34		-0.0001163	1.21E-04	-0.0003587	0.0001261	1
B-Fapp	0.0001124	1.00	0.00	106.86	<0.0001	significant	-0.001249	1.21E-04	-0.001492	-0.001007	1
C-Tapp	9.96E-08	1.00	0.00	0.10	0.76		-0.00003719	1.21E-04	-0.0002796	0.0002052	1
D-d-Omega	9.645E-08	1.00	0.00	0.09	0.76		0.0000366	1.21E-04	-0.0002058	0.000279	1
E-Inertia	4.119E-07	1.00	0.00	0.39	0.53		0.00007564	1.21E-04	-0.0001668	0.0003181	1
F-Alpha-max	0.000002531	2.00	0.00	1.20	0.31		0.0001933	1.61E-04	-0.0001299	5.17E-04	
F-Alpha-min							0.00004057	1.61E-04	-0.0002827	3.64E-04	
						Std. Dev.	0.001026		R-Squared	0.7055	
						Mean	0.013		Adj R-Squared	0.5555	
Residual	0.00005575	53	1.05E-06			C.V. %	8.07		Pred R-Squared	0.2242	
Cor Total	0.0001893	80				PRESS	0.0001469		Adeq Precision	9.809	

Figure 4.43 (a) presents a fitted straight line from the normal distribution of residuals with minimum standard error. Also, Figure 4.43 (b) shows the residuals versus simulation runs in a randomly scattered plot. It can be seen that all data are between the CIs region. Figure 4.43 (c)depicts the data from residuals versus predicted that is distributed randomly between upper and lower CI lines. Figure 4.43 (d)shows the power transformation with the best lambda value ($\lambda = -1.39$) that is recommended from the software. Figure 4.44 shows the effect of every single factor on C_p. In this section, the upper and lower limit lines present the minimum and maximum applied tolerance dimensions on the friction cones. From Figure 4.44 it can be observed that the most effective factor on C_p is applied force and other factors have almost a similar effect on C_p. Moreover, contact pressure will increase when the friction cone has the maximum tolerance dimension. It has also been proved also in the previous section (see Figure 4.22).

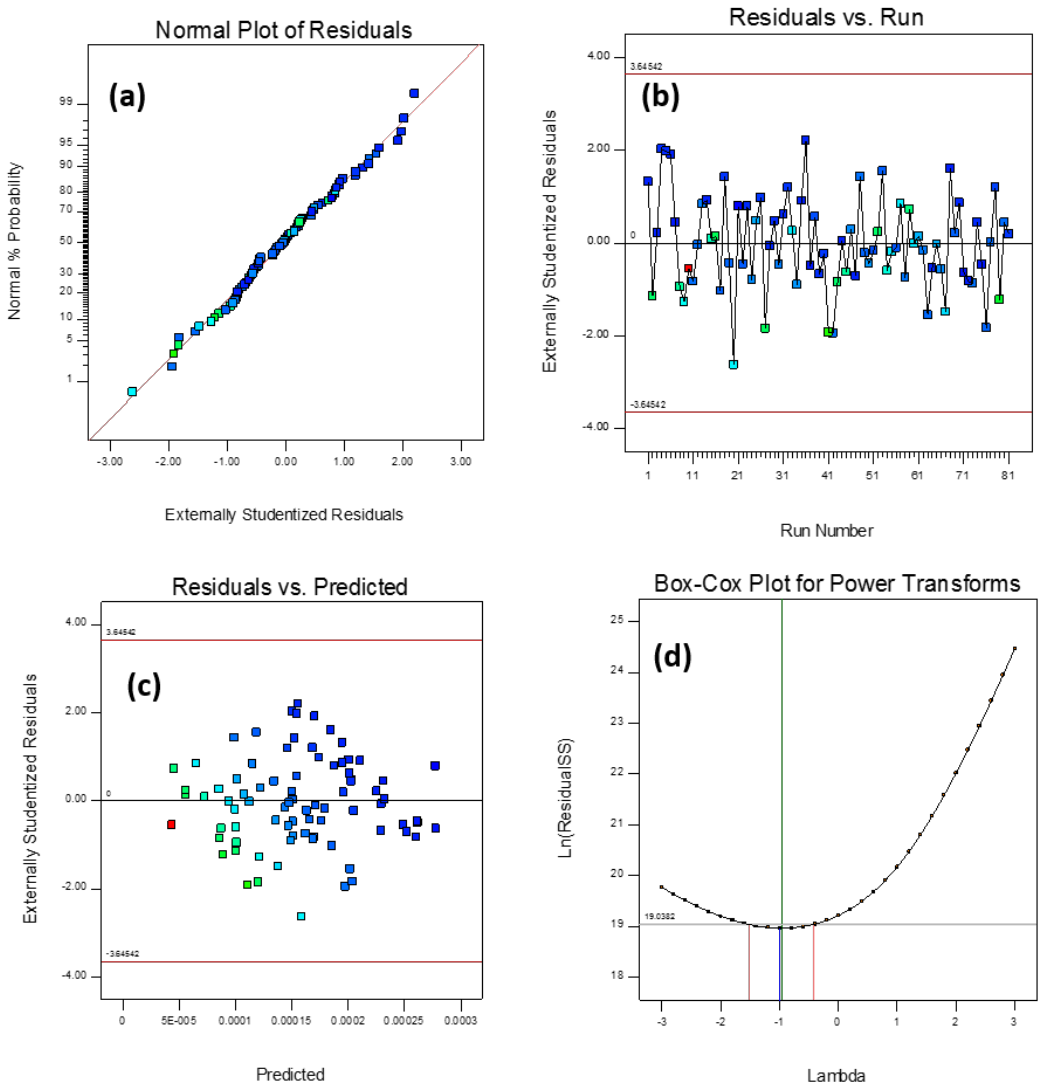

Fig. 4.43 Post ANOVA verification tools for prediction of contact pressure for SC-74 with varies cone angle.

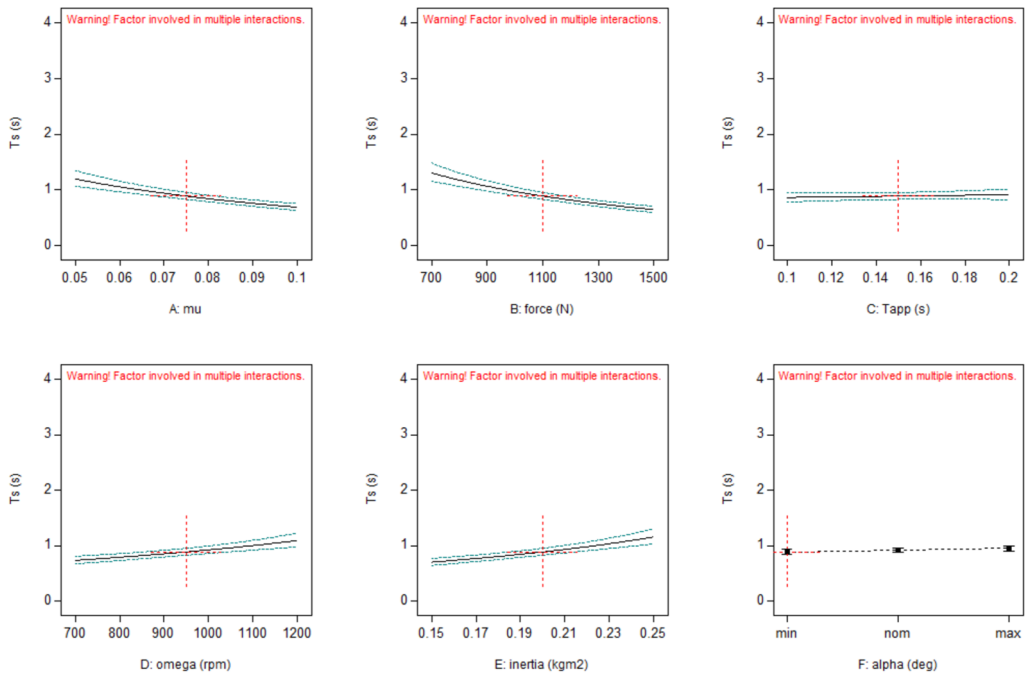

Fig. 4.44 Effect of changing main control factors on the response of contact pressure for SC-74 with varies cone angle.

To investigate the effect of the third response of SC-74 as the friction dissipated energy, (ALLFD) ANOVA analysis was performed that is shown in Table 4.8.It can be said that except time of applying force, all main factors are significant with P-value of less than 0.08 for 92% confidence. To apply the RSM on DOE table of ALLFD, a linear model regarding only main factors was proposed by the Design Expert software. The value of R-square for ALLFD response is 0.779 that shows high accuracy of the model. Moreover, the difference between Predicted R-square of 0.666 and Adjusted R-square of 0.505 is less than 0.2 which is desirable. The signal-to-noise ratio or Adequate Precision value for ALLFD is higher than 10 that shows highly confidence (much bigger than 4) in this model. Furthermore, the results between CIs prove that the main factors are significant and ALLFD can be affected by changing the main factors over the selected region. Additionally, VIF with value of 1 indicates an ideal correlation between the regression coefficients.

Table 4.8 ANOVA analysis for friction dissipated energy as the third response of DOE method for SC-74 with varies cone angle.

Source	Sum of Square	DoF	Mean Square	F- Value	p-value		Coefficient	Standard Error	95% CI Low	95% CI High	VIF
Model	2.536E-07	27	9.392E-09	6.93	<0.0001	significant					
A-Mu	1.492E-08	1	1.492E-08	11.01	0.0016	significant	0.0000144	4.34E-06	0.000005693	0.0000231	1
B-Fapp	4.025E-08	1	4.025E-08	29.69	<0.0001	significant	0.00002364	4.34E-06	0.00001494	0.00003235	1
C-Tapp	5.142E-12	1	5.142E-12	0.003792	0.9511		-2.672E-07	4.34E-06	-0.000008971	0.000008437	1
D-d-Omega	0.000000129	1	0.000000129	95.15	<0.0001	significant	-0.00004233	4.34E-06	-0.00005103	-0.00003362	1
E-Inertia	3.196E-08	1	3.196E-08	23.57	<0.0001	significant	-0.00002107	4.34E-06	-0.00002977	-0.00001236	1
F-Alpha-max	6.953E-09	2	3.476E-09	2.56	0.0865	significant	-0.000007241	5.79E-06	-0.00001885	4.36E-06	
F-Alpha-min							-0.000005837	5.79E-06	-0.00001744	5.77E-06	
						Std. Dev.	3.68217E-05		R-Squared	0.779188776	
						Mean	0.000158055		Adj R-Squared	0.666700039	
Residual	7.18594E-08	53	1.36E-09			C.V. %	23.29677588		Pred R-Squared	0.505536373	
Cor Total	3.25434E-07	80				PRESS	1.60915E-07		Adeq Precision	10.81764874	

Figure 4.45 (a) presents an acceptable normal distribution of residuals. It can be observed that all runs are fitted on a straight line which means the low residual error. Also, figure 4.45(b) shows the residuals versus simulation runs in a random scattered plot. It can be seen that all data are between the CIs region. Figure 4.45 (c) depicts the data from residuals versus predicted that is distributed randomly between upper and lower CI lines. Figure 4.45 (d) the inverse lambda transformation with the best lambda value ($\lambda = -1$) that is recommended from the software.

Figure 4.46 illustrates the effect of every single factor on ALLFD. From figure 4.46it can be seen that the applied force is slightly more effective than other factors on ALLFD. Moreover, ALLFD will be reduced when the friction cone has the maximum tolerance dimension. The dissipated friction energy in minimum and nominal conditions are almost at the same value. Due to the stiffness of the previous model, these models cannot be compared together in terms of friction dissipated energy.

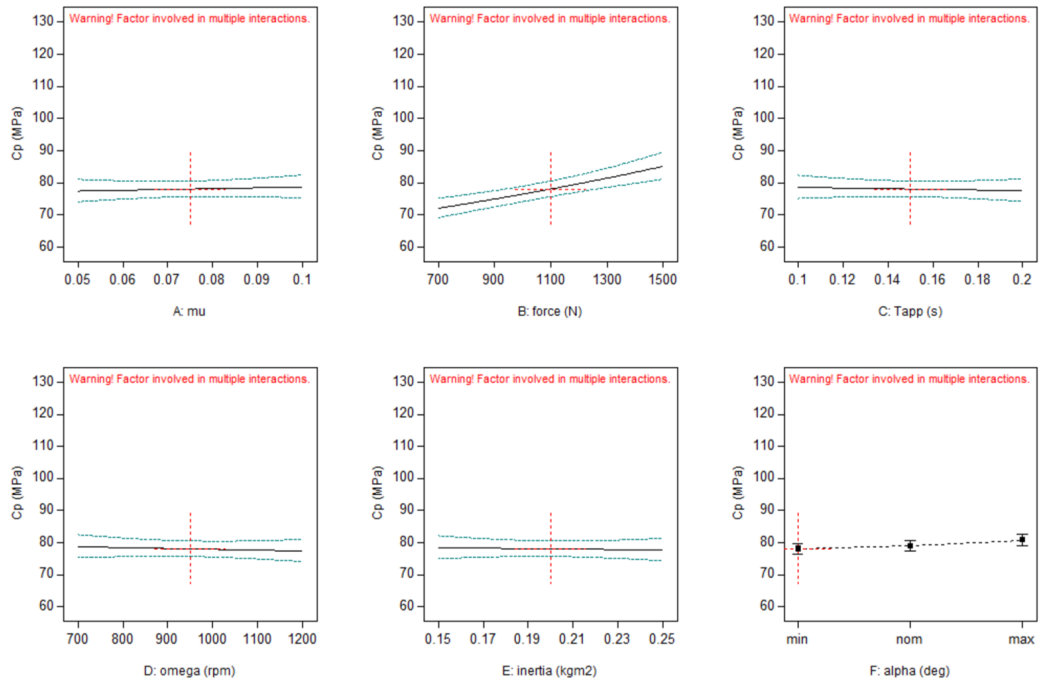

Fig. 4.45 Post ANOVA verification tools for prediction of friction dissipated energy for SC-74 with varies cone angle.

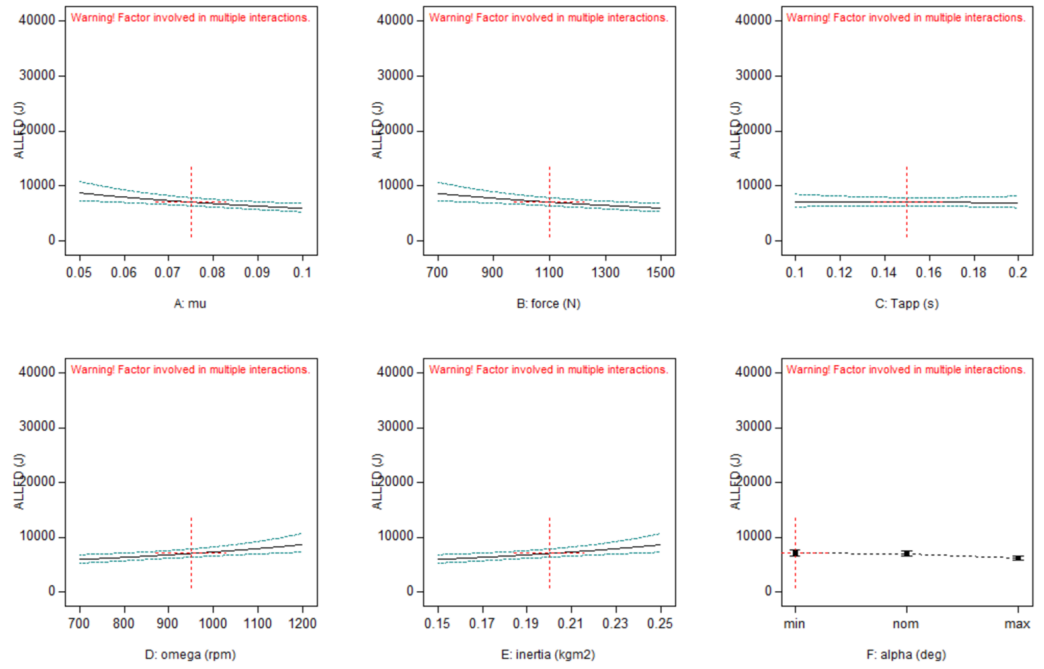

Fig. 4.46 Effect of changing main control factors on the response of friction dissipated energy for SC-74 with varies cone angle.

The empirical models for three responses (T_s, C_p and ALLFD) are available in Appendix1. For each cone angle (min, nominal, and max tolerance dimension), a separate empirical model was obtained.

4.6 Summary of this chapter

This chapter presents the results of different approaches to evaluate the dynamic behavior of three synchronizers.

1. Results of two mathematical models were presented in this chapter. The first model is only able to predict the time of synchronization. The results of the first model were compared with experimental data and the error of the model was calculated. The second model, as well as calculation of the time of synchronization, simulates the overall behavior of different parts of the synchronizer.

2. Results of natural frequency and modal dynamic analysis with different loading conditions were presented.

3. A rigid MBD model has been validated the through experiment to show the overall behavior of the synchronizer mechanism.

4. The results of flexible MBD model with higher accuracy than rigid model were compared with experimental data. Moreover, a sub-model was extracted from FMBD model for using in DOE method.

5. A multi-objective DOE analysis was performed on three types of synchronizers and after statistical verification methods, the validated empirical models were proposed to predict system responses. In addition, a sensitivity analysis was carried out in order to evaluate the effect of different control factors on the performance of the synchronizer mechanism.

Chapter 5

Conclusion

5.1 Introduction

The objectives of this study were focused on establishing different multi-body dynamic models with different approaches to investigate the dynamic behavior of three types of the synchronizer mechanism. These approaches can be applied to study the dynamic responses of shifting mechanisms regarding calculation time, the accuracy of results and complexity of the problem. The following section presents the conclusion drawn from this study.

5.2 Conclusion

In conclusion, the outcomes of this thesis can be categorized as follows:

- A critical review was carried out on different transmission systems, different synchronizer mechanisms, the existing model to simulate the shifting process, significant physical parameters during synchronization and different methods to model the shifting process.
- A new Eulerian mathematical model to predict synchronization time was proposed. This model considers applied force as a function of time. The time dependency can be considered as the novelty of this method. The calculated

error of this method in the worst case was less than 11% if compared with experimental results

- Another mathematical model for every phase of synchronization was established and the results of this model were compared with experimental data. There is a good agreement between extracted results. This model gives a rough estimation of the dynamic behavior of synchronizer regarding fast calculation time. Because of the rigid body assumption, the reliability of this model in different loading conditions and changing the geometrical dimensions can be reduced.

- A set of experiments for the purpose of validation were carried out on a universal test rig machine.

- An FE model was generated to evaluate the natural frequency and the modal dynamic behavior of the system. The modal responses of different synchronizers under various loading and boundary conditions were examined. The results highlighted the resonance frequency for each synchronizer based on transient modal dynamic.

- The developed FE model was modified in order to carry out the multi-body dynamic analysis of three synchronizers. Two different MBD methods (rigid and flexible) were created and the results of those methods were compared with experimental data. There is a good agreement between both models and experimental results. However, the accuracy of the flexible model is much closer to the real test conditions.

- A sensitivity analysis was performed in the rigid MBD model and the effect of changing the angle of friction cones was investigated. A new expression as a force ratio error was proposed as the outcome of this study.

- The flexible MBD model was simplified to a sub-model in order to use for DOE optimization method. Furthermore, the results of this validated model were used for the DOE- RSM method in order to obtain the best operational conditions for each kind of synchronizers. After performing different statistical verification tests some empirical models with more than 96% accuracy were proposed in order to predict the synchronization time, maximum contact pressure, and friction dissipated energy. The calculated synchronization time

from DOE method was compared with experimental data and shows less than 2% error for different synchronizer mechanisms.

- Based on the DOE method, a sensitivity analysis was performed to study the effect of different factors when the friction cones have different tolerance dimensions. After applying the verification test on statistical models, the final empirical models for each condition were presented.

In general, different models which were expressed in this thesis can be applied to different applications. The proposed methodology provides dynamic behavior of synchronizers regarding computational cost and detailed information of synchronization during the shifting process.

5.3 Recommendations and future works

The results of the modal dynamic of this thesis were not validated with experimental results. These results only show the trends of modal dynamics of different synchronizers under various loading conditions. Therefore, performing an experimental procedure can be suggested as an open topic for future works. The mathematical model has the capability to be linked with an optimization technique such as a genetic algorithm to find the best solution. Also, the control factors can be assumed in a wider range to see all dynamic responses of shifting mechanisms.

References

[1] Various components of a manual gearbox. https://carfromjapan.com/article/car-maintenance/how-manual-transmissions-work-explained-easy-way/, 2018.

[2] 11-speed-automatic-transmission-patent filed by ford motor. https://www.autoevolution.com/news/11-speed-automatic-transmission-patent-filed-by-ford-motor-company-with-the-uspto-94355.html year=2018,.

[3] To clutch or not to clutch: A guide to dual clutch transmissions. https://gearpatrol.com/2013/08/19/a-guide-to-dual-clutch-transmissions/ year=2013,.

[4] Automated manual transmission the eureka moment for the indian automotive scene. http://www.aventure.ac.in/automated-manual-transmission-eureka-moment-indias-automotive-scene/ year=2014,.

[5] Construction mechanic basic chapter 10. http://seabeemagazine.navylive.dodlive.mil year=2018,.

[6] Design of transmission systems. https://sites.google.com/site/designoftransmissionsystems/Design-of-Gear-Boxes/constant-mesh-gear-box year=2014,.

[7] Dog clutch free 3d model. https://www.cgtrader.com/free-3d-models/industrial/part/dog-clutch year=2016,.

[8] Giesbert Lechner and Harald Naunheimer. *Automotive transmissions: fundamentals, selection, design and application*. Springer Science and Business Media, 1999.

[9] Freewheels,sprag andtrapped roller clutches. http://pdf.directindustry.com/pdf/renold/freewheels-sprag-trapped-roller-clutches/5242-325529-_8.html year=2018,.

[10] Hydraulic multi-plate clutch. https://www.ortlinghaus.com/english/products/clutches/clutches.html year=2018,.

[11] Ver ABAQUS. 6.14 documentation. *Dassault Systemes Simulia Corporation*, 2014.

[12] Amit Sandooja and Sagar Jadhav. Analysis of gear geometry and durability with asymmetric pressure angle. *SAE International Journal of Commercial Vehicles*, 5(2012-01-1995):546–558, 2012.

[13] Adrian Irimescu, Liviu Mihon, and G Padure. Automotive transmission efficiency measurement using a chassis dynamometer. *International Journal of Automotive Technology*, 12(4):555–559, 2011.

[14] Chyuan-Yow Tseng and Chih-Hsien Yu. Advanced shifting control of synchronizer mechanisms for clutchless automatic manual transmission in an electric vehicle. *Mechanism and Machine Theory*, 84:37–56, 2015.

[15] Gu Yuming. Discuss designing-method of transmission synchronizer. *International Conference on Advanced Technology of Design and Manufacture (ATDM 2011)*, 2011.

[16] B Paffoni, R Progri, R Gras, and J Blout. The hydrodynamic phase of gearbox synchromesh operation: the influence of radial and circumferential grooves. *Proceedings of the Institution of Mechanical Engineers, Part J: Journal of Engineering Tribology*, 211(2):107–116, 1997.

[17] Peter Fietkau and Bernd Bertsche. Influence of tribological and geometrical parameters on lubrication conditions and noise of gear transmissions. *Mechanism and Machine Theory*, 69:303–320, 2013.

[18] Manish Kumar Sharma and Jinesh Savla. Shift system inertia mass optimization techniques to minimize double bump for manual transmission. Technical report, SAE Technical Paper, 2012.

[19] Joohyung Kim, Dukhwan Sung, Changsung Seok, Hyunsoo Kim, Hanlim Song, Chaehong Lim, and Jungjune Kim. Development of shift feeling simulator for a manual transmission. Technical report, SAE Technical Paper, 2002.

[20] Paul D Walker and Nong Zhang. Investigation of synchroniser engagement in dual clutch transmission equipped powertrains. *Journal of Sound and Vibration*, 331(6):1398–1412, 2012.

[21] Xu Wanli, Zhao Wei, Su Bin, and Xu Ximeng. Investigation of manual transmission synchronizer failure mechanism induced by interface material/lubricant combinations. *Wear*, 328:475–479, 2015.

[22] Gerhard Poll and Marcus Spreckels. Influence of temperature distribution on the tribological performance of automotive synchronisers. *Tribology Series*, 41:613–621, 2003.

[23] Yen-Chen Liu and Ching-Huan Tseng. Simulation and analysis of synchronisation and engagement on manual transmission gearbox. *International journal of vehicle design*, 43(1-4):200–220, 2007.

[24] Syed T Razzacki. Synchronizer design: a mathematical and dimensional treatise. Technical report, SAE Technical Paper, 2004.

[25] L Lovas, Daniel Play, J Marialigeti, and Jean-Francois Rigal. Mechanical behaviour simulation for synchromesh mechanism improvements. *Proceedings of the Institution of Mechanical Engineers, Part D: Journal of Automobile Engineering*, 220(7):919–945, 2006.

[26] Syed T Razzacki and Jonathan E Hottenstein. Synchronizer design and development for dual clutch transmission (dct). Technical report, SAE Technical Paper, 2007.

[27] Ana Pastor Bedmar. Synchronization processes and synchronizer mechanisms in manual transmissions. *Modelling and simulation of synchronization processes: Master's thesis.: Göteborg (Sweden)*, 2013.

[28] Homer Rahnejat. *Multi-body dynamics: vehicles, machines, and mechanisms*. Wiley, 1998.

[29] Hiroaki Hoshino. Analysis on synchronization mechanism of transmission. Technical report, SAE Technical Paper, 1999.

[30] NA Abdel-Halim, DC Barton, DA Crolla, and AM Selim. Performance of multicone synchronizers for manual transmissions. *Proceedings of the Institution of Mechanical Engineers, Part D: Journal of Automobile Engineering*, 214(1):55–65, 2000.

[31] Christopher Vagg, Christian J Brace, Roshan Wijetunge, Sam Akehurst, and Lloyd Ash. Development of a new method to assess fuel saving using gear shift indicators. *Proceedings of the Institution of Mechanical Engineers, Part D: Journal of Automobile Engineering*, 226(12):1630–1639, 2012.

[32] Callum J Oglieve, Mahdi Mohammadpour, and Homer Rahnejat. Optimisation of the vehicle transmission and the gear-shifting strategy for the minimum fuel consumption and the minimum nitrogen oxide emissions. *Proceedings of the Institution of Mechanical Engineers, Part D: Journal of Automobile Engineering*, 231(7):883–899, 2017.

[33] A Farokhi Nejad and G Chiandussi. Estimation of the synchronization time of a transmission system through multi body dynamic analysis. *INTERNATIONAL JOURNAL OF MECHANICAL ENGINEERING AND ROBOTICS RESEARCH*, 6(3):232–236, 2017.

[34] Harald Naunheimer, Bernd Bertsche, Joachim Ryborz, and Wolfgang Novak. *Automotive transmissions: Fundamentals, selection, design and application*. Springer Science and Business Media, 2010.

[35] GW Blankenship and A Kahraman. Steady state forced response of a mechanical oscillator with combined parametric excitation and clearance type non-linearity. *Journal of Sound and Vibration*, 185(5):743–765, 1995.

[36] Ahmet Kahraman and G Wesley Blankenship. Experiments on nonlinear dynamic behavior of an oscillator with clearance and periodically time-varying parameters. *Journal of Applied Mechanics*, 64(1):217–226, 1997.

[37] Vijaya Kumar Ambarisha and Robert G Parker. Nonlinear dynamics of planetary gears using analytical and finite element models. *Journal of sound and vibration*, 302(3):577–595, 2007.

[38] Paul D Walker and Nong Zhang. Investigation of synchroniser engagement in dual clutch transmission equipped powertrains. *Journal of Sound and Vibration*, 331(6):1398–1412, 2012.

[39] Y Zhang, X Chen, X Zhang, H Jiang, and W Tobler. Dynamic modeling and simulation of a dual-clutch automated lay-shaft transmission. *Journal of Mechanical Design*, 127(2):302–307, 2005.

[40] Robert G Parker, Vinayak Agashe, and Sandeep M Vijayakar. Dynamic response of a planetary gear system using a finite element/contact mechanics model. *Journal of Mechanical Design*, 122(3):304–310, 2000.

[41] A.Hedman. Powertrain mechanics, course. Lecture Notes, Chalmers University of Technology, Applied Mechanics department, 2011.

[42] Bernd Matthes. Dual clutch transmissions-lessons learned and future potential. Technical report, SAE Technical Paper, 2005.

[43] KruttgenSascha.Painter Jorg.Bonning, Friedhelm.KrakeRolf. *New opel six-speed manual transmission for high-performance cars with transverse engine installation*. Springer,ATZ Worldw, 2004.

[44] Geoff Davis, Rolland Donin, Mark Findlay, Peter Harman, Mark Ingram, and David Kelly. Simulationsgestützte optimierung der schaltqualität von handschaltgetrieben. *ATZ-Automobiltechnische Zeitschrift*, 106(7-8):668–675, 2004.

[45] H Drott and E Oppertshäuser. 3-konus-synchronisierungen in opel-pkw-schaltgetrieben. *VDI-Berichte*, (878):293–309, 1991.

[46] Hauser.C. Influence of oil ageing on the stabilitiy of the coefficient of friciton of multi-plate clutches. *FVA-Forschungsvorhaben*, (297), 2004.

[47] Heinz Heisler. *Advanced vehicle technology*. Elsevier, 2002.

[48] Yuji Goto, Yoichi Yagi, Yoshiro Morimoto, and Masami Kawasaki. Shift feel in manual transmissions-an analysis of unsmooth shifting and gear clashing. *JSAE Rev*, 9(4):52–55, 1988.

[49] H Winter and H Pflaum. Synchronizers in motor vehicle manual transmissions. *Antriebstechnik*, 30(8):50–58, 1991.

[50] László Lovas, Daniel Play, János Márialigeti, and Jean-Francois Rigal. Modelling of gear changing behaviour. *Periodica Polytechnica. Transportation Engineering*, 34(1-2):35, 2006.

[51] S Goll and R Schröper. The synchronizer shifting element a sophisticated assembly in passenger car and commercial vehicle transmissions. *VDI-Berichte*, 579:287–300, 1986.

[52] Mosbach C. Investigation of the causes of friction vibrations and noises of oil-cooled frictional shifting elements. *FVA-Forschungsvorhaben*, 297, 2001.

[53] Frey D Naumann W. Influencing frictional shifting elements by the oil. *VDI-Berichte*, 680, 1988.

[54] Wagner D. New friction materials and concepts for single and multiple synchronizers. *ATZ Automobiltechnische Zeitschrift*, 95, 1993.

[55] Ronald L Huston. *Multibody dynamics*. Tolley, 1990.

[56] Andreas Müller. Generic mobility of rigid body mechanisms. *Mechanism and Machine Theory*, 44(6):1240–1255, 2009.

[57] John Joseph Uicker, Gordon R Pennock, Joseph Edward Shigley, et al. *Theory of machines and mechanisms*, volume 1. Oxford University Press New York, NY, 2011.

[58] RA Wehage and EJr Haug. Generalized coordinate partitioning for dimension reduction in analysis of constrained dynamic systems. *Journal of mechanical design*, 104(1):247–255, 1982.

[59] Nicolae Orlandea, Milton A Chace, and Donald A Calahan. A sparsity-oriented approach to the dynamic analysis and design of mechanical systems part 1. *Journal of Engineering for Industry*, 99(3):773–779, 1977.

[60] MA Chace. Analysis of the time-dependence of multi-freedom mechanical systems in relative coordinates. *Journal of Engineering for Industry*, 89(1):119–125, 1967.

[61] Javier Garcia De Jalon and Eduardo Bayo. *Kinematic and dynamic simulation of multibody systems: the real-time challenge*. Springer Science and Business Media, 2012.

[62] Parviz E Nikravesh. *Computer-aided analysis of mechanical systems*, volume 186. Prentice-hall Englewood Cliffs, NJ, 1988.

[63] Werner Schiehlen. Multibody system dynamics: Roots and perspectives. *Multibody system dynamics*, 1(2):149–188, 1997.

[64] Ahmed A Shabana. Flexible multibody dynamics: review of past and recent developments. *Multibody system dynamics*, 1(2):189–222, 1997.

[65] F Reuleaux. Theoretische kinematic, 1875. translated as kinematics of machinery, 1963.

[66] J Michael McCarthy and Gim Song Soh. *Geometric design of linkages*, volume 11. Springer Science and Business Media, 2010.

[67] Parviz E Nikravesh. *Planar multibody dynamics: formulation, programming and applications*. CRC press, 2007.

[68] Robert D Cook et al. *Concepts and applications of finite element analysis*. John Wiley and Sons, 2007.

[69] Chao Yang, Weiguo Gao, Zhaojun Bai, Xiaoye S Li, Lie-Quan Lee, Parry Husbands, and Esmond Ng. An algebraic substructuring method for large-scale eigenvalue calculation. *SIAM Journal on Scientific Computing*, 27(3):873–892, 2005.

[70] Kolja Elssel and Heinrich Voss. Reducing huge gyroscopic eigenproblems by automated multi-level substructuring. *Archive of Applied Mechanics*, 76(3-4):171–179, 2006.

[71] Janusz S Przemieniecki. *Theory of matrix structural analysis*. Courier Corporation, 1985.

[72] John E Mottershead and MI Friswell. Model updating in structural dynamics: a survey. *Journal of sound and vibration*, 167(2):347–375, 1993.

[73] Ahid D Nashif, Ahid D Nashif, David IG Jones, David IG Jones, John P Henderson, et al. *Vibration damping*. John Wiley and Sons, 1985.

[74] S Rao Singiresu et al. *Mechanical vibrations*. Addison Wesley, 1995.

[75] Douglas C Montgomery. *Design and analysis of experiments*. John wiley and sons, 2017.

[76] Raymond H Myers, Douglas C Montgomery, et al. *Response surface methodology: process and product optimization using designed experiments*, volume 4. Wiley New York, 1995.

[77] George EP Box and Kenneth B Wilson. On the experimental attainment of optimum conditions. *Journal of the Royal Statistical Society: Series B (Methodological)*, 13(1):1–38, 1951.

[78] Genichi Taguchi and Yuin Wu. *Introduction to off-line quality control*. Central Japan Quality Control Assoc., 1979.

[79] Gunst R. F. Hess J. L. Mason, R. L. *Statistical design and analysis of experiments: with applications to engineering and science*. John Wiley and Sons, 2003.

[80] Thomas P. Ryan and J. P. Morgan. Modern experimental design. *Journal of Statistical Theory and Practice*, 1(3-4):501–506, 2007.

[81] Jack PC. Kleijnen. An overview of the design and analysis of simulation experiments for sensitivity analysis. *European Journal of Operational Research*, 164(2):287–300, 2005.

[82] M. Cavazzuti. *Optimization Methods: From Theory to Design*, volume 53. Springer, 2013.

[83] Frey D. Matthes B. Holzer, N. Drag torque of wet multi-plate brakes. *VDI BERICHTE*, 1323(2):469–490, 1997.

[84] Progri R. Gras R. Blouet J. Paffoni, B. The hydrodynamic phase of gearbox synchromesh operation: the influence of radial and circumferential grooves. *Proceedings of the Institution of Mechanical Engineers, Part J: Journal of Engineering Tribology*, 211(2):107–116., 1997.

[85] Progri R. Gras R. Paffoni, B. The mixed phase of gearbox synchromesh operation. *Proceedings of the Institution of Mechanical Engineers, Part J: Journal of Engineering Tribology*, 214(2):157–165, 2000.

[86] Lu, X., Khonsari, M. M., Gelinck, E. R. The Stribeck curve: experimental results and theoretical prediction Journal of tribology, 128(4):789–794, 2006.

[87] Firrone, C. M.,Zucca, S. Modelling friction contacts in structural dynamics and its application to turbine bladed disks.

[88] Zucca, S., Botto, D., Gola, M. M. Range of variability in the dynamics of semi-cylindrical friction dampers for turbine blades.

[89] Choy, F. K., Tu, Y. K., Savage, M., Townsend, D. P. Vibration signature and modal analysis of multi-stage gear transmission Journal of the Franklin Institute

[90] Razavykia, A., Farahany, S., Yusof, N. M. Evaluation of cutting force and surface roughness in the dry turning of almg2si in situ metal matrix composite inoculated with bismuth using doe approach. =Measurement,76,(170-182),2000

Appendix A

Appendix1

Table A.1 Design of Experiment's table for DC-170

		Factor 1	Factor 2	Factor 3	Factor 4	Factor 5	Factor 6	Response 1	Response 2	Response 3
Std	Run	A:Mu	B:Fapp	C:Tapp	D:d-Omega	E:Inertia	F:Td	Ts	Cp	ALLFD
		–	N	s	rad/s	kg/m^2	N.m	s	MPa	kJ
1	17	0.07	700	0.1	500	0.2	0	0.196625	18.6991	6.51075
2	36	0.12	700	0.1	500	0.2	10	0.171245	43.2716	17.7416
3	27	0.07	1500	0.1	500	0.2	10	0.135092	46.169	17.6687
4	10	0.12	1500	0.1	500	0.2	0	0.0893471	30.0205	5.86028
5	6	0.07	700	0.2	500	0.2	10	0.318053	38.2742	18.1789
6	46	0.12	700	0.2	500	0.2	0	0.184966	19.2935	5.66157
7	35	0.07	1500	0.2	500	0.2	0	0.165439	20.4766	6.32982
8	18	0.12	1500	0.2	500	0.2	10	0.170309	43.3311	23.6706
9	40	0.07	700	0.1	1200	0.2	10	0.437614	36.6816	31.2527
10	47	0.12	700	0.1	1200	0.2	0	0.255275	16.5328	8.75269
11	50	0.07	1500	0.1	1200	0.2	0	0.21422	17.9247	9.67095
12	51	0.12	1500	0.1	1200	0.2	10	0.162462	43.8569	28.074
13	44	0.07	700	0.2	1200	0.2	0	0.451899	13.3727	9.36486
14	22	0.12	700	0.2	1200	0.2	10	0.376703	37.3666	20.1729
15	23	0.07	1500	0.2	1200	0.2	10	0.297553	38.6758	19.8231
16	34	0.12	1500	0.2	1200	0.2	0	0.19575	18.7413	20.8141
17	38	0.07	700	0.1	500	0.9	10	0.745526	34.9318	25.8114
18	14	0.12	700	0.1	500	0.9	0	0.43489	13.5331	13.3114
19	32	0.07	1500	0.1	500	0.9	0	0.357912	14.45	13.694
20	41	0.12	1500	0.1	500	0.9	10	0.246282	39.973	28.6536
21	13	0.07	700	0.2	500	0.9	0	0.759811	11.7101	13.5665
22	20	0.12	700	0.2	500	0.9	10	0.556319	35.7776	29.5282
23	15	0.07	1500	0.2	500	0.9	10	0.441245	36.6467	29.3824
24	45	0.12	1500	0.2	500	0.9	0	0.279615	15.9005	8.33997
25	4	0.07	700	0.1	1200	0.9	0	1.63355	10.405	7.00101
26	1	0.12	700	0.1	1200	0.9	10	1.00945	34.2816	36.655
27	3	0.07	1500	0.1	1200	0.9	10	0.805656	34.7462	36.4801
28	52	0.12	1500	0.1	1200	0.9	0	0.481077	13.1239	15.7292
29	19	0.07	700	0.2	1200	0.9	10	1.75498	33.5014	37.7045
30	11	0.12	700	0.2	1200	0.9	0	1.02374	11.081	15.2045

		Factor 1	Factor 2	Factor 3	Factor 4	Factor 5	Factor 6	Response 1	Response 2	Response 3
Std	Run	A:Mu	B:Fapp	C:Tapp	D:d-Omega	E:Inertia	F:Td	Ts	Cp	ALLFD
		–	N	s	rad/s	kg/m^2	N.m	s	MPa	kJ
31	2	0.07	1500	0.2	1200	0.9	0	0.838989	11.4798	17.041
32	49	0.12	1500	0.2	1200	0.9	10	0.56441	35.7298	40.3472
33	12	0.0558729	1100	0.15	850	0.55	5	0.638547	23.761	20.5609
34	9	0.134127	1100	0.15	850	0.55	5	0.3197	26.6567	25.469
35	42	0.095	473.966	0.15	850	0.55	5	0.860517	23.012	20.2518
36	39	0.095	1726.03	0.15	850	0.55	5	0.290702	27.2352	25.7781
37	16	0.095	1100	0.0717458	850	0.55	5	0.365443	25.9308	22.9065
38	30	0.095	1100	0.228254	850	0.55	5	0.461482	24.875	24.1234
39	48	0.095	1100	0.15	302.22	0.55	5	0.206326	29.8433	17.9989
40	43	0.095	1100	0.15	1397.78	0.55	5	0.620598	23.8449	22.3134
41	21	0.095	1100	0.15	850	0.0022204	5	0.221804	29.2162	18.6082
42	37	0.095	1100	0.15	850	1.09778	5	0.733582	23.3848	33.7375
43	29	0.095	1100	0.15	850	0.55	0	0.396417	13.9469	5.66153
44	28	0.095	1100	0.15	850	0.55	12.8254	0.44014	43.2052	24.5237
45	8	0.095	1100	0.15	850	0.55	5	0.413462	25.3416	23.0149

Table A.2 Design of Experiment's table for TC-100

11	11	Factor 1	Factor 2	Factor 3	Factor 4	Factor 5	Factor 6	Response 1	Response 2	Response 3
Std	Run	A:Mu	B:Fapp	C:Tapp	D:d-Omega	E:Inertia	F:Td	Ts	Cp	ALLFD
		–	N	s	rad/s	kg/m^2	N.m			
1	40	0.07	700	0.1	700	0.5	0	0.148943	11.714	3.44512
2	35	0.11	700	0.1	700	0.5	10	0.164402	27.0826	55.9757
3	38	0.07	1500	0.1	700	0.5	10	0.18834	26.3095	54.3564
4	6	0.11	1500	0.1	700	0.5	0	0.118816	13.4164	4.31868
5	49	0.07	700	0.2	700	0.5	10	0.308029	24.2464	57.1248
6	25	0.11	700	0.2	700	0.5	0	0.168031	10.9513	6.10754
7	31	0.07	1500	0.2	700	0.5	0	0.210637	9.74749	4.87213
8	3	0.11	1500	0.2	700	0.5	10	0.276566	24.6158	60.0526
9	22	0.07	700	0.1	1200	0.5	10	0.228408	25.3781	59.0569
10	33	0.11	700	0.1	1200	0.5	0	0.155566	11.4281	9.6934
11	24	0.07	1500	0.1	1200	0.5	0	0.195012	10.1279	7.73266
12	42	0.11	1500	0.1	1200	0.5	10	0.193703	26.1625	62.0697
13	19	0.07	700	0.2	1200	0.5	0	0.275789	8.62596	10.9356
14	29	0.11	700	0.2	1200	0.5	10	0.315177	24.1728	69.6388
15	1	0.07	1500	0.2	1200	0.5	10	0.35893	23.7861	64.2323
16	36	0.11	1500	0.2	1200	0.5	0	0.220004	9.54538	13.7085
17	45	0.07	700	0.1	700	1.1	10	0.255346	24.9163	55.9063
18	10	0.11	700	0.1	700	1.1	0	0.176232	10.6743	6.40564
19	30	0.07	1500	0.1	700	1.1	0	0.222012	9.50425	5.13524
20	47	0.11	1500	0.1	700	1.1	10	0.210978	25.7398	57.6686
21	43	0.07	700	0.2	700	1.1	0	0.312426	8.20076	7.22654
22	37	0.11	700	0.2	700	1.1	10	0.337879	23.9596	62.2812
23	11	0.07	1500	0.2	700	1.1	10	0.394228	22.6486	51.4852
24	4	0.11	1500	0.2	700	1.1	0	0.24923	9.01236	9.05895
25	28	0.07	700	0.1	1200	1.1	0	0.309164	8.23453	12.259
26	44	0.11	700	0.1	1200	1.1	10	0.266438	24.7532	66.6019
27	5	0.07	1500	0.1	1200	1.1	10	0.312497	23.9197	63.5808
28	46	0.11	1500	0.1	1200	1.1	0	0.233104	9.28992	14.5249
29	27	0.07	700	0.2	1200	1.1	10	0.475831	23.1016	68.8677
30	16	0.11	700	0.2	1200	1.1	0	0.326318		

11	11	Factor 1	Factor 2	Factor 3	Factor 4	Factor 5	Factor 6	Response 1	Response 2	Response 3
Std	Run	A:Mu	B:Fapp	C:Tapp	D:d-Omega	E:Inertia	F:Td	Ts	Cp	ALLFD
		–	N	s	rad/s	kg/m^2	N.m			
31	15	0.07	1500	0.2	1200	1.1	0	0.409164	7.44401	16.2242
32	26	0.11	1500	0.2	1200	1.1	10	0.399771	23.5014	74.9099
33	41	0.0586983	1100	0.15	950	0.8	5	0.318615	16.1386	33.3869
34	7	0.121302	1100	0.15	950	0.8	5	0.236706	17.2246	37.8762
35	9	0.09	473.966	0.15	950	0.8	5	0.266482	16.7526	35.7553
36	17	0.09	1726.03	0.15	950	0.8	5	0.266482	16.7526	35.7553
37	39	0.09	1100	0.0717458	950	0.8	5	0.177369	18.6379	32.1587
38	8	0.09	1100	0.228254	950	0.8	5	0.343702	15.9095	38.8719
39	48	0.09	1100	0.15	558.729	0.8	5	0.216546	17.618	30.1402
40	20	0.09	1100	0.15	1341.27	0.8	5	0.307244	16.2547	42.5077
41	50	0.09	1100	0.15	950	0.330475	5	0.190288	18.2552	32.6801
42	12	0.09	1100	0.15	950	1.26953	5	0.323639	16.0899	38.0622
43	13	0.09	1100	0.15	950	0.8	-2.82542	0.237065	9.21826	19.568
44	51	0.09	1100	0.15	950	0.8	12.8254	0.307793	28.7696	66.5497
45	14	0.09	1100	0.15	950	0.8	5	0.266482	16.7526	35.7553

Table A.3 Design of Experiment's table for SC-74- sensitivity analysis

		Factor 1	Factor 2	Factor 3	Factor 4	Factor 5	Factor 6	Response 1	Response 2	Response 3
Std	Run	A:mu	B:force	C:Tapp	D:omega	E:inertia	F:alpha	Ts	Cp	ALLFD
			N	s	rpm	kgm2	deg	s	MPa	J
1	13	0.05	700	0.1	700	0.25	min	1.98	69.54	7236
2	35	0.1	700	0.1	700	0.15	min	0.56	67.4	4242
3	42	0.05	1500	0.1	700	0.15	min	0.54	87.6	6850
4	11	0.1	1500	0.1	700	0.25	min	0.46	80.9	6775
5	62	0.05	700	0.2	700	0.15	min	1.1	72	7138
6	50	0.1	700	0.2	700	0.25	min	1.8	74	8073.4
7	26	0.05	1500	0.2	700	0.25	min	0.9	88.1	4987.5
8	37	0.1	1500	0.2	700	0.15	min	0.48	94.5	4028
9	45	0.05	700	0.1	1200	0.15	min	1.8	76	14253
10	53	0.1	700	0.1	1200	0.25	min	1.5	79	6240
11	43	0.05	1500	0.1	1200	0.25	min	1.4	80.2	15890
12	29	0.1	1500	0.1	1200	0.15	min	0.46	83.4	4619
13	10	0.05	700	0.2	1200	0.25	min	2.95	65.2	35120
14	24	0.1	700	0.2	1200	0.15	min	0.95	71.5	7706
15	30	0.05	1500	0.2	1200	0.15	min	0.92	80.1	7238
16	58	0.1	1500	0.2	1200	0.25	min	0.8	78.2	7037
17	48	0.025	1100	0.15	950	0.2	min	2.15	75.2	6872
18	74	0.125	1100	0.15	950	0.2	min	0.55	77.4	4598
19	8	0.075	300	0.15	950	0.2	min	2.57	65.1	14348
20	14	0.075	1900	0.15	950	0.2	min	0.53	92.4	4325
21	78	0.075	1100	0.05	950	0.2	min	0.81	83.7	5389
22	36	0.075	1100	0.25	950	0.2	min	0.56	79.3	4442
23	63	0.075	1100	0.15	450	0.2	min	0.48	76	6604
24	2	0.075	1100	0.15	1450	0.2	min	1.2	75.9	15950
25	31	0.075	1100	0.15	950	0.1	min	0.47	78.2	4507
26	54	0.075	1100	0.15	950	0.3	min	1.2	81.8	12357
27	77	0.075	1100	0.15	950	0.2	min	0.85	78.6	6585
28	19	0.05	700	0.1	700	0.25	nom	1.95	68.2	6500
29	28	0.1	700	0.1	700	0.15	nom	0.87	67.2	4390
30	44	0.05	1500	0.1	700	0.15	nom	0.56	111	4281
31	73	0.1	1500	0.1	700	0.25	nom	0.54	88.2	6900
32	1	0.05	700	0.2	700	0.15	nom	1.32	68.3	4342
33	69	0.1	700	0.2	700	0.25	nom	0.91	65	6412
34	76	0.05	1500	0.2	700	0.25	nom	0.89	93	6449
35	72	0.1	1500	0.2	700	0.15	nom	0.39	88.1	4205
36	60	0.05	700	0.1	1200	0.15	nom	1.76	69.8	10651
37	79	0.1	700	0.1	1200	0.25	nom	1.59	66.4	17905
38	15	0.05	1500	0.1	1200	0.25	nom	1.33	84.8	13352
39	20	0.1	1500	0.1	1200	0.15	nom	0.61	124	11056.5
40	59	0.05	700	0.2	1200	0.25	nom	2.05	79.7	15304.1
41	46	0.1	700	0.2	1200	0.15	nom	0.97	78.5	7700.5
42	67	0.05	1500	0.2	1200	0.15	nom	0.9	81.2	10256.7
43	65	0.1	1500	0.2	1200	0.25	nom	0.74	86.2	8947

		Factor 1	Factor 2	Factor 3	Factor 4	Factor 5	Factor 6	Response 1	Response 2	Response 3
Std	Run	A:mu	B:force	C:Tapp	D:omega	E:inertia	F:alpha	Ts	Cp	ALLFD
			N	s	rpm	kgm2	deg	s	MPa	J
44	80	0.025	1100	0.15	950	0.2	nom	2.15	76.4	6720
45	6	0.125	1100	0.15	950	0.2	nom	0.51	80.2	4315
46	27	0.075	300	0.15	950	0.2	nom	2.7	61.3	16345
47	68	0.075	1900	0.15	950	0.2	nom	0.55	79.5	4235
48	4	0.075	1100	0.05	950	0.2	nom	0.75	71.3	4652
49	38	0.075	1100	0.25	950	0.2	nom	0.86	74.5	5786
50	64	0.075	1100	0.15	450	0.2	nom	0.57	76.2	4327
51	16	0.075	1100	0.15	1450	0.2	nom	1.2	80.1	16540
52	40	0.075	1100	0.15	950	0.1	nom	0.61	84.2	5064.36
53	55	0.075	1100	0.15	950	0.3	nom	1.1	85.3	10730
54	18	0.075	1100	0.15	950	0.2	nom	0.79	79.8	4922
55	81	0.05	700	0.1	700	0.25	max	2.1	64.2	4978.9
56	39	0.1	700	0.1	700	0.15	max	0.72	80.1	4748.61
57	75	0.05	1500	0.1	700	0.15	max	0.59	93.1	4021.7
58	3	0.1	1500	0.1	700	0.25	max	0.52	93.5	4322.87
59	17	0.05	700	0.2	700	0.15	max	1.16	78.6	6348
60	32	0.1	700	0.2	700	0.25	max	0.95	79.8	4975
61	47	0.05	1500	0.2	700	0.25	max	0.9	80.1	4298
62	71	0.1	1500	0.2	700	0.15	max	0.44	84.2	3839.15
63	33	0.05	700	0.1	1200	0.15	max	1.8	67.1	10815
64	61	0.1	700	0.1	1200	0.25	max	1.5	66.8	8954
65	9	0.05	1500	0.1	1200	0.25	max	1.49	84.3	11548
66	22	0.1	1500	0.1	1200	0.15	max	0.6	84.1	6110
67	52	0.05	700	0.2	1200	0.25	max	3.1	78.5	16014
68	25	0.1	700	0.2	1200	0.15	max	1.02	72.8	8712
69	66	0.05	1500	0.2	1200	0.15	max	0.95	86.4	7615
70	34	0.1	1500	0.2	1200	0.25	max	0.8	86.3	8021
71	5	0.025	1100	0.15	950	0.2	max	2.41	72.9	4587.2
72	23	0.125	1100	0.15	950	0.2	max	0.55	79.1	4678
73	41	0.075	300	0.15	950	0.2	max	3.07	63.4	20145
74	7	0.075	1900	0.15	950	0.2	max	0.61	103	4064.39
75	51	0.075	1100	0.05	950	0.2	max	0.82	80.9	5763
76	49	0.075	1100	0.25	950	0.2	max	0.94	87.2	6418
77	21	0.075	1100	0.15	450	0.2	max	0.49	87.3	3293.5
78	57	0.075	1100	0.15	1450	0.2	max	1.28	84.5	10785
79	70	0.075	1100	0.15	950	0.1	max	0.46	76.8	4480
80	12	0.075	1100	0.15	950	0.3	max	1.4	90.6	6838.4
81	56	0.075	1100	0.15	950	0.2	max	0.9	88.5	5978

Table A.4 ANOVA analysis for synchronization time as the first response of DOE method for DC-170.

Source	Sum of Square	DoF	Mean Square	F- Value	p-value		Coefficient	Standard Error	95% CI Low	95% CI High	VIF
Model	2.26	21.00	0.11	83.86	<0.0001	significant					
A-Mu	0.17	1.00	0.17	131.33	<0.0001	significant	-0.068	5.89E-03	-0.08	-0.055	1
B-Fapp	0.39	1.00	0.39	303.22	<0.0001	significant	-0.1	5.89E-03	-0.11	-0.091	1
C-Tapp	0.03	1.00	0.03	19.95	0.00	significant	0.026	5.89E-03	0.014	0.038	1
D-d-Omega	0.42	1.00	0.42	328.57	<0.0001	significant	0.11	5.89E-03	0.095	0.12	1
E-Inertia	1.06	1.00	1.06	830.36	<0.0001	significant	0.17	5.89E-03	0.16	0.18	1
F-Td	0.01	1.00	0.01	6.64	0.02	significant	0.015	6.01E-03	0.003208	2.80E-02	1
Residual	0.038	30	1.28E-03			Std. Dev.	0.036		R-Squared	0.9833	
Lack of Fit	0.038	23	1.67E-03			Mean	0.66		Adj R-Squared	0.9715	
Pure Error	0	7	0			C.V. %	5.46		Pred R-Squared	0.9581	
Cor Total	2.29	51				PRESS	0.096		Adeq Precision	41.968	

Table A.5 ANOVA analysis for contact pressure as the second response of DOE method for DC-170.

Source	Sum of Square	DoF	Mean Square	F- Value	p-value		Coefficient	Standard Error	95% CI Low	95% CI High	VIF
Model	5066.44	27.00	187.65	280.61	<0.0001	significant					
A-Mu	39.55	1.00	39.55	59.15	<0.0001	significant	1.04	1.30E-01	0.76	1.31	1
B-Fapp	94.79	1.00	94.79	141.76	<0.0001	significant	1.6	1.30E-01	1.32	1.88	1
C-Tapp	22.63	1.00	22.63	33.84	<0.0001	significant	-0.78	1.30E-01	-1.06	-0.51	1
D-d-Omega	112.21	1.00	112.21	167.80	<0.0001	significant	-1.74	1.30E-01	-2.02	-1.47	1
E-Inertia	296.19	1.00	296.19	442.94	<0.0001	significant	-2.83	1.30E-01	-3.11	-2.56	1
F-Td	4292.16	1.00	4292.16	6418.67	<0.0001	significant	11.14	1.40E-01	10.85	1.14E+01	1.03
Residual	16.05	24	6.70E-01			Std. Dev.	0.82		R-Squared	0.9968	
Lack of Fit	16.05	17	9.40E-01			Mean	26.68		Adj R-Squared	0.9933	
Pure Error	0	7	0			C.V. %	3.06		Pred R-Squared	0.9785	
Cor Total	5082.48	51				PRESS	109.19		Adeq Precision	60.661	

Table A.6 ANOVA analysis for friction dissipated energy as the third response of DOE method for DC-170.

Source	Sum of Square	DoF	Mean Square	F- Value	p-value		Coefficient	Standard Error	95% CI Low	95% CI High	VIF
Model	3660.41	27.00	135.57	10.79	<0.0001	significant					
A-Mu	19.35	1.00	19.35	1.54	0.23		0.72	5.80E-01	-0.48	1.93	1
B-Fapp	30.98	1.00	30.98	2.46	0.13		0.92	5.80E-01	-0.29	2.12	1
C-Tapp	5.44	1.00	5.44	0.43	0.52		0.38	5.80E-01	-0.82	1.59	1
D-d-Omega	254.63	1.00	254.63	20.26	0.00	significant	2.63	5.80E-01	1.42	3.83	1
E-Inertia	550.95	1.00	550.95	43.84	<0.0001	significant	3.86	5.80E-01	2.66	5.07	1
F-Td	2449.58	1.00	2449.58	194.91	<0.0001	significant	8.42	6.00E-01	7.17	9.66E+00	1.03
Residual	301.62	24	1.26E+01			Std. Dev.	3.55		R-Squared	0.9239	
Lack of Fit	301.62	17	1.77E+01			Mean	20.46		Adj R-Squared	0.8382	
Pure Error	0	7	0			C.V. %	17.32		Pred R-Squared	0.3754	
Cor Total	3962.03	51				PRESS	2474.71		Adeq Precision	13.073	

Table A.7 ANOVA analysis for synchronization time as the first response of DOE method for TC-100.

Source	Sum of Square	DoF	Mean Square	F- Value	p-value		Coefficient	Standard Error	95% CI Low	95% CI High	VIF
Model	0.26	27.00	0.01	663.00	<0.0001	significant					
A-Mu	0.02	1.00	0.02	1554.70	<0.0001	significant	-0.025	6.33E-04	-0.026	-0.024	1
B-Fapp	0.00	1.00	0.00	1.76	0.20		-0.0008397	6.33E-04	-0.002146	0.0004664	1
C-Tapp	0.10	1.00	0.10	6756.06	<0.0001	significant	0.052	6.33E-04	0.051	0.053	1
D-d-Omega	0.03	1.00	0.03	2118.24	<0.0001	significant	0.029	6.33E-04	0.028	0.03	1
E-Inertia	0.07	1.00	0.07	4537.48	<0.0001	significant	0.043	6.33E-04	0.041	0.044	1
F-Td	0.03	1.00	0.03	2086.97	<0.0001	significant	0.029	6.33E-04	0.028	3.00E-02	1
Residual	0.0003547	24	1.48E-05			Std. Dev.	0.003844		R-Squared	0.9987	
Lack of Fit	0.0003547	17	2.09E-05			Mean	0.26		Adj R-Squared	0.9972	
Pure Error	0	7	0			C.V. %	1.45		Pred R-Squared	0.9921	
Cor Total	0.26	51				PRESS	0.002106		Adeq Precision	126.539	

Table A.8 ANOVA analysis for contact pressure as the second response of DOE method for TC-100.

Source	Sum of Square	DoF	Mean Square	F- Value	p-value		Coefficient	Standard Error	95% CI Low	95% CI High	VIF
Model	466800	27	1729000	1515.85	<0.0001	significant					
A-Mu	128100	1	128100	112.29	<0.0001	significant	58.91	5.56	47.44	70.39	1
B-Fapp	841.05	1	841.05	0.74	0.399		-4.77	5.56	-16.25	6.7	1
C-Tapp	645100	1	645100	565.6	<0.0001	significant	-132.22	5.56	-143.7	-120.75	1
D-d-Omega	127500	1	127500	111.82	<0.0001	significant	-58.79	5.56	-70.26	-47.31	1
E-Inertia	368800	1	368800	323.34	<0.0001	significant	-99.97	5.56	-111.45	-88.5	1
F-Td	42550000	1	42550000	37303.67	<0.0001	significant	1073.8	5.56	1062.33	1085.28	1
Residual	27373.01	24	1.14E+03			Std. Dev.	33.77		R-Squared	0.9994	
Lack of Fit	27373.01	17	1.61E+03			Mean	1230.14		Adj R-Squared	0.9988	
Pure Error	0	7	0			C.V. %	2.75		Pred R-Squared	0.9956	
Cor Total	46710000	51				PRESS	207000		Adeq Precision	137.236	

Table A.9 ANOVA analysis for friction dissipated energy as the third response of DOE method for TC-100.

Source	Sum of Square	DoF	Mean Square	F- Value	p-value		Coefficient	Standard Error	95% CI Low	95% CI High	VIF
Model	23153.53	6.00	3858.92	231.87	<0.0001	significant					
A-Mu	90.96	1.00	90.96	5.47	0.02	significant	1.57	6.70E-01	0.22	2.92	1
B-Fapp	1.70	1.00	1.70	0.10	0.75		-0.21	6.70E-01	-1.57	1.14	1
C-Tapp	128.41	1.00	128.41	7.72	0.01	significant	1.87	6.70E-01	0.51	3.22	1
D-d-Omega	628.66	1.00	628.66	37.77	<0.0001	significant	4.13	6.70E-01	2.77	5.48	1
E-Inertia	89.83	1.00	89.83	5.40	0.02	significant	1.56	6.70E-01	0.21	2.91	1
F-Td	22213.97	1.00	22213.97	1334.74	<0.0001	significant	24.54	6.70E-01	23.18	2.59E+01	1
Residual	748.93	45	1.66E+01			Std. Dev.	4.08		R-Squared	0.9687	
Lack of Fit	748.93	38	1.97E+01			Mean	35.87		Adj R-Squared	0.9645	
Pure Error	0	7	0			C.V. %	11.37		Pred R-Squared	0.9601	
Cor Total	23902.46	51				PRESS	954.86		Adeq Precision	51.311	